UNIVERSITÀ DEGLI STUDI DI MESSINA

Dipartimento di Scienze chimiche, biologiche, farmaceutiche ed ambientali

Dottorato di ricerca in scienze chimiche (Ciclo XXXIV)

The hydrogen bond: actor and stage in the theater of chemistry

Settore scientifico-disciplinare CHIM/03

PhD student

Giovanni Bella

Thesis Supervisor

Prof. Giuseppe Bruno

Anno Accademico 2021/2022

"Quantum mechanics is not boring,
quantum mechanics is *bohring*"

Giovanni Bella

Index

CHAPTER 1

CHAPTER 2

Summary

Hydrogen bond plays a key role in a wide range of inorganic, organic, as well as biological systems. The understanding on how the chemical environment can affect this kind of interaction is crucial to predict its binding strength, and consequently the robustness and the dynamic properties of many supramolecular systems. Both in nature and in artificial system hydrogen bonding offers a plethora of possible assembling and arrangement between molecules. In this thesis, a theoretical approach was adopted to spotlight the intimate nature of hydrogen interactions in two unprecedented chemical H-bonded architecture: 1) an AA-DD pattern in a amine-borane azacrown involving a double dihydrogen interaction; 2) a BODIPY dyad generated by two complementary chromophores directly bearing in meso position an acceptor-donor-acceptor (A-D-A) and a donor-acceptor-donor (D-A-D) frontier geometry. Both cases were computationally treated by means density functional theory (DFT) in order to highlight hydrogen bond strengths, directionality and function-structure relationship.

CHAPTER 1

INTRODUCTION

Hydrogen, the most ubiquitous element in the universe always seems to find new roles to play in the chemical theatre, its non-directional valence orbital and the total lack of core electron density allows it to get involved in many interactions[1]. Hydrogen bonds lie at the heart of chemistry to such an extent that we can consider it as the "fundamental interaction" that governs life. In some ways, it is possible to assert that nature "choose" hydrogen bond because it has exactly the correct strength. Such sentence can be justified because the hydrogen bond shows enough binding stability to held together supramolecular complex structures as DNA, and at the same time, it is labile enough to be easily broken allowing DNA replication.

Among the various attractive electrostatic forces holding molecules together, hydrogen bonds are the most effective, due to their pronounced directionality and relatively low bonding energies, which are particularly important for noncovalent supramolecular aggregation[2]. It is clear that intermolecular hydrogen bonding has a profound impact on the structure, stability, and stereochemistry of inorganic, organic, organometallic, and bioorganic molecules and molecular assemblies built *via* hydrogen bonds[3]. Hydrogen bond is massively used in supramolecular chemistry and crystal

engineering, whereas together with metal-coordination interactions, performs key roles in all the systems where dynamic features and thermodynamic control are requested[4]. Despite the relative weakness of hydrogen bonds due to cooperativity, they are responsible for the spontaneous formation of the three-dimensional shape of proteins and for the double helix of DNA and other complex molecular aggregates[5].

In some sense, intermolecular hydrogen bonds act as glue in the build-up and design of molecular crystals[6]. The main advantage of hydrogen-bonded crystals is the fact that they are weak and energetically flexible enough to allow annealing and editing[7]. On the other hand, they are strong enough to impart stability to crystal systems. The role of hydrogen bonding is also well recognized in proton transfer reactions, where hydrogen bonds act as organizing interactions[8]. The first pioneers to reveal the existence of this interaction were Moore and Winmill with their studies about the changing in basicity of trimethylammonium hydroxide[9]. Typically, hydrogen bond involves a stabilizing electrostatic interaction between two molecules: a partially positive charged hydrogen of a proton donor (D) and the lone pair of a strongly electronegative element of a proton acceptor (A) (Figure 1).

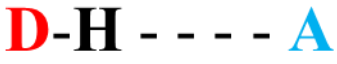

Figure 1. Electrostatic attractive interaction between a proton donor D-H and a proton acceptor A, where D and A are electronegative atoms such as O, N, F etc.

According to their interaction energy in solution, H-bonds are often classified as strong (15 to 22 kcal/mol), moderate (4 to 15 kcal/mol), and weak (<4 kcal/mol)[10]. An important characteristic of this interaction is its directionality, i.e. the angle θ between the D-H and H---A bonds (see Figure 2). Usually θ lies in the range from 140° to 180°[10], where typically smaller θ values go together with a weaker H-bonds strength. For smaller angles the hydrogen bonding is believed to be largely due to the van der Waals (vdW) interaction[11].

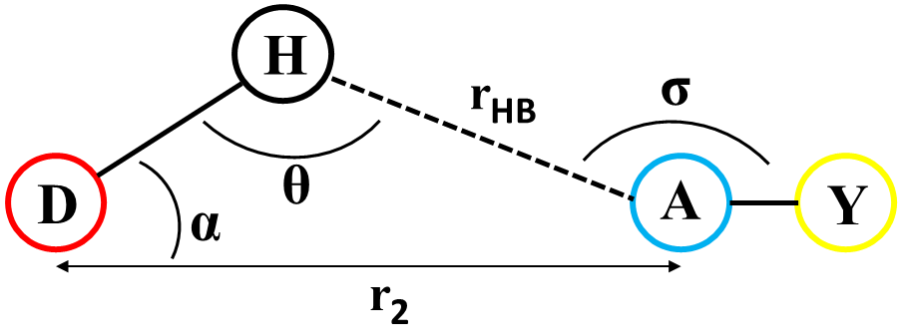

Figure 2. Parameters for describing the hydrogen bond geometry

The classical electrostatic model of the hydrogen bond gives quantitative description of the structure, vibrations, dipole moments, intensities, and cooperatives of many H-bonded systems[12]. Unfortunately, this method has limitations in describing some electronic features: the changes due to hydrogen bonding in the electric field gradient at a nucleus, and in dipole moment derivatives with respect to displacement of the nuclei actually involved in the hydrogen bond, where charge distortion related to short-range overlap effects (such as intermolecular charge transfer and exchange

repulsion) might be relatively more important[13]. Moreover, this model is unlikely to be successful for excited states, like anions that have diffuse electron clouds.

In these terms theoretical calculations have played a fundamental role in determining the properties of hydrogen-bonded systems[14], but at the same time no theory of hydrogen bonding *per se* is enough to explain the intimate nature of this interaction[15]. Nowadays computational methods based on quantum theory and developed for the treatment of chemical bonding, intermolecular forces, reactivity, and interaction with electromagnetic field have reached a level of competitiveness with the best experimental data[16]. However, the treatment of the dynamics of hydrogen bonds, particularly those biological interest that interact between them or with the medium requires specific adaptations of theory of the condensed states[17]. Current DFT (density functional theory) methods has made an unparalleled impact on the application of quantum mechanics to interesting and challenging problems regarding hydrogen bonds[18].

The Schrodinger equation that describes the quantum phenomena of matter is

$$\hat{\mathbf{H}}\psi = \mathbf{E}\psi$$

where the Hamiltonian, $\hat{\mathbf{H}}$, for a Coulombic system is given by

$$\hat{\mathbf{H}} = -\sum_i \frac{1}{2} \nabla_i^2 - \sum_{ia} \frac{Za}{|Ri - Ra|} + \sum_{i>j} \frac{1}{Rij}$$

With a specified set of nuclei with charges Za, position Ra and a number of electrons N. The goal is to simply minimize the energy over all possible antisymmetric wave functions, $\Psi(x_1,x_2,x_3...x_N)$, where x_i contains the spatial coordinate Ri and spin coordinate σ_i. This enables us to find the minimizing Ψ and hence the ground state energy, E. The basic principles of density functional theory is fundamentally based upon Hohenberg–Kohn theorems[19], which states that the external potential is a functional of the ground-state density. In this context, the density (an observable in 3D space) is used to describe the complicated physics behind the interactions between electrons and, therefore, determines everything about the quantum system.

Theorem I:

Total ground state energy of a quantum mechanical system is a unique functional of the electron density: $\boldsymbol{E=E[\rho(r)]}$ where $\rho(r)$ is the electronic density.

Theorem II:

The electron density that minimizes the overall functional is the true ground state electron density: $\mathbf{E[\rho(r)]>E_0\ [\rho_0(r)]}$ where, $\rho_0(r)$ is the ground state density.

In Kohn-Sham (KS) theory[20], these are formulated as a simple expression for the ground state energy:

$$\mathbf{E[\rho(r)] = T_s[\rho(r)] + V_{ne}[\rho(r)] + J[\rho(r)] + E_{xc}[\rho(r)]}$$

where the forms of some of the functionals are explicitly known. The kinetic energy for the KS non-interacting reference system is

$$\mathbf{T_s[\rho(r)] = \sum_i < \phi i \mid -\frac{1}{2}\nabla^2 \mid \phi i >}$$

in terms of {ϕi}, the set of one electron KS orbitals. The electron density of the KS reference system is given by

$$\mathbf{[\rho(r)] = \sum_i \mid \phi i\,(r)\mid^2}$$

The other two known energy components are the nucleus electron potential energy, expressed in terms of the external potential due to the nuclei,

$$\boldsymbol{v} = \mathbf{-\sum_a}\left(\frac{\boldsymbol{Za}}{|\boldsymbol{r}-\boldsymbol{Ra}|}\right)$$

$$\mathbf{V_{ne}[\rho(r)] = \int \rho(r)\, v(r)\, dr}$$

and the classical electron-electron repulsion energy is

$$\mathbf{J[\rho(r)] = \frac{1}{2}\iint \frac{\rho(r)\rho(r')}{r-r'} drdr'}$$

Much is known about the key remaining term, the exchange-correlation functional, $\mathbf{E_{xc}[\rho(r)]}$, although no explicit form is available. It can be expressed in the constrained search formulation for density functionals

$$\mathbf{E_{xc}[\rho(r)] = \min_{\psi\to\rho} <\psi|T + V_{ee}|\psi> - T_s[\rho(r)] - J[\rho(r)] = (T[\rho(r)] - T_s[\rho(r)])}$$

$$\mathbf{+ (V_{ee}[\rho(r)] - J[\rho(r)])}$$

It can also be expressed elegantly through the adiabatic connection:

$$\mathbf{E_{xc}[\rho(r)] = \int_0^1 < \psi_\lambda | V_{ee} | \psi_\lambda > d\lambda - d[\rho(r)]}$$

Finding effective formulations for the exchange-correlation functional is one of the crucial points of DFT methods.

The first methods were based on the LDA[21] (local density approximation): this approximation implies that the value of $\mathbf{E_{xc}[\rho(r)]}$ at a certain point r^k of the space depends only on the value of the electron density $\boldsymbol{\rho(r^k)}$ at that point. $\mathbf{E_{xc} = E_{xc}[\rho(r^k)]}$

Although the methods based on the LDA approximation were pioneering and played a key role in the development of functionals, they fail in molecular simulation[22]. The move from LDA to GGA (generalized gradient approximation) brought about a massive improvement in functionals, of roughly an order of magnitude in binding energies[23]. GGA approach assumes that $\mathbf{E_{xc}[\rho(r)]}$ depends on the density $\boldsymbol{\rho(r^k)}$ and its gradient $\boldsymbol{\nabla \rho(r^k)}$.

$$\mathbf{E_{xc} = E_{xc}[\rho(r^k), \nabla \rho(r^k)]}$$

The next obvious step is to include higher-order derivatives of the density, then a further gradient expansion leads to Meta-GGA[24]:

$$\mathbf{E_{xc} = E_{xc}[\rho(r^k), \nabla \rho(r^k), \nabla^2 \rho(r^k)]}$$

Functionals based on the LSDA, GGA and MGGA approximations are also known as “pure DFT functionals”, probably the last clear advance in the

development of exchange-correlation functionals came in 1993, with the inclusion of some Hartree-Fock exchange that gave rise to "hybrid functionals"[25].

This class of functionals benefits from the studies of Vladimir Aleksandrovič Fock and Douglas Hartree, the latter, in 1928, introduced the Self Consistent Field (SCF) philosophy to the embryonic field of quantum chemistry. He proposed a model in which the *i*th electron in an atom moves completely independently of the others in an orbital $\Psi_i(r)$, Within this uncorrelated picture, the total kinetic energy is simply the sum of the kinetic energies of the individual electrons which, as Schrodinger had shown, is given by

$$\mathbf{E_T} = -\frac{\mathbf{1}}{\mathbf{2}}\sum_i^n \int \boldsymbol{\psi_i}\,(\boldsymbol{r})\boldsymbol{\nabla^2}\boldsymbol{\psi_j}\,(\boldsymbol{r})\mathbf{dr}$$

The early applications of Hartree's independent-electron model were confined to atoms but, by 1930, Lennard-Jones, Mulliken and Hund had shown that the model can be readily extended to molecules by allowing the $\psi_i\,(r)$ to delocalize over several atoms. This marked the birth of molecular orbital theory. It should be emphasized that the previous equation does not yield the exact kinetic energy (except in one-electron systems) because, in reality, the electrons do not move independently of one another, correlation effects must be considered. Almost parallel, in 1930, Fock pointed out that the Hartree wavefunction violates the Pauli Exclusion Principle because it is not properly antisymmetric. He showed that this deficiency can be

remedied by antisymmetrizing the wavefunction but that electrons of the same spin avoid one another, a phenomenon called Fermi correlation or exchange. Fock showed that this treatment corresponds to the exchange functional:

$$\mathbf{Ex} = -\frac{\mathbf{1}}{\mathbf{2}}\sum_{i}^{n}\sum_{i}^{n}\iint \frac{\psi_i\,(r_1)\psi_j\,(r_1)\psi_i\,(r_2)\psi_j\,(r_2)}{|r_1 - r_2|}\mathbf{dr_1 dr_2}$$

[1] S. J. Grabowski, *Chem. Rev.*, **2011**, *111*, 2597–2625.

[2] X. Fu, Q. Zhang, G. Wu, W. Zhou, Q-C. Wanga, D-H. Qu, *Polym. Chem*., **2014**,*5*, 6662-6666.

[3] a) L. Brammer, J.C. Mareque Rivas, R. Atencio, S. Fanga, F. C. Piggea, *J. Chem. Soc., Dalton Trans*., **2000**, 3855-3867. b) D. A. Leigh, C. C. Robertson, A. M. Z. Slawin, P. I. T. Thomson, *J. Am. Chem. Soc*. **2013**, *135* (26), 9939–9943.

[4] a) J. Holub, A. Santoro, J.-M. Lehn, *Inorg. Chim. Acta*, **2019**, *494*, 223-231. b) F. Nastasi, A. Santoro, S. Serroni, S. Campagna, N. Kaveevivitchai, R.P. Thummel, Photochem. *Photobiol. Sci*., **2019**, *18* (9), 2164-2173.

[5] C. F. Guerra, F. M. Bickelhaupt, J. G. Snijders, E. J. Baerends, *J. Am. Chem. Soc*. **2000**, *122* (17), 4117–4128.

[6] S. J. Grabowski, *Crystals*, **2016**, *6*, 59.

[7] C. Guzmán-Afonso, Y-L. Hong, H. Colaux, H. Iijima, A. Saitow, T. Fukumura, Y. Aoyama, S. Motoki, T. Oikawa, T. Yamazaki, K. Yonekura, Y. Nishiyama. *Nat Commun*, **2019**, *10*, 3537.

[8] T. Pilati, S. Quici, M. R. Chierotti, C. Nervi, R. Gobetto, G. Resnati, *Chem. Eur. J.* **2017**, *23*, 14462–14468.

[9] T. S. Moore, T. F. Winmill, *J. Chem. Soc.,* **1912**, *101*, 1635–1676.

[10] T. Steiner, *Angew. Chem., Int. Ed.* **2002**, *41*, 48.

[11] a) J. J. Novoa, P. Fuente, F. Mota, *Chem. Phys. Lett.* **1998**, *290*, 159. (b) T. Steiner, G. R. Desiraju, *Chem. Commun.* **1998**, 891.

[12] J. D. Bernal, R. H. Fowler, *J. Chem. Phys.* **1933**, *1*, 515.

[13] S. C. C. van der Lubbe, C. Fonseca Guerra, *Chem. Asian J.* **2019**, *14*, 2760.

[14] M. S. Gordon, J. H. Jensen, *Acc. Chem. Res.* **1996**, *29*, 536-543.

[15] M. Rozenberg, *RSC Adv.,* **2014**,*4*, 26928-26931.

[16] a) L. M. Roch, K. K. Baldridge, *Phys. Chem. Chem. Phys.*, **2017**,*19*, 26191-26200. b) L. M. Debefve, C. J. Pollock, *Phys. Chem. Chem. Phys.*, **2021**,*23*, 24780-24788.

[17] R. Pang, L-J. Yu, M. Zhang, Z-Q. Tian, D-Y. Wu, *J. Phys. Chem. A,* **2016**, *120* (42) 8273–8284.

[18] A. J. Cohen, P. Mori-Sánchez, W. Yang, *Chem. Rev.* **2012**, *112* (1), 289–320.

[19] P. Hohenberg, W. Kohn, *Phys. Rev.,* **1964**, *136*, 864-871.

[20] W. Kohn, L.J. Sham, *Phys. Rev.,* **1965**, *140,* 1133-1138.

[21] F. Xuan, J-D. Chai, H. Su, *ACS Omega,* **2019**, *4* (4), 7675–7683.

[22] O. V. Gritsenko , Ł. M. Mentel, E. J. Baerends, *J. Chem. Phys.* **2016**, *144*, 204114.

[23] E. Bright-Wilson, In Structural Chemistry and Molecular Biology; Rich, A., Davidson, N., Eds.; W. H. Freeman, San Francisco, **1968**, pp 753-760.

[24] J. P. Perdew, K. Schmidt Jacob's ladder of density functional approximations for the exchange-correlation energy. In Density Functional Theory and Its Application to Materials; VanDoren, V., VanAlsenoy,C., Geerlings, P., Eds.; **2001**; Vol. *577*, pp 1-20.

[25] A. D. Becke *J. Chem. Phys*. **1993**, *98*, 1372.

DIHYDROGEN BONDING

Hydrogen bonding, one of the oldest fundamental concepts in chemistry, is constantly evolving, due to the appearance of new experimental and theoretical methods[26]. Recently, an unconventional interaction in which both donor and acceptor atoms are hydrogens has attracted considerable attention and it was called *dihydrogen bond*[27]. Although ideas about the interaction between two hydrogen atoms with opposite partial charges have been exploited by chemists for a long time, formulation of this interaction as a bonding between two hydrogen atoms was first suggested in 1993[28]. Among the various nonconventional hydrogen bonds, dihydrogen bonds are the most unusual and intriguing. These bonds are formed between two hydrogen atoms, the first positively charged and acting as a proton-donor component (acidic hydrogen), the second negatively charged and acting as a proton-acceptor site (hydridic hydrogen) (see Figure 3). It should be noted that the term *dihydrogen bond* should be differentiated from the term *dihydrogen ligand*, which corresponds to the binding of molecular hydrogen to a transition metal in a $^{2}\eta$-H_2 fashion[29].

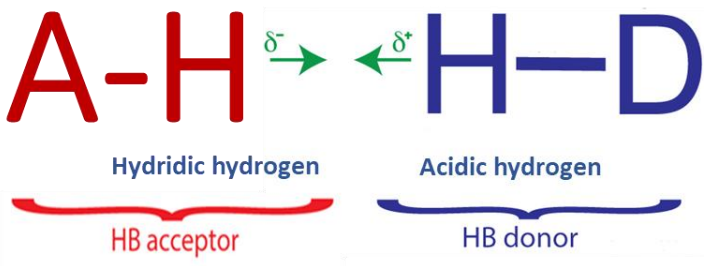

Figure 3. Typical dihydrogen bond involving a stabilizing electrostatic interaction between hydridic hydrogen and acidic hydrogen.

Despite its unusual character, this kind of proton–hydride interaction is now recognized as a common phenomenon in chemistry. Experimental data and theory have demonstrated that metal–hydrogen (M–H) and B–H σ-bonds act as proton acceptors with respect to acidic groups such as N–H, O–H or S-H, yielding medium or strong dihydrogen bonds that affect markedly even the physical properties of supramolecular aggregates[30]. In order to evaluate how much this apparently weak interaction can influence the molecules it is possible to perform a logical comparison: CH_3CH_3 and BH_3NH_3. These two molecules have: 1) the same number of atoms (8), 2) the same number of electrons (isoelectronic) 3) almost the same molar mass (30.07 g/mol for CH_3CH_3, 30.86 g/mol for BH_3NH_3) but surprisingly their physicochemical properties differ strongly. The melting point is −180° C for CH_3CH_3 and +104° C for BH_3NH_3 so ethane is a gas while the amine-borane adduct is a crystalline solid, *de facto* in the ethane dimer can be seen only very weak London interactions while in BH_3NH_3 the dihydrogen bonds allow the formation of an extended network in the solid state. These

simple considerations lead to the conclusion that dihydrogen bonding with its strength and directionality can actually affect the structure of compounds in solution and in the solid state and also the reactivity and even the selectivity of reactions[31].

[26] D. Herschlag, M. M. Pinney, *Biochemistry* **2018**, *57* (24) 3338–3352.

[27] V. I. Bakhmutov, Dihydrogen Bonds: Principles, Experiments, and Applications, John Wiley & Sons, Inc, 2008.

[28] T. B. Richardson, S. de Gala,R. H. Crabtree, *J. Am. Chem. SOC*. **1995**,*117*, 12875-12876.

[29] I. Alkorta, I. Rozas, J. Elguero, *Chem. Soc. Rev*. **1998**, *27*, 163.

[30] J. Wessel, J. C. Lee, E. Peris, G. P. A. Yap, J. B. Fortin, J. S. Ricci, G. Sini, A. Albinati, T. F. Koetzle, O. Eisenstein, A. L. Rheingold, R. H. Crabtree, *Angew. Chem. Int. Ed. Engl*. **1995**, *34*, 2507.

[31] R. Custelcean, J. E. Jackson, *Chem. Rev*. **2001**, *101*, 1963−1980.

PURPOSE OF THE WORK

In this study, I present a novel amine-borane aza-coronand, strategically designed to have both AA and DD pattern in order to involve them in a stabilizing self-assembly based on multiple dihydrogen bond (see Figure 4). The current investigation focuses on the determination and understanding of the electrostatic forces as an alternative way to elucidate the behavior of the secondary electrostatic interactions (SEIs) in the multiple dihydrogen bond. In this context, a good prevision of intermolecular hydrogen distances and angles becomes very important to have a reliable vectorial forces model. For this purpose, I began my study analysing which DFT functional better reproduce the H---H intermolecular bond length, NH---H and BH---H intermolecular angles, experimentally obtained by SCXRD analysis. Over 250 functionals were computationally evaluated to select the best method to reproduce the binding interaction geometry of this new pattern. Moreover, a new vector force model was used to split the contribution of primary and secondary electrostatic interactions (SEIs), in order to evaluate how the latter one can modify the binding strength of this unusual hydrogen-hydrogen interaction. Energy decomposition analyses was performed in order to rationalize which electronic factor can markedly affect the interaction region of dihydrogen bond. Lastly, NCI mapped

surfaces illustrated how some topologist features turn out to be crucial for the comprehension of the interaction geometry.

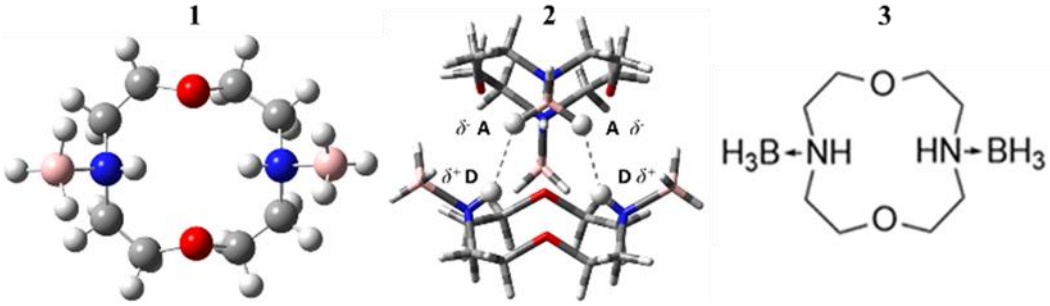

Figure 4. (**1**) and (**2**) are Xray pictures of the synthesized monomer and the self-assembled supramolecular complex respectively, ball and stick pattern was used to highlight hydrogens donors and acceptors. On the right the atomic skeleton of the aza-coronand (3).

SECONDARY ELECTROSTATIC INTERACIONS

Despite the seeming simplicity of the task, in reality it is not easy to say what a hydrogen bond is, it is well known that hydrogen bonds are dynamic in nature, and hydrogen-bonded complexes are often unstable, populating an area on the potential energy surface that does not correspond to an energy minimum[32]. Apparently, the hydrogen bonding mechanism seems easily rationalizable by simple interactions of spherical opposite charges. However, this model becomes puzzling when systems composed of multiple adjacent hydrogen bonds are investigated. In these systems, the transversal interaction (attractive or repulsive) between the two adjacent

hydrogen bonds of the two components of the system is called secondary electrostatic interactions (SEIs) (Figure 5).

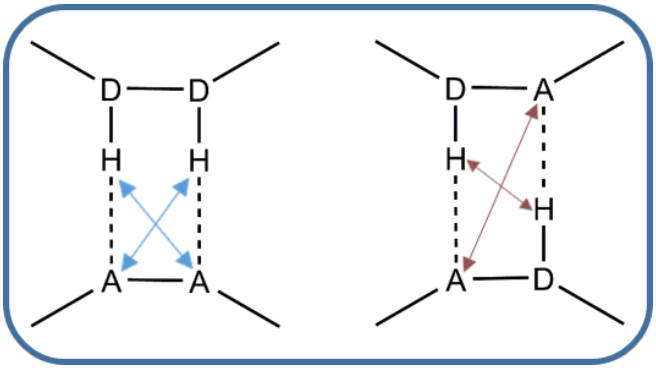

Figure 5. Electrostatic interactions between H-bond acceptors and donors in doubly H-bonded model. Blue arrows are related to attractive diagonally atoms, in a DD-AA system (left), whereas, in AD-DA system (right) the diagonal forces are repulsive, here represented by red arrows.

Jorgensen and Severance illustrated that the monomers in which all of the donor atoms (D) are aligned on one monomer and all of the acceptor atoms (A) are aligned on the other one exhibit the strongest hydrogen-bonded pairs[33]. This model simplifies the hydrogen bond dynamics by describing the latter as interacting point charges. However, despite valid criticisms[34] experimental binding strengths are often in line with the predictions[35]. Recent findings highlighted how the grouping of proton donor and acceptor groups in poli H-bonded aggregates drastically changes the association constants (hence the interaction energies) with respect to dimers in which the proton donor and acceptor components are alternating[35] (Figure 6).

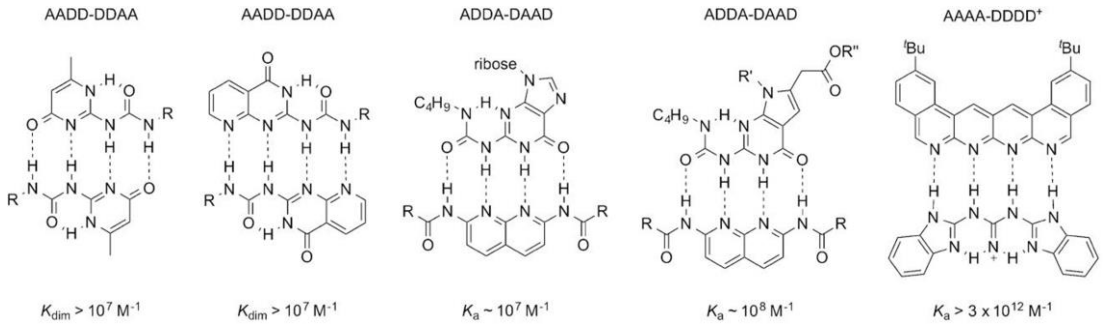

Figure 6. Hydrogen bonding pairs with quadruple bonds.

[32] C. Zhou, X. Li, Z. Gong, C. Jia, Y. Lin, C. Gu, G. He, Y. Zhong, J. Yang, X. Guo, *Nat Commun* **2018**, *9*, 807.

[33] W.L. Jorgensen, D.L. Severance, *J. Am. Chem. SOC.* **1991**,*113*, 209-216.

[34] O. Lukin, J. Leszczynski, *J. Phys. Chem. A* **2002**, *106*, 6775 – 6782.

[35] B. A. Blight, C. A. Hunter, D. A. Leigh, H. McNab, P. I. T. Thomson, *Nat. Chem*. **2011**, *3,* 244– 247. b) S. K. Yang, S. C. Zimmerman, *Isr. J. Chem*. **2013**, *53*, 1–10.

GEOMETRY OPTIMIZATION

Many problems in computational chemistry can be formulated as an optimization of a multi-dimensional function. Optimization is a general term for finding stationary points of a function, i.e. points where the first derivative is zero. In the majority of cases, the desired stationary point is a minimum, i.e. all the second derivatives are positive. In some cases, the desired point is a first-order saddle point, i.e. the second derivative is negative in one, and positive in all other, directions (transition state). In a few special cases, a higher order saddle point is desired (Figure 7). The optimizing procedure calculates the wave function and the energy at a starting geometry and then proceeds to search a new geometry of a lower energy. This is repeated until the lowest energy geometry is found.

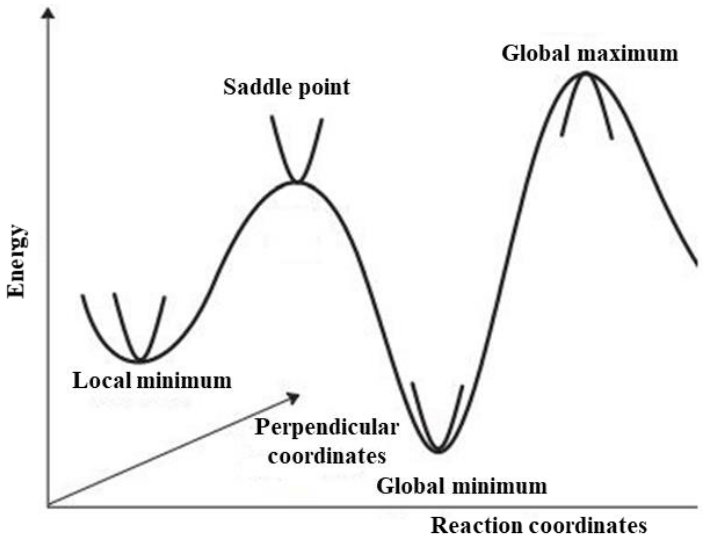

Figure 7 Illustrating a multi-dimensional energy surface.

The simple-minded approach for minimizing a function is to step one variable at a time until the function has reached a minimum, and then switch to another variable. This requires only the ability to calculate the function value for a given set of variables. As the variables are not independent, however, several cycles through the whole set are necessary for finding a minimum. This is impractical for more than five–ten variables and may not work anyway. Since optimization problems in computational chemistry tend to have many variables, essentially all commonly used methods assume that at least the first derivative of the function with respect to all variables, the gradient g, can be calculated analytically (i.e. directly, and not as a numerical differentiation by stepping the variables). Some methods also assume that the second derivative matrix, the Hessian H, can be calculated. It should be noted that the target function and its derivative(s) are calculated with a finite precision, which depends on the computational implementation. A stationary point can therefore not be located exactly, the gradient can only be reduced to a certain value. Below this value, the numerical inaccuracies due to the finite precision will swamp the "true" functional behaviour. In practice, the optimization is considered converged if the gradient is reduced below a suitable "cut-off" value, or if the function change between two iterations becomes sufficiently small. Both these criteria may in some cases lead to problems, as a function with a very flat surface in a certain region may meet the criteria without containing a stationary point.

TESTING OF FUNCTIONALS IN THE OPTIMIZATION PROCESS

In this study, a wide range of functionals (270) were assessed to obtain the best matching between theoretical and experimental intermolecular bond length and angles involved in dihydrogen bond. First, 210 pure functionals given by combining exchange and correlation functionals were tested: SVWN[36,37], SVWN5[36,37], SLYP[36,38], SPL[36,39], SP86[36,40], SPW9[36,41], SB95[36,42], SPBE[36,43], STPSS[36,44], SRevTPSS[36,45], SKCIS[36,46], SBRC[36,47], SPKZB[36,48], SVP86[36,49], SV5LYP[36,50], XAVWN[36,37], XAVWN5[36,37], XALYP[36,38], XAPL[36,39], XAP86[36,40], XAPW9[36,41], XAB95[36,42], XAPBE[36,43], XATPSS[36,44], XARevTPSS[36,45], XAKCIS[36,46], XABRC[36,47], XAPKZB[36,48], XAVP86[36,49], XAV5LYP[36,50], BVWN[51,37], BVWN5[51,37], BLYP[51,38], BPL[51,39], BP86[51,40], BPW91[51,41], BB95[51,42], BPBE[51,43], BTPSS[51,44], BRevTPSS[51,45], BKCIS [51,46], BBRC[51,47], BPKZB[51,48], BVP86[51,49], BV5LYP[51,50], PW91VWN[41,37], PW91VWN5[41,37], PW91LYP[41,38], PW91PL[41,39], PW91P86[41,40], PW91PW91[41], PW91B95[41,42], PW91PBE[41,43], PW91TPSS[41,44], PW91RevTPSS[41,45], PW91KCIS[41,46], PW91BRC[41,47], PW91PKZB[41,48], PW91VP86[41,49], PW91V5LYP[41,50], mPWVWN[52,37], mPWVWN5[52,37], mPWLYP[52,38], mPWPL[52,39], mPWP86[52,40], mPWPW91[52,41], mPWB95[52,42], mPWPBE[52,43], mPWTPSS[52,44], mPWRevTPSS[52,45], mPWKCIS[52,46], mPWBRC[52,47], mPWPKZB[52,48], mPWVP86[52,49], mPWV5LYP[52,50],

G96VWN[53,37], G96VWN5[53,37], G96LYP[53,38], G96PL[53,39], G96P86[53,40], G96PW91[53,41], G96B95[53,42], G96PBE[53,43], G96TPSS[53,44], G96RevTPSS[53,45], G96KCIS[53,46], G96BRC[53,47], G96PKZB[53,48], G96VP86[53,49], G96V5LYP[53,50], PBEVW[43,37], PBEVWN5[43,37], PBELYP[43,38], PBEPL[43,39], PBEP86[43,40], PBEPW91[43,41], PBEB95[43,42], PBEPBE[43], PBETPSS[43,44], PBERevTPSS[43,45], PBEKCIS[43,46], PBEBRC[43,47], PBEPKZB[43,48], PBEVP86[43,49], PBEV5LYP[43,50], OVWN[54,37], OVWN5[54,37], OLYP[54,38], OPL[54,39], OP86[54,40], OPW91[54,41], OB95[54,42], OPBE[54,43], OTPSS[54,44], ORevTPSS[54,45], OKCIS[54,46], OBRC[54,47], OPKZB[54,48], OVP86[54,49], OV5LYP[54,50], TPSSVWN[44,37], TPSSVWN5[44,37], TPSSLYP[44,38], TPSSPL[44,39], TPSSP86[44,40], TPSSPW91[44,41], TPSSB95[44,42], TPSSPBE[44,43], TPSSTPSS[44], TPSSRevTPSS[44,45], TPSSKCIS[44,46], TPSSBRC[44,47], TPSSPKZB[44,48], TPSSVP86[44,49], TPSSV5LYP[44,50], RevTPSSVWN[45,37], RevTPSSVWN5[45,37], RevTPSSLYP[45,38], RevTPSSPL[45,39], RevTPSSP86[45,40], RevTPSSPW91[45,41], RevTPSSB95[45,42], RevTPSSPBE[45,43], RevTPSSTPSS[45,44], RevTPSSRevTPSS[45], RevTPSSKCIS[45,46], RevTPSSBRC[45,47], RevTPSSPKZB[45,48], RevTPSSVP86[45,49], RevTPSSV5LYP[45,50], BRxVWN[55,37], BRxVWN5[55,37], BRxLYP[55,38], BRxPL[55,39], BRxP86[55,40], BRxPW91[55,41], BRxB95[55,42], BRxPBE[55,43], BRxTPSS[55,44], BRxRevTPSS[55,45], BRxKCIS[55,46], BRxBRC[55,47], BRxPKZB[55,48], BRxVP86[55,49], BRxV5LYP[55,50], PKZBVWN[48,37], PKZBVWN5[48,37], PKZBLYP[48,38], PKZBPL[48,39], PKZBP86[48,40], PKZBPW91[48,41], PKZBB95[48,42], PKZBPBE[48,43], PKZBTPSS[48,44], PKZBRevTPSS[48,45], PKZBKCIS[48,46], PKZBBRC[48,47],

PKZBPKZB[48], PKZBVP86[48,49], PKZBV5LYP[48,50], wPBEhVWN[56,37], wPBEhVWN5[56,37], wPBEhLYP[56,38], wPBEhPL[56,39], wPBEhP86[56,40], wPBEhPW91[56,41], wPBEhB95[56,42], wPBEhPBE[56,43], wPBEhTPSS[56,44], wPBEhRevTPSS[56,45], wPBEhKCIS[56,46], wPBEhBRC[56,47], wPBEhPKZB[56,48], wPBEhVP86[56,49], wPBEhV5LYP[56,50], PBEhVWN[57,37], PBEhVWN5[57,37], PBEhLYP[57,38], PBEhPL[57,39], PBEhP86[57,40], PBEhPW91[57,41], PBEhB95[57,42], PBEhPBE[57,43] PBEhTPSS[57,44], PBEhRevTPSS[57,45], PBEhKCIS[57,46], PBEhBRC[57,47], PBEhPKZB[57,48], PBEhVP86[57,49], PBEhV5LYP[57,50].

In addition, 14 pure standalone functionals were investigated: VSXC[58], HCTH[59], HCTH93[59], HCTH147[59], HCTH407[59], tHCTH[60], B97D[61], B97D3[62], M06L[63], SOGGA11[64], M11L[65], MN12L[66], N12[67], MN15L[68].

Finally 46 hybrid functionals were used: B3LYP[69,38], B3P86[69,40], B3PW91[70,41], O3LYP[70], APFD[71], APF[71], wB97XD[72], LC-wHPBE[73], LC-wPBE[74], CAM-B3LYP[75], wB97[76], wB97X[76], MN15[77], M11[78], SOGGA11X[79], N12SX[80], MN12SX[80], PW6B95[81], PW6B95D3[81], M08HX[82], M06[83], M06HF[84], M062X[85], M05[86], M052X[87], PBE1PBE[88], HSEH1PBE[89], OHSE2PBE[89], OHSE1PBE[89], PBEh1PBE[89], B1B95[90,42], B1LYP[90,38], mPW1PW91[50,41], mPW1LYP[52,38], mPW1PBE[52,43], mPW3PBE[91], B98[92], B971[93], B972[94], TPSSh[95], tHCTHhyb[96], BMK[97], HISSbPBE[98], X3LYP[99], BHandH[100], BHandHLYP[101].

For dispersion corrections, I used both D2[102] and D3[103] when specified, whereas some functionals (B97-D, APFD, wB97XD etc.) have a built-in

dispersion term. Pople's 6-311++G basis set was chosen as it represents a good compromise between accuracy and CPU time demand. In all cases, counterpoise corrections were not applied because they generate errors quite similar to those without cp-corrections in systems hold together by hydrogen bonds[104]. All the DFT geometry optimization, unless specifically mentioned, were carried out using *Gaussian09*[105].

It was quite challenging to find the suitable functional that accurately reproduced the structural parameters that most influence the multiple dihydrogen bond interaction, i.e. H---H bond length, NH---H and BH---H angles. Despite the wide number of functional tested, none of them produced an excellent agreement between theoretical and experimental data for all three parameters mentioned above (Table 1,2,3).

Table 1. Comparison between calculated values (related to pure functionals from combinations) of the dihydrogen bond geometry (Å and °) with data of the crystal structures for selected complex (**2**) of Figure 4. Where Δ (E-C) is the difference between experimental and calculated parameters.

	Pure combination functionals					
Type	**(Å)**	**(°)**	**(°)**	**Δ (E-C)**	**Δ (E-C)**	**Δ (E-C)**
	H---H	**N-H---H**	**B-H---H**	**H---H**	**N-H---H**	**B-H---H**
Exp X-ray	**2.095**	**145.951**	**137.668**	-	-	-
SVWN	1.616	157.919	138.624	0.479	-11.968	-2.956
SVWN5	1.627	158.074	138.773	0.468	-12.123	-3.105
SLYP	1.563	155.538	136.150	0.532	-9.587	-0.482

SPL	1.627	158.040	138.747	0.468	-12.089	-3.079
SP86	1.519	151.771	132.461	0.576	-5.820	3.207
SPW91	1.526	151.848	132.569	0.569	-5.897	3.099
SB95	1.578	143.413	128.590	0.517	2.538	7.078
SPBE	1.523	151.454	132.212	0.572	-5.503	3.456
STPSS	1.533	151.775	132.470	0.562	-5.824	3.198
SRevTPSS	1.538	152.179	132.857	0.557	-6.228	2.811
SKCIS	1.543	153.180	133.448	0.552	-7.229	2.220
SBRC	1.543	155.267	136.148	0.552	-9.316	-0.480
SPKZB	1.542	151.820	132.733	0.553	-5.869	2.935
SVP86	1.519	151.799	132.476	0.576	-5.848	3.192
SV5LYP	1.563	155.538	136.150	0.532	-9.587	-0.482
XAVWN	1.574	158.182	138.738	0.521	-12.231	-3.070
XAVWN5	1.585	158.329	138.873	0.511	-12.378	-3.205
XALYP	1.528	155.576	136.091	0.567	-9.625	-0.423
XAPL	1.585	158.295	138.844	0.510	-12.344	-3.176
XAP86	1.491	151.429	132.023	0.604	-5.478	3.645
XAPW91	1.497	151.602	132.216	0.598	-5.651	3.452
XAB95	1.544	143.536	128.648	0.551	2.415	7.020
XAPBE	1.492	151.369	131.998	0.603	-5.418	3.670
XATPSS	1.502	151.641	132.206	0.593	-5.690	3.462
XARevTPSS	1.508	151.916	132.479	0.587	-5.965	3.189
XAKCIS	1.509	153.279	133.397	0.586	-7.328	2.271
XABRC	1.534	138.742	123.682	0.561	7.209	11.986
XAPKZB	1.511	151.778	132.533	0.584	-5.827	3.135
XAVP86	1.490	151.496	132.091	0.605	-5.545	3.577

XAV5LYP	1.528	155.576	136.091	0.567	-9.625	-0.423
BVWN	2.353	155.917	140.128	-0.258	-9.966	-4.460
BVWN5	2.411	155.577	139.770	-0.316	-9.626	-4.102
BLYP	1.993	160.468	142.068	0.102	-14.517	-6.400
BPL	2.410	155.583	139.788	-0.315	-9.632	-4.120
BP86	1.870	159.980	141.455	0.225	-14.029	-5.787
BPW91	1.971	158.710	141.187	0.125	-12.759	-5.519
BB95	1.924	156.621	139.746	0.171	-10.670	-4.078
BPBE	1.976	158.147	141.139	0.119	-12.196	-5.471
BTPSS	2.013	157.058	140.873	0.082	-11.107	-5.205
BRevTPSS	2.001	158.372	140.977	0.094	-12.421	-5.309
BKCIS	2.055	157.522	140.960	0.040	-11.571	-5.292
BBRC	2.133	157.099	141.068	-0.038	-11.148	-5.400
BPKZB	2.032	156.650	140.759	0.063	-10.699	-5.091
BVP86	1.867	160.208	141.618	0.228	-14.257	-5.950
BV5LYP	1.994	160.455	142.064	0.101	-14.504	-6.396
PW91VWN	2.154	157.343	140.698	-0.059	-11.392	-5.030
PW91VWN5	2.190	157.038	140.469	-0.095	-11.087	-4.801
PW91LYP	1.914	160.085	141.842	0.182	-14.134	-6.174
PW91PL	2.188	157.066	140.501	-0.093	-11.115	-4.833
PW91P86	1.808	159.357	141.196	0.287	-13.406	-5.528
PW91PW91	1.875	158.860	140.837	0.220	-12.909	-5.169
PW91B95	1.864	155.787	139.472	0.231	-9.836	-3.804
PW91PBE	1.876	158.736	140.733	0.219	-12.785	-5.065
PW91TPSS	1.901	158.609	140.602	0.194	-12.658	-4.934
PW91RevTPSS	1.903	158.657	140.640	0.192	-12.706	-4.972

PW91KCIS	1.933	158.984	140.977	0.163	-13.033	-5.309
PW91BRC	1.990	158.583	141.289	0.105	-12.632	-5.621
PW91PKZB	1.914	158.509	140.553	0.181	-12.558	-4.885
PW91VP86	1.808	159.379	141.206	0.287	-13.428	-5.538
PW91V5LYP	1.914	160.085	141.842	0.182	-14.134	-6.174
mPWVWN	2.250	156.581	140.371	-0.155	-10.630	-4.703
mPWVWN5	2.292	156.388	140.140	-0.197	-10.437	-4.472
mPWLYP	1.952	160.448	142.053	0.143	-14.497	-6.385
mPWPL	2.291	156.378	140.148	-0.196	-10.427	-4.480
mPWP86	1.839	159.761	141.385	0.256	-13.810	-5.717
mPWPW91	1.916	159.226	141.163	0.179	-13.275	-5.495
mPWB95	1.893	156.278	139.601	0.202	-10.327	-3.933
mPWPBE	1.918	159.084	141.066	0.177	-13.133	-5.398
mPWTPSS	1.945	158.593	140.943	0.150	-12.642	-5.275
mPWrevVTPSS	1.946	158.989	140.944	0.149	-13.038	-5.276
mPWKCIS	1.985	159.030	141.139	0.110	-13.079	-5.471
mPWBRC	2.061	158.263	141.212	0.034	-12.312	-5.544
mPWPKZB	1.959	158.841	140.918	0.136	-12.890	-5.250
mPWVP86	1.839	159.769	141.412	0.256	-13.818	-5.744
mPWV5LYP	1.952	160.448	142.053	0.143	-14.497	-6.385
G96VWN	3.182	152.058	136.921	-1.087	-6.107	-1.253
G96VWN5	3.255	152.122	136.739	-1.160	-6.171	-1.071
G96LYP	2.059	155.603	142.369	0.036	-9.652	-6.701
G96PL	3.256	152.111	136.738	-1.161	-6.160	-1.070
G96P86	1.883	161.057	142.192	0.212	-15.106	-6.524
G96PW91	2.229	153.076	140.857	-0.134	-7.125	-5.189

G96B95	1.922	157.419	140.588	0.174	-11.468	-4.920
G96PBE	2.311	152.754	140.351	-0.216	-6.803	-4.683
G96TPSS	2.425	152.451	139.842	-0.330	-6.500	-4.174
G96RevTPSS	2.233	152.869	140.745	-0.138	-6.918	-5.077
G96KCIS	2.322	153.435	140.710	-0.227	-7.484	-5.042
G96BRC	2.532	154.025	140.105	-0.437	-8.074	-4.437
G96PKZB	2.805	151.239	137.824	-0.710	-5.288	-2.156
G96VP86	1.884	161.028	142.190	0.211	-15.077	-6.522
G96V5LYP	2.059	155.603	142.369	0.036	-9.652	-6.701
PBEVWN	2.147	157.986	140.834	-0.052	-12.035	-5.166
PBEVWN5	2.177	157.804	140.709	-0.082	-11.853	-5.041
PBELYP	1.927	160.128	141.786	0.168	-14.177	-6.118
PBEPL	2.180	157.690	140.624	-0.085	-11.739	-4.956
PBEP86	1.824	159.311	141.121	0.271	-13.360	-5.453
PBEPW91	1.889	158.860	140.780	0.206	-12.909	-5.112
PBEB95	1.880	155.841	139.389	0.215	-9.890	-3.721
PBEPBE	1.890	158.736	140.674	0.205	-12.785	-5.006
PBETPSS	1.916	158.650	140.525	0.179	-12.699	-4.857
PBERevTPSS	1.918	158.702	140.565	0.177	-12.751	-4.897
PBEKCIS	1.947	159.015	140.863	0.148	-13.064	-5.195
PBEBRC	1.998	158.752	141.287	0.098	-12.801	-5.619
PBEPKZB	1.928	158.575	140.496	0.167	-12.624	-4.828
PBEVP86	1.824	159.335	141.130	0.271	-13.384	-5.462
PBEV5LYP	1.927	160.128	141.786	0.168	-14.177	-6.118
OVWN	2.837	155.450	137.121	-0.742	-9.499	-1.453
OVWN5	2.867	155.526	137.102	-0.772	-9.575	-1.434

OLYP	2.624	155.376	137.722	-0.529	-9.425	-2.054
OPL	2.867	155.513	137.102	-0.772	-9.562	-1.434
OP86	2.542	154.458	137.351	-0.447	-8.507	-1.683
OPW91	2.747	154.053	136.539	-0.652	-8.102	-0.871
OB95	2.776	152.842	136.477	-0.681	-6.891	-0.809
OPBE	2.756	154.036	136.264	-0.661	-8.085	-0.596
OTPSS	2.770	154.227	136.298	-0.675	-8.276	-0.630
ORevTPSS	2.747	154.228	136.404	-0.652	-8.277	-0.736
OKCIS	2.763	154.920	136.666	-0.668	-8.969	-0.998
OBRC	2.770	155.132	137.079	-0.675	-9.181	-1.411
OPKZB	2.770	154.200	136.340	-0.675	-8.249	-0.672
OVP86	2.543	154.463	137.350	-0.448	-8.512	-1.682
OV5LYP	2.624	155.376	137.722	-0.529	-9.425	-2.054
TPSSVWN	2.261	155.073	139.534	-0.166	-9.122	-3.866
TPSSVWN5	2.302	154.914	139.302	-0.207	-8.963	-3.634
TPSSLYP	1.922	159.657	141.915	0.173	-13.706	-6.247
TPSSPL	2.301	154.906	139.307	-0.206	-8.955	-3.639
TPSSP86	1.811	159.209	141.412	0.284	-13.258	-5.744
TPSSPW91	1.894	158.558	141.118	0.201	-12.607	-5.450
TPSSB95	1.870	155.309	139.263	0.225	-9.358	-3.595
TPSSPBE	1.899	158.364	140.977	0.196	-12.413	-5.309
TPSSTPSS	1.932	158.023	140.732	0.163	-12.072	-5.064
TPSSRevTPSS	1.929	158.182	140.760	0.166	-12.231	-5.092
TPSSKCIS	1.969	158.145	141.026	0.126	-12.194	-5.358
TPSSBRC	2.059	156.563	140.632	0.036	-10.612	-4.964
TPSSPKZB	1.946	157.931	140.776	0.149	-11.980	-5.108

TPSSVP86	1.811	159.166	141.385	0.284	-13.215	-5.717
TPSSV5LYP	1.922	159.657	141.915	0.173	-13.706	-6.247
RevTPSSVWN	2.178	155.154	139.720	-0.083	-9.203	-4.052
RevTPSSVWN5	2.216	154.867	139.504	-0.121	-8.916	-3.836
RevTPSSLYP	1.892	159.150	141.229	0.203	-13.199	-5.561
RevTPSSPL	2.215	154.858	139.505	-0.120	-8.907	-3.837
RevTPSSP86	1.799	158.106	140.274	0.296	-12.155	-4.606
RevTPSSPW91	1.860	158.045	140.244	0.235	-12.094	-4.576
RevTPSSB95	1.841	153.133	138.001	0.254	-7.182	-2.333
RevTPSSPBE	1.860	157.961	140.175	0.235	-12.010	-4.507
RevTPSSTPSS	1.883	157.848	140.079	0.212	-11.897	-4.411
RevTPSSRevTPSS	1.885	157.869	140.097	0.210	-11.918	-4.429
RevTPSSKCIS	1.917	158.101	140.363	0.179	-12.150	-4.695
RevTPSSBRC	1.970	157.788	140.866	0.125	-11.837	-5.198
RevTPSSPKZB	1.895	157.783	140.062	0.200	-11.832	-4.394
RevTPSSVP86	1.799	158.152	140.308	0.296	-12.201	-4.640
RevTPSSV5LYP	1.892	159.150	141.229	0.203	-13.199	-5.561
BRxVWN	2.214	156.971	140.386	-0.119	-11.020	-4.718
BRxVWN5	2.249	156.715	140.200	-0.154	-10.764	-4.532
BRxLYP	1.977	160.126	141.576	0.118	-14.175	-5.908
BRxPL	2.248	156.673	140.174	-0.153	-10.722	-4.506
BRxP86	1.885	158.889	140.574	0.210	-12.938	-4.906
BRxPW91	1.941	158.690	140.421	0.154	-12.739	-4.753
BRxB95	1.920	156.191	139.200	0.175	-10.240	-3.532
BRxPBE	1.942	158.601	140.339	0.154	-12.650	-4.671
BRxTPSS	1.961	158.867	140.446	0.134	-12.916	-4.778

BRxRevTPSS	1.962	158.916	140.495	0.133	-12.965	-4.827
BRxKCIS	1.995	159.154	140.653	0.100	-13.203	-4.985
BRxBRC	2.049	158.346	140.906	0.046	-12.395	-5.238
BRxPKZB	1.972	158.780	140.396	0.123	-12.829	-4.728
BRxVP86	1.886	158.898	140.565	0.210	-12.947	-4.897
BRxV5LYP	1.977	160.127	141.576	0.118	-14.176	-5.908
PKZBVWN	2.472	154.037	136.648	-0.377	-8.086	-0.980
PKZBVWN5	2.500	154.137	136.624	-0.405	-8.186	-0.956
PKZBLYP	2.239	155.309	137.331	-0.144	-9.358	-1.663
PKZBPL	2.501	154.069	136.593	-0.406	-8.118	-0.925
PKZBP86	2.125	154.503	136.662	-0.029	-8.552	-0.994
PKZBPW91	2.232	154.067	136.381	-0.137	-8.116	-0.713
PKZBB95	2.187	151.717	134.357	-0.092	-5.766	1.311
PKZBPBE	2.240	153.887	136.248	-0.145	-7.936	-0.580
PKZBTPSS	2.260	153.904	136.236	-0.165	-7.953	-0.568
PKZBRevTPSS	2.251	154.052	136.313	-0.156	-8.101	-0.645
PKZBKCIS	2.295	154.272	136.460	-0.200	-8.321	-0.792
PKZBBRC	2.353	153.325	136.390	-0.258	-7.374	-0.722
PKZBPKZB	2.269	153.854	136.236	-0.174	-7.903	-0.568
PKZBVP86	2.125	154.446	136.678	-0.029	-8.495	-1.010
PKZBV5LYP	2.239	155.309	137.331	-0.144	-9.358	-1.663
wPBEhVWN	2.137	157.976	141.024	-0.042	-12.025	-5.356
wPBEhVWN5	2.173	157.696	140.790	-0.078	-11.745	-5.122
wPBEhLYP	1.900	160.572	142.179	0.195	-14.621	-6.511
wPBEhPL	2.172	157.699	140.795	-0.077	-11.748	-5.127
wPBEhP86	1.802	159.612	141.371	0.293	-13.661	-5.703

wPBEhPW91	1.861	159.286	141.191	0.234	-13.335	-5.523
wPBEhB95	1.856	155.944	139.681	0.239	-9.993	-4.013
wPBEhPBE	1.862	159.191	141.100	0.233	-13.240	-5.432
wPBEhTPSS	1.886	159.108	140.973	0.209	-13.157	-5.305
wPBEhRevTPSS	1.896	160.001	138.459	0.199	-14.050	-2.791
wPBEhKCIS	1.920	159.339	141.194	0.175	-13.388	-5.526
wPBEhBRC	1.979	158.831	141.511	0.116	-12.880	-5.843
wPBEhPKZB	1.897	159.033	140.961	0.198	-13.082	-5.293
wPBEhVP86	1.804	159.553	141.315	0.291	-13.602	-5.647
wPBEhV5LYP	1.900	160.572	142.180	0.195	-14.621	-6.512
PBEhVWN	2.137	157.976	141.024	-0.042	-12.025	-5.356
PBEhVWN5	2.173	157.696	140.790	-0.078	-11.745	-5.122
PBEhLYP	1.900	150.572	142.179	0.195	-4.621	-6.511
PBEhPL	2.172	157.699	140.795	-0.077	-11.748	-5.127
PBEhP86	1.802	159.612	141.371	0.293	-13.661	-5.703
PBEhPW91	1.861	159.286	141.191	0.234	-13.335	-5.523
PBEhB95	1.856	155.944	139.681	0.239	-9.993	-4.013
PBEhPBE	1.862	159.191	141.100	0.233	-13.240	-5.432
PBEhTPSS	1.886	159.108	140.973	0.209	-13.157	-5.305
PBEhRevTPSS	1.889	159.139	140.980	0.206	-13.188	-5.312
PBEhKCIS	1.920	159.339	141.194	0.175	-13.388	-5.526
PBEhBRC	1.979	158.831	141.511	0.116	-12.880	-5.843
PBEhPKZB	1.897	159.033	140.961	0.198	-13.082	-5.293
PBEhVP86	1.804	159.553	141.315	0.291	-13.602	-5.647
PBEhV5LYP	1.900	160.572	142.179	0.195	-14.621	-6.511

Table 2. Comparison between calculated values (related to standalone pure functionals) of the dihydrogen bond geometry (Å and °) with data of the crystal structures for selected complex (**2**) of Figure 4. Where Δ (E-C) is the difference between experimental and calculated parameters.

Standalone pure functionals						
Type	**(Å)**	**(°)**	**(°)**	**Δ (E-C)**	**Δ (E-C)**	**Δ (E-C)**
	H---H	**N-H---B**	**B-H---N**	**H---H**	**N-H---H**	**B-H---H**
Exp X-ray	**2.095**	**145.951**	**136.668**	-	-	-
VSXC	3.146	100.824	93.932	-1.051	45.127	41.736
HCTH	2.382	154.592	140.524	-0.287	-8.641	-4.856
HCTH93	2.632	155.523	139.443	-0.537	-9.572	-3.775
HCTH147	2.261	154.552	140.560	-0.166	-8.601	-4.892
HCTH407	2.382	154.592	140.524	-0.287	-8.641	-4.856
tHCTH	2.174	154.783	140.387	-0.079	-8.832	-4.719
B97D	1.814	151.284	140.046	0.281	-5.333	-4.378
B97D3	1.801	153.249	141.653	0.294	-7.298	-5.985
M06L	1.798	157.084	139.645	0.297	-11.133	-3.977
SOGGA11	2.700	146.595	130.416	-0.605	-0.644	5.252
M11L	2.123	134.209	135.431	-0.026	11.742	0.237
MN12L	1.962	140.659	135.303	0.133	5.292	0.365
N12	1.881	154.098	136.818	0.214	-8.147	-1.150
MN15L	2.043	145.482	137.320	0.052	0.469	-1.652

Table 3. Comparison between calculated values (related to hybrid functionals) of the dihydrogen bond geometry (Å and °) with data of the crystal structures for selected complex (**2**) of Figure 4. Where Δ (E-C) is the difference between experimental and calculated parameters.

	Hybrid functional					
Type	**(Å)**	**(°)**	**(°)**	**Δ (E-C)**	**Δ (E-C)**	**Δ (E-C)**
	H---H	**N-H---B**	**B-H---N**	**H---H**	**N-H---H**	**B-H---H**
Exp X-ray	**2.095**	**144.951**	**136.668**	-	-	-
B3LYP	2.285	144.939	129.777	-0.190	1.012	5.891
B3P86	1.853	159.679	140.710	0.242	-13.728	-5.042
B3PW91	1.968	153.052	139.029	0.127	-7.101	-3.361
O3LYP	2.567	154.491	139.677	-0.472	-8.540	-4.009
APFD	1.789	159.526	140.562	0.306	-13.575	-4.894
APF	1.916	158.783	140.026	0.179	-12.832	-4.358
wB97XD	1.798	158.053	140.148	0.297	-12.102	-4.480
LC-wHPBE	1.996	148.525	138.388	0.099	-2.574	-2.720
LC-wPBE	1.998	148.703	138.466	0.097	-2.752	-2.798
CAM-B3LYP	1.903	159.692	140.324	0.192	-13.741	-4.656
wB97	1.860	149.142	139.227	0.235	-3.191	-3.559
wB97X	1.883	157.235	138.758	0.212	-11.284	-3.090
MN15	1.945	143.254	136.643	0.150	2.697	-0.975
M11	1.880	142.459	136.508	0.215	3.492	-0.840
SOGGA11X	1.838	160.035	140.446	0.257	-14.084	-4.778
N12SX	1.868	159.237	140.101	0.227	-13.286	-4.433
MN12SX	1.979	143.270	128.729	0.116	2.681	6.939
PW6B95	2.090	143.143	128.765	0.005	2.808	6.903

PW6B95D3	1.960	142.771	128.600	0.135	3.180	7.068
M08HX	1.884	141.419	127.281	0.211	4.532	8.387
M06	1.876	145.611	129.392	0.219	0.340	6.276
M06HF	1.784	146.280	128.203	0.311	-0.329	7.465
M062X	1.888	143.353	128.571	0.207	2.598	7.097
M05	2.193	145.464	129.694	-0.098	0.487	5.974
M052X	2.035	143.558	128.407	0.060	2.393	7.261
PBE1PBE	2.120	144.615	129.334	-0.024	1.336	6.334
HSEH1PBE	2.060	144.730	129.468	0.035	1.221	6.200
OHSE2PBE	2.065	144.806	129.522	0.030	1.145	6.146
OHSE1PBE	2.067	144.823	129.508	0.028	1.128	6.160
PBEh1PBE	2.071	144.705	129.508	0.025	1.246	6.160
B1B95	2.104	142.979	128.612	-0.009	2.972	7.056
B1LYP	2.293	145.102	129.865	-0.198	0.849	5.803
mPW1PW91	2.200	144.291	129.238	-0.105	1.660	6.430
mPW1LYP	2.226	145.337	129.979	-0.131	0.614	5.689
mPW1PBE	2.214	144.099	129.107	-0.120	1.852	6.561
mPW3PBE	2.199	144.296	129.289	-0.104	1.655	6.379
B98	2.258	144.675	129.596	-0.163	1.276	6.072
B971	2.188	144.984	129.821	-0.093	0.967	5.847
B972	2.582	142.706	128.059	-0.487	3.245	7.609
TPSSh	2.461	141.228	127.669	-0.366	4.723	7.999
tHCTHhyB	2.181	144.556	129.692	-0.086	1.395	5.976
BMK	1.952	146.185	130.733	0.143	-0.234	4.935
HISSbPBE	2.068	144.836	129.284	0.027	1.115	6.384

X3LYP	2.218	145.226	129.960	-0.123	0.725	5.708
BHandH	1.788	144.347	128.517	0.307	1.604	7.151
BHandHLYP	2.193	145.610	129.904	-0.098	0.341	5.764

Speaking of "accurate" geometries, by considering the well-known problem of H localization in X-ray structural determinations, and also the uncertainties of our experimental model, a deviation from the experimental data that do not exceed 0.02 Å for bond lengths and 1-2° for angles is considered a good approximation[105]. As it possible to see from Table 1,2 and 3 this condition never occurred simultaneously for all three parameters. Therefore, a careful inspection was necessary to understand which functional proposed the best compromise of accuracy between the angles and the bond intermolecular distance (with a slight preference for the latter). This analysis is essential to obtain an adequate interaction geometry, keeping in mind that even small variations in the geometric parameters cause large changing in the calculation of electrostatic forces. Analyzing Table 1, it is possible to notice that only 2 out of 210 pure functionals deriving from the combinations provide optimal H---H lengths: PKZBP86 and PKZBVP86 (green labelled). As regard the standalone pure functionals (Table 2) only M11L functional, from the Truhlar group, presents a good matching between experimental and calculated intermolecular bond length (green labelled). Undoubtedly, the set of hybrid functionals (Table 3) is the one that on average provides the best

agreement with the experimental data about H---H distance, specifically the functionals employing PBE correlation (green labelled). NH---H and BH---H angles are more difficult to rationalize and evaluate. Almost all pure functionals from combinations considerably overestimate the experimental NH---H value, with the exception of SB95 and XAB95 (yellow labelled). Approximately the same trend is also maintained for pure standalone functionals, in fact only SOGGA11 and MN15L (yellow labelled) exhibit accurate values. The situation improves markedly by focusing on hybrid functionals, as a matter of fact, about half of them (yellow labelled) well describe the values from X-ray analysis. For BH---H angle all three functionals sets have a discrete "flexibility" (grey labelled), examining these trends it is possible to argue that the functionals tested roughly describe the BH---H angle better than the NH---H one. We believe that this behavior is due to the NH---H angle comprises an endocyclic atom (nitrogen) which is most affected by the wide conformational variability of the ether bridges to which it is linked, this phenomenon minimally disturbs the boron of the BH---H angle, as it is an exocyclic atom. (Figure 8)

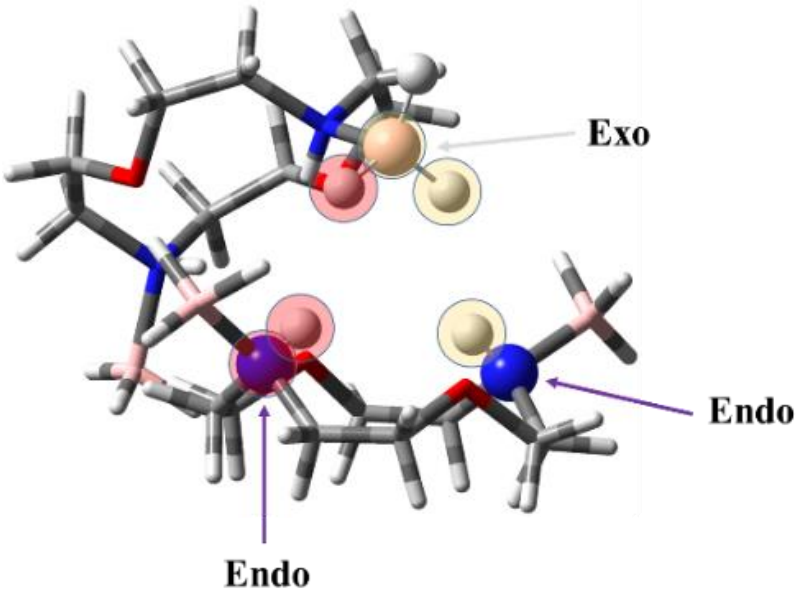

Figure 8. Perspective view of the interacting optimized complex (PBE1PBE/6-311++G), "endo" is referred to the endocyclic acceptors nitrogens while "exo" is related to the boron exocyclic donor. The atoms circled in green constitute the BH---H angle, while the ones circled in red are referred to the NH---H angle.

[36] a) P. Hohenberg, W. Kohn, *Phys. Rev.,* **1964**, *136*, B864-B71. b) W. Kohn, L. J. Sham, *Phys. Rev.,* **1965***, 140*, A1133-A38. c) J. C. Slater, The Self-Consistent Field for Molecular and Solids, Quantum Theory of Molecular and Solids, *Vol. 4* (McGraw-Hill, New York, **1974**).

[37] S. H. Vosko, L. Wilk, M. Nusair,, *Can. J. Phys.,* **1980**, *58*, 1200-11.

[38] a) C. Lee, W. Yang, R. G. Parr, *Phys. Rev. B,* **1988**, *37*, 785-89. b) B. Miehlich, A. Savin, H. Stoll, H. Preuss, *Chem. Phys. Lett.,* **1989**, *157*, 200-06.

[39] J. P. Perdew, A. Zunger, *Phys. Rev. B,* **1981**, *23*, 5048-79.

[40] J. P. Perdew, *Phys. Rev. B,* **1986**, *33*, 8822-24.

[41] a) J. P. Perdew, in *Electronic Structure of Solids '91*, Ed. P. Ziesche and H. Eschrig (Akademie Verlag, Berlin, **1991**) *11*. b) J. P. Perdew, J. A. Chevary, S. H. Vosko, K. A. Jackson, M. R. Pederson, D. J. Singh, C. Fiolhais*, Phys. Rev. B*, **1992**,*46*, 6671-87. c) J. P. Perdew, J. A. Chevary, S. H. Vosko, K. A. Jackson, M. R. Pederson, D. J. Singh C. Fiolhais, *Phys. Rev. B*, **1993**, *48*, 4978. d) J. P. Perdew, K. Burke, Y. Wang*, Phys. Rev. B,***1996**, *54*,16533-39. e) K. Burke, J. P. Perdew, Y. Wang, in Electronic Density Functional Theory: Recent Progress and New Directions, Ed. J. F. Dobson, G. Vignale, and M. P. Das (Plenum, **1998**).

[42] A. D. Becke, J. Chem. Phys., **1996**, *104*, 1040-46.

[43] a) J. P. Perdew, K. Burke, M. Ernzerhof, *Phys. Rev. Lett.,* **1996**, *77*, 3865-68. b) J. P. Perdew, K. Burke, M. Ernzerhof, *Phys. Rev. Lett*., **1997**, *78*,1396.

[44] J. M. Tao, J. P. Perdew, V. N. Staroverov, G. E. Scuseria, *Phys. Rev. Lett.,* **2003**, *91*, 146401.

[45] a) J. P. Perdew, A. Ruzsinszky, G. I. Csonka, L. A. Constantin, J. Sun, *Phys. Rev. Lett.*, **2009**, *103*, 026403. b) J.P. Perdew, A. Ruzsinszky, G. I. Csonka, L. A. Constantin, J. Sun, *Phys. Rev. Lett.*, **2011**, *106* ,179902(E).

[46] a) J. Rey, A. Savin, *Int. J. Quantum Chem*., **1998**, *69*, 581-90. b) J. B. Krieger, J. Q. Chen, G. J. Iafrate, A. Savin, in Electron Correlations and Materials Properties, Ed. A. Gonis, N. Kioussis, and M. Ciftan (Kluwer Academic, New York, **1999**) 463-77. c) J. B. Krieger, J. Q. Chen, and S. Kurth, in *Density Functional Theory and its Application to Materials*, Ed. V. VanDoren, C. VanAlsenoy, and P. Geerlings, *A.I.P. Conference Proceedings*, Vol. 577 (A.I.P., New York, **2001**) 48-69. d) J. Toulouse, A. Savin, C. Adamo, *J. Chem. Phys.,* **2002**, *117*, 10465-73.

[47] A. D. Becke, M. R. Roussel, *Phys. Rev. A*,**1989**, *39*, 3761-67.

[48] J. P. Perdew, S. Kurth, A. Zupan, P. Blaha, *Phys. Rev. Lett.,* **1999**, *82*, 2544-47.

[49] a) S. H. Vosko, L. Wilk, M. Nusair,, *Can. J. Phys.,* **1980**, *58*, 1200-11. b) J. P. Perdew, *Phys. Rev. B,* **1986**, *33*, 8822-24.

[50] a) S. H. Vosko, L. Wilk, M. Nusair,, *Can. J. Phys.,* **1980**, *58*, 1200-11. b) C. Lee, W. Yang, R. G. Parr, Phys. Rev. B, 1988, 37, 785-89. c) B. Miehlich, A. Savin, H. Stoll, H. Preuss, Chem. Phys. Lett., 1989, 157, 200-06.

[51] a) A. D. *Becke, Phys. Rev. A*, **1988**, *38*, 3098-100.

[52] a) C. Adamo V. Barone, *J. Chem. Phys.,* **1998**, *108*, 664-75.

[53] a) P. M. W. Gill, *Mol. Phys.,* **1996**, *89*, 433-45. b) C. Adamo, V. Barone, *J. Comp. Chem.,* **1998**, *19*, 418-29.

[54] a) N. C. Handy, A. J. Cohen, *Mol. Phys.,* **2001**, *99*, 403-12. b) W.-M. Hoe, A. Cohen, N. C. Handy, *Chem. Phys. Lett.,* **2001**, *341*, 319-28.

[55] A. D. Becke, M. R. Roussel, *Phys. Rev. A*, **1989**, *39*, 3761-67.

[56] a) J. Heyd, G. Scuseria, M. Ernzerhof, *J. Chem. Phys.,* **2003**, *118*, 8207-15. b) A. F. Izmaylov, G. Scuseria, M. J. Frisch, *J. Chem. Phys.,* **2006**, *125*, 104103. c) T. M. Henderson, A. F. Izmaylov, G. Scalmani, G. E. Scuseria, *J. Chem. Phys.,* **2009**, *131*, 044108.

[57] M. Ernzerhof, J. P. Perdew, *J. Chem. Phys.,* **1998**, *109*.

[58] T. Van Voorhis, G. E. Scuseria, *J. Chem. Phys.*, **1998**, *109*, 400-10.

[59] a) F. A. Hamprecht, A. Cohen, D. J. Tozer, N. C. Handy, *J. Chem. Phys.*, **1998**, *109,* 6264-71. b) A. D. Boese, N. L. Doltsinis, N. C. Handy, M. Sprik, *J. Chem. Phys.*, **2000**, *112*, 1670-78. c) A. D. Boese, N. C. Handy, *J. Chem. Phys.*, **2001**, *114*, 5497-503.

[60] A. D. Boese, N. C. Handy, *J. Chem. Phys.*, **2002**, *116*, 9559-69.

[61] S. Grimme, *J. Comp. Chem.*, **2006**, *27*, 1787-99.

[62] S. Grimme, S. Ehrlich, L. Goerigk, *J. Comp. Chem*., **2011**, *32,* 1456-65.

[62] Y. Zhao, D. G. Truhlar, *J. Chem. Phys.*, **2006**, *125*, 194101: 1-18.

[63] R. Peverati, Y. Zhao, D. G. Truhlar, *J. Phys. Chem. Lett.*, **2011**, *2*, 1991-1997.

[64] R. Peverati, D. G. Truhlar, *J. Phys. Chem. Lett.*, **2012**, *3*, 117-124.

[65] R. Peverati, D. G. Truhlar, *Phys. Chem. Chem. Phys.,* **2012**, *10*, 13171.

[66] R. Peverati, D. G. Truhlar, *J. Chem. Theory and Comput.*, **2012**, *8*, 2310-2319.

[67] H. S. Yu, X. He, D. G. Truhlar, *Journal of Chemical Theory and Computation,* **2016**, *12*, 1280-1293.

[68] A. D. Becke, *J. Chem. Phys.*, **1993**, *98*, 5648-52.

[69] A. J. Cohen,N. C. Handy, *Mol. Phys.*, **2001**, *99,* 607-15.

[70] A. Austin, G. Petersson, M. J. Frisch, F. J. Dobek, G. Scalmani, K. Throssell, *J. Chem. Theory and Comput*.**, 2012**, *8*, 4989.

[71] J.-D. Chai and M. Head-Gordon, *Phys. Chem. Chem. Phys.*, **2008**, *10*, 6615-20.

[72] T. M. Henderson, A. F. Izmaylov, G. Scalmani, G. E. Scuseria, *J. Chem. Phys.*, **2009**, *131*, 044108.

[73] a) O. A. Vydrov, G. E. Scuseria, *J. Chem. Phys.*, **2006**, *125*, 234109. b) O. A. Vydrov, J. Heyd, A. Krukau, G. E. Scuseria, *J. Chem. Phys.*, **2006**, *125*, 074106. c) O. A. Vydrov, G. E. Scuseria, and J. P. Perdew, *J. Chem. Phys.*, **2007**, *126*, 154109.

[74] T. Yanai, D. Tew, N. Handy, *Chem. Phys. Lett.*, **2004**, *393*, 51-57.

[75] J.-D. Chai, M. Head-Gordon, *J. Chem. Phys.*, **2008**, *128*, 084106.

[76] H. S. Yu, X. He, S. L. Li, D. G. Truhlar, *Chem. Sci.,* **2016**, *7*, 5032-5051.

[77] R. Peverati, D. G. Truhlar, *J. Phys. Chem. Lett.*, **2011**, *2*, 2810-2817.

[78] R. Peverati, D. G. Truhlar, *J. Chem. Phys.*, **2011**, *135*, 191102.

[79] R. Peverati, D. G. Truhlar, *Phys. Chem. Chem. Phys.*, **2012**, *14*, 16187.

[80] Y. Zhao, D. G. Truhlar, *J. Phys. Chem. A*, **2005**, *109*, 5656.

[81] Y. Zhao, D. G. Truhlar, *J. Chem. Theory Compute.* **2008**, *4*, 1849.

[82] Y. Zhao, D. G. Truhlar, *Theor. Chem. Acc.*, **2008**, *120*, 215-41.

[83] a) Y. Zhao, D. G. Truhlar, *J. Phys. Chem.*, **2006**, *110*, 5121-29. b) Y. Zhao, D. G. Truhlar, *J. Phys. Chem. A*, **2006**, *110*, 13126-30.

[84] Y. Zhao, D. G. Truhlar, *Theor. Chem. Acc.*, **2008**, *120*, 215-41.

[85] Y. Zhao, N. E. Schultz, D. G. Truhlar, *J. Chem. Phys.*, **2005**, *123*, 161103.

[86] Y. Zhao, N. E. Schultz, D. G. Truhlar, *J. Chem. Theory and Comput.*, **2006**, *2*, 364-82.

[87] a) C. Adamo, V. Barone, *J. Chem. Phys.*, **1999**, *110*, 6158-69. b) M. Ernzerhof, G. E. Scuseria, *The Journal of Chemical Physics*, **1999**, *110*, 5029-36.

[88 b]a) J. Heyd, G. Scuseria, *J. Chem. Phys.*, **2004**, *121*, 1187-92. b) J. Heyd, G. E. Scuseria, *J. Chem. Phys.*, **2004**, *120*, 7274. c) J. Heyd, J. E. Peralta, G. E. Scuseria, R. L. Martin, *J. Chem. Phys.*, **2005**, *123*, 174101: 1-8. d) J. Heyd, G. E. Scuseria, M. Ernzerhof, *J. Chem. Phys.*, **2006**, *124*, 219906. e) T. M. Henderson, A. F. Izmaylov, G. Scalmani, G. E. Scuseria, *J. Chem. Phys.*, **2009**, *131*, 044108. f) A. F. Izmaylov, G. Scuseria, M. J. Frisch, *J. Chem. Phys.*, **2006**, *125*, 104103: 1-8. A. V. Krukau, O. A. Vydrov, A. F. Izmaylov, G. E. Scuseria, *J. Chem. Phys.*, **2006**, *125*, 224106.

[89] A. D. Becke, *J. Chem. Phys.*, **1996**, *104*, 1040-46.

[90] C. Adamo, V. Barone, *J. Chem. Phys.,* **1998**,*108*, 664.

[91] H. L. Schmider, A. D. Becke, *J. Chem. Phys.*, **1998**, *108*, 9624-31.

[92] F. A. Hamprecht, A. Cohen, D. J. Tozer, N. C. Handy, *J. Chem. Phys.*, **1998**, *109*, 6264-71.

[93] P. J. Wilson, T. J. Bradley, D. J. Tozer, *J. Chem. Phys.*, **2001**, *115*, 9233-42.

[94] a) J. M. Tao, J. P. Perdew, V. N. Staroverov, G. E. Scuseria, *Phys. Rev. Lett.*, **2003**, *91*, 146401. b) V. N. Staroverov, G. E. Scuseria, J. Tao, J. P. Perdew, *J. Chem. Phys.*, **2003**, *119*, 12129.

[95] A. D. Boese, N. C. Handy, *J. Chem. Phys.*, **2002**, *116*, 9559-69.

[96] A. D. Boese, J. M. L. Martin, *J. Chem. Phys.*, **2004**, *121*, 3405-16.

[97] T. M. Henderson, A. F. Izmaylov, G. E. Scuseria, A. Savin, *J. Chem. Theory and Comput.*, **2008**, *4*, 1254.

[98] X. Xu, W. A. Goddard III, *Proc. Natl. Acad. Sci. USA*, **2004**, *101*, 2673-77.

[99] M. Waller, A. Robertazzi, J. Platts, D. Hibbs, P. Williams, *J Comput Chem,* **2006**, *27,* 491-504.

[100] Becke, A. D. *J Chem Phys* **1993***, 98, 1372.*

[101] S. Grimme, *J. Comput. Chem.* **2006**, *27*, 1787.

[102] a) S. Grimme, J. Antony, S. Ehrlich, H. Krieg, *J. Chem. Phys.*, **2010**, *132*, 154104. b) S. Grimme, S. Ehrlich, L. Goerigk, *J. Comput. Chem.,* **2011**, *32*, 1456.

[103] A. D. Boese, J. M. L. Martin, W. Klopper, *J. Phys. Chem. A,* **2007**, *111*, 11122.

[104] Frisch, M. J.; Trucks, G. W.; Schlegel, H. B.; Scuseria, G. E.; Robb, M. A.; Cheeseman, J. R.; Scalmani, G.; Barone, V.; Petersson, G. A.; Nakatsuji, H.; Li, X.; Caricato, M.; Marenich, A. V.; Bloino, J.; Janesko, B. G.; Gomperts, R.; Mennucci, B.; Hratchian, H. P.; Ortiz, J. V.; Izmaylov, A. F.; Sonnenberg, J. L.; Williams-Young, D.; Ding, F.; Lipparini,

F.; Egidi, F.; Goings, J.; Peng, B.; Petrone, A.; Henderson, T.; Ranasinghe, D.; Zakrzewski, V. G.; Gao, J.; Rega, N.; Zheng, G.; Liang, W.; Hada, M.; Ehara, M.; Toyota, K.; Fukuda, R.; Hasegawa, J.; Ishida, M.; Nakajima, T.; Honda, Y.; Kitao, O.; Nakai, H.; Vreven, T.; Throssell, K.; Montgomery, J. A., Jr.; Peralta, J. E.; Ogliaro, F.; Bearpark, M. J.; Heyd, J. J.; Brothers, E. N.; Kudin, K. N.; Staroverov, V. N.; Keith, T. A.; Kobayashi, R.; Normand, J.; Raghavachari, K.; Rendell, A. P.; Burant, J. C.; Iyengar, S. S.; Tomasi, J.; Cossi, M.; Millam, J. M.; Klene, M.; Adamo, C.; Cammi, R.; Ochterski, J. W.; Martin, R. L.; Morokuma, K.; Farkas, O.; Foresman, J. B.; Fox, D. J. *Gaussian 16*, Revision A.03; Gaussian, Inc.: Wallingford, CT, 2016.

[105] J. B. Foresman and Æ Frisch, Exploring Chemistry with Electronic Structure Methods, 3rd ed., Gaussian, Inc.: Wallingford, CT, 2015.

THE VECTORIAL MODEL

In my work, I adopted a different approach, based not on electrostatic energy but on electrostatic force. In non-planar molecules such as DNA, RNA, proteins and cryptands hydrogen bonds are surrounded by atoms in a three-dimensional model. In such a situation, the electrostatic force (based on Coulomb's law) with its directionality turns out to be a better descriptor than electrostatic energy[106]. In order to calculate the vectorial sum of the electrostatic forces involved in our molecular system I adopted a schematic representation based on vector algebra, depicted in Figure 9. The optimized complex arranges the frontier atoms (four hydrogens: two partially positive and two partially negative) in such a way as to create an equilateral trapezoid-shaped pattern.

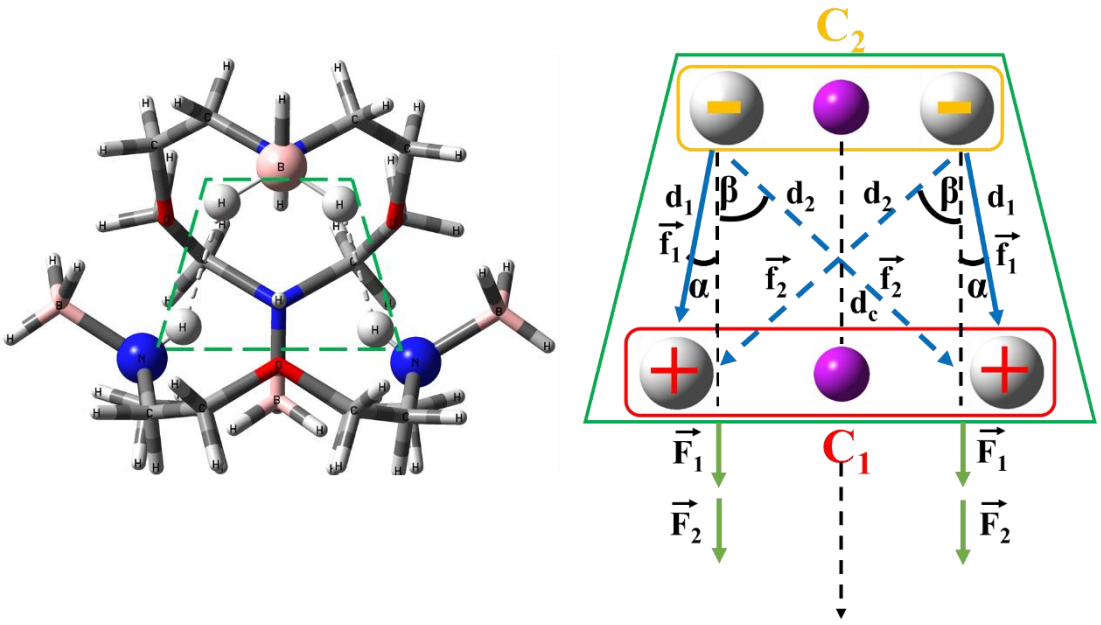

Figure 9. Left: crystal structure of dihydrogen bonded complex. Right: simple 2D model that illustrates how the two partners organize their frontier atoms during the self-assembly. The straight blue arrows indicate the primary electrostatic interactions while the dotted blue ones refer to the secondary electrostatic interactions. (It is worth noting that for symmetry reasons the frontier hydrogens have the same charge value in pairs: $\mathbf{Q}^{-} = \mathbf{Q}^{-}$ and $\mathbf{Q}^{+} = \mathbf{Q}^{+}$)

To compute the net electrostatic force experienced by each fragment a preferential direction of approach between the two molecules was chosen. It is quite intuitive to note that the line joining the centers of the masses, of the charges and of the geometric coordinates i.e. $\mathbf{C}_1$ and $\mathbf{C}_2$ for donor and acceptor hydrogens respectively (purple spherical points) represents the most favourable electrostatically direction of interaction. It is to be noted that this approach was made possible because the frontier hydrogens pairs (circled in gold and red in Figure 9) occupy the corners of an equilateral trapezoid and have the same mass and the same charge respectively. The forces were calculated by employing Coulomb's law considering atoms as

point charges, the latter were determined by NBO charge analysis[107]. Mulliken method[108] was not taken into account because it is less suitable in calculating charges in heterocyclic systems[109] and due to its considerable dependence on the basis set used[110]. In the model represented in Figure 9, $\vec{\mathbf{f}}_1$ and $\vec{\mathbf{f}}_2$ are the forces vectors experienced by the corresponding charged particles due to the charges on the other partner, while $\vec{\mathbf{F}}_1$ and $\vec{\mathbf{F}}_2$ are the projections of the vectors $\vec{\mathbf{f}}_1$ and $\vec{\mathbf{f}}_2$ along the direction of approach. $\mathbf{d}_1$ and $\mathbf{d}_2$ indicate the distances between atoms along which the primary and secondary electrostatic interactions occur respectively. $\mathbf{d}_c$ is the distance between $\mathbf{C}_1$ and $\mathbf{C}_2$, finally $\boldsymbol{\alpha}$ and $\boldsymbol{\beta}$ define the angles subtended by the vectors $\vec{\mathbf{f}}_1$ and $\vec{\mathbf{f}}_2$ along the line of interaction respectively. Therefore, every partner perceives a total electrostatic force $\mathbf{F}_{tot}$ given by the sum of all the individual force vectors (Scheme 1).

$$\vec{f}_1 = \frac{K\,Q_+Q_-}{d_1^{\,2}} \qquad \vec{f}_2 = \frac{K\,Q_+Q_-}{d_2^{\,2}}$$

$$\vec{F}_1 = \vec{f}_1\cos(\alpha) \qquad \vec{F}_2 = \vec{f}_2\cos(\beta)$$

$$F_{tot} = 2\,\vec{F}_1 + 2\,\vec{F}_2$$

Scheme 1. Rapid illustration of the method used for the calculation of $\mathbf{F}_{tot}$, I used the value of the vacuum Coulomb's constant K equal to $8.987*10^9$ Nm^2/C^2.

[106] M. K. Tiwari, K. Vanka, *Chem. Sci.,* **2017**, *8*, 1378.

[107] A. E. Reed, R. B. Weinstock, F. Weinhold, *J. Chem. Phys.,* **1985**, *83*, 735–746.

[108] R. S. Mulliken, *J. Chem. Phys.,* **1955**, *23*, 1833-1840.

[109] G. Bella, A. Santoro, M. Cordaro, F. Nicolò, G. Bruno, *Chin. J. Chem.*, **2019**, *37,* 163-168.

[110] F. Martin, H. Zipse, *J. Comput. Chem.* **2005,** *26* (1), 97-105.

THE RELATIONSHIP BETWEEN THE INTERACTION ENERGIES AND NEWTONIAN FORCES

Finally, based on all previous consideration about the tested functionals for the optimization of aggregated system in Figure 9 (left), I decided to adopt the PBE1PBE hybrid functional (red labelled) to develop the vector model shown in Figure 9 (right). This functional provides an excellent agreement (one of the best of the whole set) for dihydrogen intermolecular length and a good one for NH---H angle (thus satisfying 2 of the 3 structural parameters). I preferred PBE1PBE to MN15L (blue labelled) because, despite the excellent agreement with the experimental values for NH---H and BH---H angle, it fails to reproduce the H---H distance. It is well known that electrostatic forces (calculated by Coulomb's law) have an inversely quadratic dependence on distance and therefore they are more influenced by it, while an error of a few degrees of angle does not produce appreciable changes in the magnitude of the projection of the force vector.

I defined the interaction energy $\mathbf{E_{int}}$, using the following formula:

$$\mathbf{E_{int} = E_c - (E_1 + E_2)}$$

where Ec is the energy of the noncovalently bonded complex, E1 and E2 are the single-point energies of two partners infinitely separated from the

optimized complex (keeping the geometry of the monomers frozen as in the complex).

Primary and secondary electrostatic interactions were analysed as a function of $\mathbf{E_{int}}$ scanning the distance between $\mathbf{C_1}$ and $\mathbf{C_2}$. In this approach $\mathbf{d_c}$ was varied over a certain range from 2.10276 Å (PBE1PBE optimized complex) to 2.60276 Å with 0.01 Å per step (50) keeping the monomers frozen in the same geometry of the fully optimized complex (see Table 4). *De facto* a change of 0.5 Å in $\mathbf{d_c}$ should not lead to any appreciable change in the geometries. Therefore, in each of the 50 steps both $\mathbf{F_{tot}}$ and $\mathbf{E_{int}}$ were calculated using the PBE1PBE/6-311++G level (Table 5,6), the calculated interaction energy and the total electrostatic forces (obtained by NBO charge analysis) were compared by a linear correlation plot (Graph 1). Satisfactorily, I obtained a near linear correlation ($R^2 = 0.91$) between the total electrostatic force on the y axis and the corresponding interaction energy on the x axis. Obviously, as shown in the Graph 1 the net total force is attractive (negative sign), because the charges of frontier hydrogens in one monomer are positive and the charges in the other partner are negative. In conclusion, the very good linear correlation indicates that in the scanned distance range the greater interaction energy, the greater the magnitude of the total electrostatic force. To further corroborate the electrostatic force method here proposed, a CHelpG[108] (Charges from Electrostatic Potentials using a Grid based method) charge analysis was

also performed, reaching a good correlation. Explicit charge values of both methods (NBO and CHelpG) are summarized in Table 6.

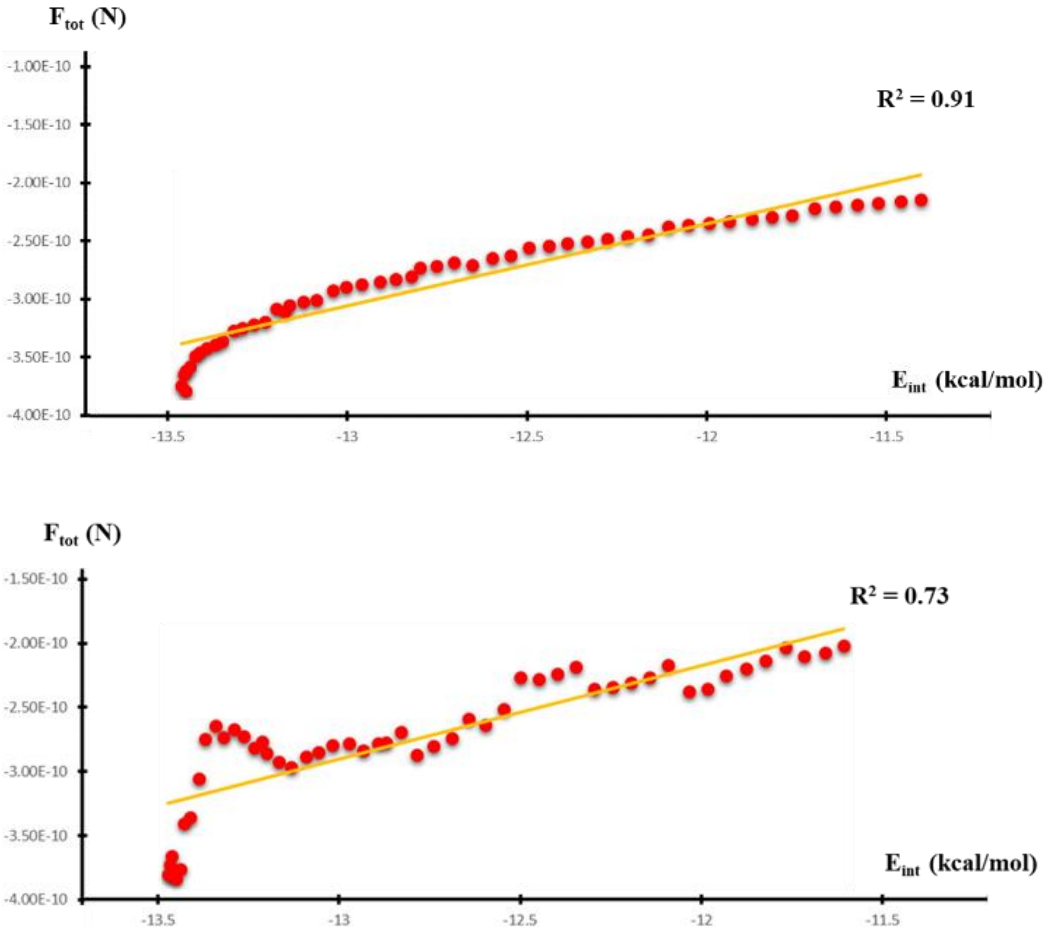

Graph 1. Correlation graphs between **Ftot** and **Eint** for dihydrogen bonded complex in a range of 0.5 Å (top graph is referred to NBO while bottom one to CHelpG).

From the previous graphs it is clear that NBO charge analysis turns out to be a better method to calculate the partial charge on the atoms involved in multiple dihydrogen bond than ChelpG.

Table 4. Changing of geometric parameters as $\mathbf{d_c}$ varies keeping the monomers frozen.

d_c (Å)	d_1 (Å)	d_2 (Å)	α (°)	β (°)	cos (α)	cos (β)
2.10276	2.11958	3.10694	7.22300	47.40600	0.99206	0.67680
2.11276	2.12950	3.11372	7.18900	47.27100	0.99214	0.67853
2.12276	2.13942	3.12051	7.15600	47.13600	0.99221	0.68026
2.13276	2.14934	3.12732	7.12200	47.00200	0.99228	0.68197
2.14276	2.15927	3.13415	7.09000	46.86800	0.99235	0.68368
2.15276	2.16919	3.14099	7.05700	46.73500	0.99242	0.68537
2.16276	2.17912	3.14786	7.02500	46.60200	0.99249	0.68706
2.17276	2.18904	3.15474	6.99300	46.47000	0.99256	0.68873
2.18276	2.19897	3.16163	6.96100	46.33900	0.99263	0.69039
2.19276	2.20889	3.16854	6.92900	46.20800	0.99270	0.69204
2.20276	2.21882	3.17547	6.89800	46.07800	0.99276	0.69368
2.21276	2.22875	3.18242	6.86700	45.94800	0.99283	0.69531
2.22276	2.23868	3.18938	6.83700	45.81900	0.99289	0.69693
2.23276	2.24861	3.19636	6.80600	45.69100	0.99295	0.69853
2.24276	2.25854	3.20335	6.77600	45.56300	0.99302	0.70012
2.25276	2.26847	3.21036	6.74700	45.43500	0.99307	0.70172
2.26276	2.27840	3.21738	6.71700	45.30800	0.99314	0.70330
2.27276	2.28833	3.22442	6.68800	45.18200	0.99320	0.70486
2.28276	2.29826	3.23148	6.65900	45.05600	0.99325	0.70642
2.29276	2.30820	3.23855	6.63000	44.93100	0.99331	0.70796
2.30276	2.31813	3.24564	6.60100	44.80600	0.99337	0.70950
2.31276	2.32806	3.25274	6.57300	44.68200	0.99343	0.71102
2.32276	2.33800	3.25986	6.54500	44.55900	0.99348	0.71253
2.33276	2.34793	3.26699	6.51700	44.43600	0.99354	0.71403
2.34276	2.35787	3.27414	6.49000	44.31300	0.99359	0.71553
2.35276	2.36780	3.28130	6.46200	44.19100	0.99365	0.71702
2.36276	2.37774	3.28848	6.43500	44.07000	0.99370	0.71849
2.37276	2.38768	3.29567	6.40800	43.94900	0.99375	0.71996
2.38276	2.39762	3.20288	6.38200	43.82800	0.99380	0.72142
2.39276	2.40756	3.31010	6.35500	43.70800	0.99386	0.72287
2.40276	2.41749	3.31734	6.32900	43.58900	0.99391	0.72430
2.41276	2.42743	3.32459	6.30300	43.47000	0.99396	0.72573
2.42276	2.43737	3.33185	6.27700	43.35200	0.99400	0.72715
2.43276	2.44731	3.33913	6.25200	43.23400	0.99405	0.72856
2.44276	2.45725	3.34642	6.22600	43.11700	0.99410	0.72996
2.45276	2.46720	3.35373	6.20100	43.00000	0.99415	0.73135
2.46276	2.47714	3.36105	6.17600	42.88400	0.99420	0.73273
2.47276	2.48708	3.36838	6.15100	42.76800	0.99424	0.73411
2.48276	2.49702	3.37573	6.12700	42.65300	0.99429	0.73547
2.49276	2.50697	3.38309	6.10200	42.53800	0.99433	0.73683
2.50276	2.51691	3.39047	6.07800	42.42400	0.99438	0.73817

2.51276	2.52685	3.39786	6.05400	42.31000	0.99442	0.73951
2.52276	2.53680	3.40526	6.03000	42.19700	0.99447	0.74084
2.53276	2.54674	3.41267	6.00700	42.08400	0.99451	0.74216
2.54276	2.55669	3.42010	5.98300	41.97200	0.99455	0.74347
2.55276	2.56663	3.42754	5.96000	41.86000	0.99459	0.74478
2.56276	2.57658	3.43500	5.93700	41.74900	0.99464	0.74607
2.57276	2.58653	3.44247	5.91400	41.63800	0.99468	0.74736
2.58276	2.59647	3.44995	5.89100	41.52700	0.99472	0.74864
2.59276	2.60642	3.45744	5.86900	41.41800	0.99476	0.74990
2.60276	2.61637	3.46494	5.84600	41.30800	0.99480	0.75117

Table 5. $\mathbf{F_{tot}}$ and $\mathbf{E_{int}}$ as $\mathbf{d_c}$ varies keeping the monomers frozen (for the calculation of the total forces the charges were converted into Coulomb by multiplying their value ,both NBO and ChelpG, by the charge of the electron, i.e. $-1{,}602\times10^{-19}$ C).

$\mathbf{d_c}$ (Å)	$\mathbf{F_{tot}}$ (N)		$\mathbf{E_{int}}$ (kcal/mol)
	NBO	CHelpG	
2.10276	-3.7177e-10	-3.8146e-10	-13.4224
2.11276	-3.6749e-10	-3.8195e-10	-13.4350
2.12276	-3.5763e-10	-3.7421e-10	-13.4287
2.13276	-3.5426e-10	-3.6728e-10	-13.4224
2.14276	-3.5094e-10	-3.8497e-10	-13.4099
2.15276	-3.4145e-10	-3.7773e-10	-13.3973
2.16276	-3.3826e-10	-3.4182e-10	-13.3848
2.17276	-3.3512e-10	-3.3684e-10	-13.3659
2.18276	-3.3201e-10	-3.0692e-10	-13.3408
2.19276	-3.2895e-10	-2.7605e-10	-13.3220
2.20276	-3.1999e-10	-2.6565e-10	-13.2906
2.21276	-3.1772e-10	-2.7469e-10	-13.2655
2.22276	-3.1481e-10	-2.6842e-10	-13.2342
2.23276	-3.1194e-10	-2.7391e-10	-13.2028
2.24276	-3.0337e-10	-2.7788e-10	-13.1463
2.25276	-3.0062e-10	-2.8288e-10	-13.1714
2.26276	-2.9790e-10	-2.8672e-10	-13.1338
2.27276	-2.9521e-10	-2.9344e-10	-13.0961
2.28276	-2.9318e-10	-2.9758e-10	-13.0585
2.29276	-2.8507e-10	-2.8979e-10	-13.0145
2.30276	-2.8252e-10	-2.8615e-10	-12.9769
2.31276	-2.8000e-10	-2.8090e-10	-12.9330
2.32276	-2.7751e-10	-2.7900e-10	-12.8828
2.33276	-2.7564e-10	-2.8450e-10	-12.8388
2.34276	-2.7320e-10	-2.7939e-10	-12.7949

2.35276	-2.6558e-10	-2.7825e-10	-12.7698
2.36276	-2.6382e-10	-2.7060e-10	-12.7259
2.37276	-2.6150e-10	-2.8794e-10	-12.6757
2.38276	-2.6376e-10	-2.8136e-10	-12.6255
2.39276	-2.5751e-10	-2.7532e-10	-12.5690
2.40276	-2.5527e-10	-2.5967e-10	-12.5188
2.41276	-2.4809e-10	-2.6495e-10	-12.4686
2.42276	-2.4648e-10	-2.5233e-10	-12.4121
2.43276	-2.4435e-10	-2.2789e-10	-12.3619
2.44276	-2.4277e-10	-2.2893e-10	-12.3055
2.45276	-2.4068e-10	-2.2497e-10	-12.2490
2.46276	-2.3862e-10	-2.1919e-10	-12.1925
2.47276	-2.3710e-10	-2.3683e-10	-12.1360
2.48276	-2.3038e-10	-2.3559e-10	-12.0795
2.49276	-2.2892e-10	-2.3174e-10	-12.0231
2.50276	-2.2697e-10	-2.2779e-10	-11.9666
2.51276	-2.2555e-10	-2.1838e-10	-11.9101
2.52276	-2.2364e-10	-2.3859e-10	-11.8474
2.53276	-2.2225e-10	-2.3637e-10	-11.7909
2.54276	-2.2038e-10	-2.2620e-10	-11.7344
2.55276	-2.1455e-10	-2.2104e-10	-11.6717
2.56276	-2.1275e-10	-2.1498e-10	-11.6152
2.57276	-2.1144e-10	-2.0446e-10	-11.5524
2.58276	-2.1015e-10	-2.1143e-10	-11.4960
2.59276	-2.0840e-10	-2.0840e-10	-11.4332
2.60276	-2.0714e-10	-2.0313e-10	-11.3767

According to Table 6 it is possible to see that as the distance $\mathbf{d_c}$ increases both acidic and hydric hydrogen charge decrease, this is a confirmation of the fact that frontier hydrogens mutate their charge distributions mutually in a range of 0.5 Å from the equilibrium geometry.

Table 6. NBO and CHelpG charges as $\mathbf{d_c}$ varies keeping the monomers frozen (it is worth noting that for symmetry reasons the frontier hydrogens have the same charge value in pairs: $\mathbf{Q^-} = \mathbf{Q^-}$ and $\mathbf{Q^+} = \mathbf{Q^+}$).

d_c (Å)	NBO		CHelpG	
	H^-	H^+	H^-	H^+
2.10276	-0.05700	0.48600	-0.18700	0.15200
2.11276	-0.05700	0.48400	-0.17700	0.16200
2.12276	-0.05600	0.48300	-0.17800	0.15900
2.13276	-0.05600	0.48200	-0.17600	0.15900
2.14276	-0.05600	0.48100	-0.17800	0.16600
2.15276	-0.05500	0.48000	-0.17700	0.16500
2.16276	-0.05500	0.47900	-0.17400	0.15300
2.17276	-0.05500	0.47800	-0.17500	0.15100
2.18276	-0.05500	0.47700	-0.17200	0.14100
2.19276	-0.05500	0.47600	-0.16900	0.13000
2.20276	-0.05400	0.47500	-0.16900	0.12600
2.21276	-0.05400	0.47500	-0.17600	0.12600
2.22276	-0.05400	0.47400	-0.17600	0.12400
2.23276	-0.05400	0.47300	-0.17800	0.12600
2.24276	-0.05300	0.47200	-0.17100	0.13400
2.25276	-0.05300	0.47100	-0.17400	0.13500
2.26276	-0.05300	0.47000	-0.17500	0.13700
2.27276	-0.05300	0.46900	-0.17400	0.14200
2.28276	-0.05300	0.46900	-0.17400	0.14500
2.29276	-0.05200	0.46800	-0.17300	0.14300
2.30276	-0.05200	0.46700	-0.17200	0.14300
2.31276	-0.05200	0.46600	-0.17000	0.14300
2.32276	-0.05200	0.46500	-0.17000	0.14300
2.33276	-0.05200	0.46500	-0.17700	0.14100
2.34276	-0.05200	0.46400	-0.17500	0.14100
2.35276	-0.05100	0.46300	-0.17300	0.14300
2.36276	-0.05100	0.46300	-0.17300	0.14000
2.37276	-0.05100	0.46200	-0.18400	0.14100
2.38276	-0.05100	0.46100	-0.19000	0.13200
2.39276	-0.05100	0.46100	-0.18900	0.13300
2.40276	-0.05100	0.46000	-0.18500	0.12900
2.41276	-0.05000	0.45900	-0.19000	0.12900
2.42276	-0.05000	0.45900	-0.18500	0.12700
2.43276	-0.05000	0.45800	-0.18100	0.11800
2.44276	-0.05000	0.45800	-0.18300	0.11800
2.45276	-0.05000	0.45700	-0.18100	0.11800
2.46276	-0.05000	0.45600	-0.17900	0.11700
2.47276	-0.05000	0.45600	-0.19300	0.11800
2.48276	-0.04900	0.45500	-0.19000	0.12000
2.49276	-0.04900	0.45500	-0.18500	0.12200
2.50276	-0.04900	0.45400	-0.18300	0.12200
2.51276	-0.04900	0.45400	-0.18100	0.11900

2.52276	-0.04900	0.45300	-0.18500	0.12800
2.53276	-0.04900	0.45300	-0.18300	0.12900
2.54276	-0.04900	0.45200	-0.17900	0.12700
2.55276	-0.04800	0.45200	-0.17600	0.12700
2.56276	-0.04800	0.45100	-0.17500	0.12500
2.57276	-0.04800	0.45100	-0.17300	0.12100
2.58276	-0.04800	0.45100	-0.18000	0.12100
2.59276	-0.04800	0.45000	-0.18000	0.12000
2.60276	-0.04800	0.45000	-0.17800	0.11900

[108] C. M. Breneman, K. B. Wiberg, *J. Comput. Chem.,* **1990**, *11*, 361–373.

SPLITTING OF TOTAL FORCES IN SECONDARY ELECTROSTIC FORCES AND PRIMARY ONE

My approach (confirmed by both NBO and CHelpG) provides the advantage of understanding whether the SEIs, expressed in terms of electrostatic forces (Table7, 8), actually play a relevant role in the AA-DD multiple dihydrogen bond. Focusing on Graph 1 we can observe which each point represents the sum of the primary and secondary electrostatic forces for each energetic value given, in these terms it is possible to split the two contributions and therefore analyse their trend as the $\mathbf{d_c}$ increases (Graph 2).

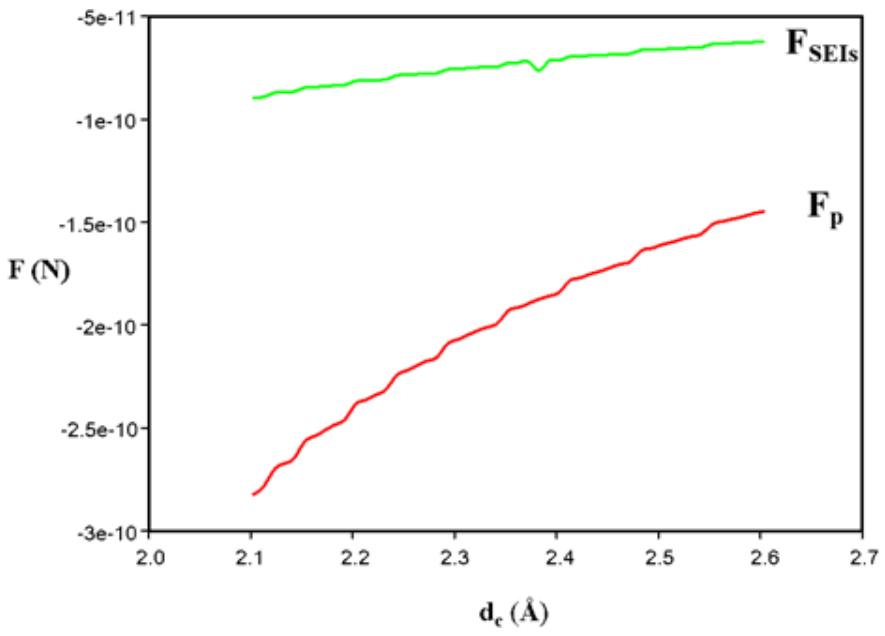

Graph 2. Trend of electrostatic forces as the $\mathbf{d_c}$ distance varies, red curve refers to primary electrostatic forces while the green one to SEIs forces (NBO method). $\mathbf{F_{SEIs}}$ and $\mathbf{F_p}$ correspond to $\mathbf{F_2}$ and $\mathbf{F_1}$ in Scheme 1 respectively.

As depicted in Graph 2 both curves have a rather regular trend, secondary electrostatic forces present a straight line (green) while primary ones are described by a slightly curved line. At ~ 2.1 Å the $\mathbf{F_p/F_{SEIs}}$ ratio is 3.15, consequently, the $\mathbf{F_{SEIs}}$ at the equilibrium distance in the optimized complex is about 1/3 of the $\mathbf{F_p}$, while at the other end of the range (~ 2.6 Å) the ratio is 2.36, in the latter case $\mathbf{F_{SEIs}}$ is just less than 1/2 of the $\mathbf{F_p}$. It is clear that for distances mildly greater than 2.6 Å, the two curves coalesce and approach zero asymptotically, making a distinction between primary and secondary forces meaningless.

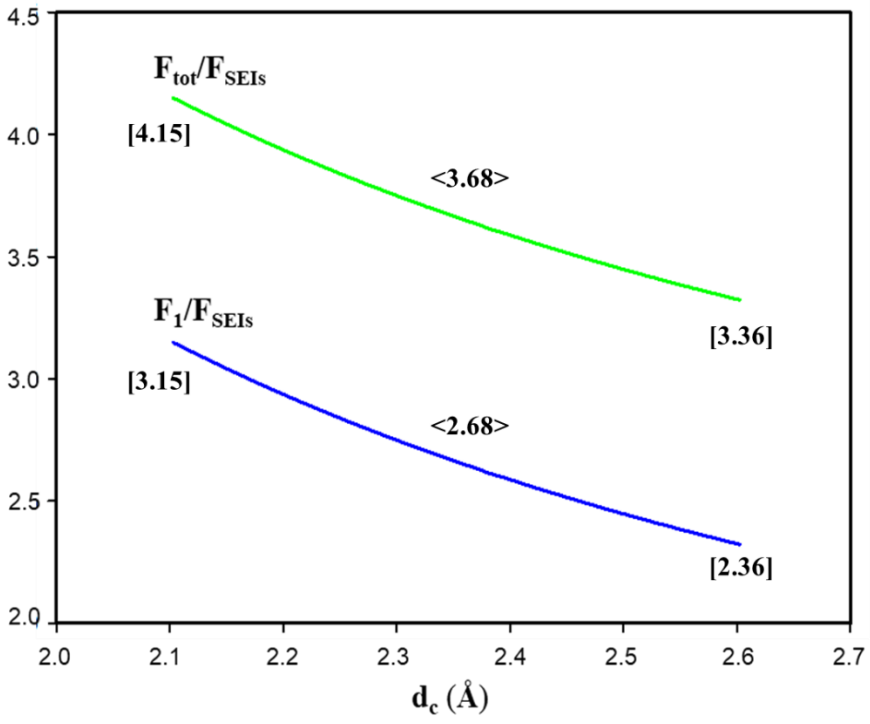

Graph 3. Trend of electrostatic forces ratio as the $\mathbf{d_c}$ varies, blue curve refers to $\mathbf{F_1/F_{SEIs}}$ while the yellow one to $\mathbf{F_{tot}/F_{SEIs}}$ (NBO method).

Throughout the interval 2.1-2.6 Å the ratio $\mathbf{F_{tot}/F_{SEIs}}$ has an average value of 3.68 (see Table 9 and Graph 3), therefore secondary electrostatic forces constitute about 27% of the total electrostatic forces ($\mathbf{F_{tot}}$). This percentage value reveals which secondary electrostatic forces play an important role in multiple AA-DD dihydrogen bond in the immediate proximity of the frontier atoms. Although obtained on different systems, our results are in good agreement with a work by Uchimaru et al.[109] according to which SEIs contribution represent the 25-35% of hydrogen-bonded complex interactions.

Table 7. $\vec{f}_1$,$\vec{f}_2$,$\vec{F}_1$,$\vec{F}_2$ forces as d_c varies keeping the monomers frozen. For the calculation of the forces the charges were converted into Coulomb by multiplying their value (NBO method), by the charge of the electron, i.e. -1,602×10^{-19} C.

d_c (Å)	NBO			
	$\vec{f}_1$ (N)	$\vec{F}_1$ (N)	$\vec{f}_2$ (N)	$\vec{F}_2$ (N)
2.10276	-1.4222e-10	-1.4109e-10	-6.6189e-11	-4.4797e-11
2.11276	-1.4032e-10	-1.3921e-10	-6.5630e-11	-4.4532e-11
2.12276	-1.3630e-10	-1.3523e-10	-6.4065e-11	-4.3581e-11
2.13276	-1.3476e-10	-1.3372e-10	-6.3655e-11	-4.3411e-11
2.14276	-1.3325e-10	-1.3223e-10	-6.3246e-11	-4.3240e-11
2.15276	-1.2940e-10	-1.2842e-10	-6.1718e-11	-4.2300e-11
2.16276	-1.2796e-10	-1.2700e-10	-6.1321e-11	-4.2131e-11
2.17276	-1.2654e-10	-1.2560e-10	-6.0926e-11	-4.1962e-11
2.18276	-1.2514e-10	-1.2421e-10	-6.0534e-11	-4.1792e-11
2.19276	-1.2375e-10	-1.2285e-10	-6.0144e-11	-4.1622e-11
2.20276	-1.2017e-10	-1.1930e-10	-5.8669e-11	-4.0698e-11
2.21276	-1.1910e-10	-1.1824e-10	-5.8413e-11	-4.0615e-11
2.22276	-1.1780e-10	-1.1696e-10	-5.8036e-11	-4.0447e-11
2.23276	-1.1651e-10	-1.1569e-10	-5.7661e-11	-4.0278e-11
2.24276	-1.1311e-10	-1.1232e-10	-5.6228e-11	-3.9366e-11
2.25276	-1.1188e-10	-1.1111e-10	-5.5864e-11	-3.9201e-11
2.26276	-1.1068e-10	-1.0992e-10	-5.5502e-11	-3.9034e-11

2.27276	-1.0948e-10	-1.0874e-10	-5.5142e-11	-3.8867e-11
2.28276	-1.0854e-10	-1.0781e-10	-5.4902e-11	-3.8783e-11
2.29276	-1.0535e-10	-1.0465e-10	-5.3517e-11	-3.7887e-11
2.30276	-1.0423e-10	-1.0354e-10	-5.3169e-11	-3.7723e-11
2.31276	-1.0312e-10	-1.0244e-10	-5.2824e-11	-3.7559e-11
2.32276	-1.0203e-10	-1.0136e-10	-5.2481e-11	-3.7394e-11
2.33276	-1.0116e-10	-1.0051e-10	-5.2252e-11	-3.7309e-11
2.34276	-1.0010e-10	-9.9456e-11	-5.1912e-11	-3.7145e-11
2.35276	-9.7141e-11	-9.6523e-11	-5.0582e-11	-3.6269e-11
2.36276	-9.6330e-11	-9.5723e-11	-5.0362e-11	-3.6184e-11
2.37276	-9.5323e-11	-9.4728e-11	-5.0034e-11	-3.6022e-11
2.38276	-9.4330e-11	-9.3745e-11	-5.2860e-11	-3.8135e-11
2.39276	-9.3553e-11	-9.2978e-11	-4.9491e-11	-3.5776e-11
2.40276	-9.2585e-11	-9.2020e-11	-4.9169e-11	-3.5613e-11
2.41276	-8.9832e-11	-8.9289e-11	-4.7890e-11	-3.4756e-11
2.42276	-8.9100e-11	-8.8566e-11	-4.7682e-11	-3.4672e-11
2.43276	-8.8186e-11	-8.7661e-11	-4.7371e-11	-3.4512e-11
2.44276	-8.7474e-11	-8.6958e-11	-4.7164e-11	-3.4428e-11
2.45276	-8.6580e-11	-8.6073e-11	-4.6856e-11	-3.4269e-11
2.46276	-8.5699e-11	-8.5201e-11	-4.6551e-11	-3.4109e-11
2.47276	-8.5015e-11	-8.4525e-11	-4.6348e-11	-3.4025e-11
2.48276	-8.2471e-11	-8.2000e-11	-4.5124e-11	-3.3188e-11
2.49276	-8.1818e-11	-8.1354e-11	-4.4928e-11	-3.3104e-11
2.50276	-8.0995e-11	-8.0539e-11	-4.4635e-11	-3.2948e-11
2.51276	-8.0359e-11	-7.9911e-11	-4.4441e-11	-3.2864e-11
2.52276	-7.9554e-11	-7.9114e-11	-4.4150e-11	-3.2708e-11
2.53276	-7.8934e-11	-7.8501e-11	-4.3959e-11	-3.2625e-11
2.54276	-7.8148e-11	-7.7722e-11	-4.3671e-11	-3.2468e-11
2.55276	-7.5961e-11	-7.5551e-11	-4.2595e-11	-3.1723e-11
2.56276	-7.5209e-11	-7.4806e-11	-4.2316e-11	-3.1571e-11
2.57276	-7.4632e-11	-7.4234e-11	-4.2132e-11	-3.1488e-11
2.58276	-7.4061e-11	-7.3670e-11	-4.1950e-11	-3.1406e-11
2.59276	-7.3334e-11	-7.2949e-11	-4.1676e-11	-3.1253e-11
2.60276	-7.2777e-11	-7.2399e-11	-4.1496e-11	-3.1170e-11

Table 8. $\vec{f}_1$,$\vec{f}_2$,$\vec{F}_1$,$\vec{F}_2$ forces as d_c varies keeping the monomers frozen. For the calculation of the forces the charges were converted into Coulomb by multiplying their value (CHelpG method), by the charge of the electron, i.e. -1,602×10^{-19} C.

d_c (Å)	CHelpG			
	$\vec{f}_1$ (N)	$\vec{F}_1$ (N)	$\vec{f}_2$ (N)	$\vec{F}_2$ (N)
2.10276	-1.4592e-10	-1.4477e-10	-6.7914e-11	-4.5964e-11

2.11276	-1.4584e-10	-1.4469e-10	-6.8213e-11	-4.6285e-11
2.12276	-1.4261e-10	-1.4150e-10	-6.7036e-11	-4.5602e-11
2.13276	-1.3971e-10	-1.3864e-10	-6.5994e-11	-4.5006e-11
2.14276	-1.4617e-10	-1.4505e-10	-6.9379e-11	-4.7433e-11
2.15276	-1.4315e-10	-1.4207e-10	-6.8275e-11	-4.6794e-11
2.16276	-1.2931e-10	-1.2834e-10	-6.1965e-11	-4.2574e-11
2.17276	-1.2719e-10	-1.2624e-10	-6.1239e-11	-4.2177e-11
2.18276	-1.1568e-10	-1.1482e-10	-5.5958e-11	-3.8633e-11
2.19276	-1.0385e-10	-1.0310e-10	-5.0472e-11	-3.4929e-11
2.20276	-9.9759e-11	-9.9037e-11	-4.8706e-11	-3.3786e-11
2.21276	-1.0297e-10	-1.0223e-10	-5.0502e-11	-3.5115e-11
2.22276	-1.0044e-10	-9.9722e-11	-4.9484e-11	-3.4486e-11
2.23276	-1.0231e-10	-1.0159e-10	-5.0631e-11	-3.5367e-11
2.24276	-1.0361e-10	-1.0288e-10	-5.1503e-11	-3.6058e-11
2.25276	-1.0528e-10	-1.0455e-10	-5.2567e-11	-3.6887e-11
2.26276	-1.0652e-10	-1.0579e-10	-5.3419e-11	-3.7569e-11
2.27276	-1.0883e-10	-1.0809e-10	-5.4812e-11	-3.8634e-11
2.28276	-1.1017e-10	-1.0943e-10	-5.5726e-11	-3.9365e-11
2.29276	-1.0710e-10	-1.0638e-10	-5.4403e-11	-3.8515e-11
2.30276	-1.0557e-10	-1.0487e-10	-5.3852e-11	-3.8208e-11
2.31276	-1.0345e-10	-1.0277e-10	-5.2994e-11	-3.7680e-11
2.32276	-1.0257e-10	-1.0191e-10	-5.2763e-11	-3.7595e-11
2.33276	-1.0441e-10	-1.0374e-10	-5.3931e-11	-3.8508e-11
2.34276	-1.0237e-10	-1.0171e-10	-5.3089e-11	-3.7987e-11
2.35276	-1.0177e-10	-1.0113e-10	-5.2994e-11	-3.7998e-11
2.36276	-9.8806e-11	-9.8184e-11	-5.1656e-11	-3.7115e-11
2.37276	-1.0496e-10	-1.0430e-10	-5.5092e-11	-3.9664e-11
2.38276	-1.0063e-10	-1.0000e-10	-5.6388e-11	-4.0679e-11
2.39276	-1.0002e-10	-9.9408e-11	-5.2914e-11	-3.8250e-11
2.40276	-9.4183e-11	-9.3609e-11	-5.0017e-11	-3.6228e-11
2.41276	-9.5938e-11	-9.5358e-11	-5.1145e-11	-3.7118e-11
2.42276	-9.1216e-11	-9.0669e-11	-4.8814e-11	-3.5495e-11
2.43276	-8.2247e-11	-8.1758e-11	-4.4181e-11	-3.2188e-11
2.44276	-8.2485e-11	-8.1998e-11	-4.4475e-11	-3.2465e-11
2.45276	-8.0927e-11	-8.0453e-11	-4.3797e-11	-3.2031e-11
2.46276	-7.8719e-11	-7.8262e-11	-4.2759e-11	-3.1331e-11
2.47276	-8.4918e-11	-8.4429e-11	-4.6295e-11	-3.3986e-11
2.48276	-8.4339e-11	-8.3858e-11	-4.6147e-11	-3.3939e-11
2.49276	-8.2827e-11	-8.2358e-11	-4.5482e-11	-3.3513e-11
2.50276	-8.1286e-11	-8.0829e-11	-4.4795e-11	-3.3067e-11
2.51276	-7.7805e-11	-7.7371e-11	-4.3028e-11	-3.1820e-11
2.52276	-8.4869e-11	-8.4399e-11	-4.7100e-11	-3.4894e-11
2.53276	-8.3948e-11	-8.3487e-11	-4.6751e-11	-3.4697e-11
2.54276	-8.0212e-11	-7.9775e-11	-4.4825e-11	-3.3326e-11

2.55276	-7.8258e-11	-7.7835e-11	-4.3882e-11	-3.2683e-11
2.56276	-7.5998e-11	-7.5590e-11	-4.2760e-11	-3.1902e-11
2.57276	-7.2167e-11	-7.1782e-11	-4.0741e-11	-3.0448e-11
2.58276	-7.4513e-11	-7.4119e-11	-4.2206e-11	-3.1597e-11
2.59276	-7.3334e-11	-7.2949e-11	-4.1676e-11	-3.1253e-11
2.60276	-7.1369e-11	-7.0998e-11	-4.0693e-11	-3.0567e-11

Table 9. $\vec{F}_1/F_{SEIs}$ and F_{tot}/F_{SEIs} ratio as a function of d_c (to maintain a label compatible with the manuscript $\vec{F}_2$ is F_{SEIs} and F_p is $\vec{F}_1$), the values between <> are referred to mean values.

d_c (Å)	NBO			
	F_1/F_{SEIs}	F_{tot}/F_{SEIs}	$<F_1/F_{SEIs}>$	$<F_{tot}/F_{SEIs}>$
2.10276	3.14953	4.14953	2.68	3.68
2.11276	3.12612	4.12612		
2.12276	3.10304	4.10304		
2.13276	3.08037	4.08037		
2.14276	3.05801	4.05801		
2.15276	3.03604	4.03604		
2.16276	3.01439	4.01439		
2.17276	2.99313	3.99313		
2.18276	2.97218	3.97218		
2.19276	2.95158	3.95158		
2.20276	2.93129	3.93129		
2.21276	2.91130	3.91130		
2.22276	2.89162	3.89162		
2.23276	2.87229	3.87229		
2.24276	2.85321	3.85321		
2.25276	2.83440	3.83440		
2.26276	2.81589	3.81589		
2.27276	2.79769	3.79769		
2.28276	2.77974	3.77974		
2.29276	2.76206	3.76206		
2.30276	2.74464	3.74464		
2.31276	2.72750	3.72750		
2.32276	2.71061	3.71061		
2.33276	2.69396	3.69396		
2.34276	2.67752	3.67752		
2.35276	2.66135	3.66135		
2.36276	2.64543	3.64543		
2.37276	2.62970	3.62970		
2.38276	2.61228	3.61228		
2.39276	2.59891	3.59891		
2.40276	2.58389	3.58389		

2.41276	2.56904	3.56904
2.42276	2.55442	3.55442
2.43276	2.53999	3.53999
2.44276	2.52577	3.52577
2.45276	2.51172	3.51172
2.46276	2.49790	3.49790
2.47276	2.48425	3.48425
2.48276	2.47080	3.47080
2.49276	2.45751	3.45751
2.50276	2.44443	3.44443
2.51276	2.43152	3.43152
2.52276	2.41877	3.41877
2.53276	2.40618	3.40618
2.54276	2.39378	3.39378
2.55276	2.38154	3.38154
2.56276	2.36947	3.36947
2.57276	2.35754	3.35754
2.58276	2.34576	3.34576
2.59276	2.33417	3.33417
2.60276	2.32268	3.32268

[109] S. Kahawara, T. Uchimaru, *J. Comput. Chem. Jpn.,* **2004**, *3*, 41-48.

QUANTUM MODEL OF HYDROGEN BONDING

The nature of hydrogen bonding can be rationalized in the framework of modern theoretical calculations that provide estimates of the total energy of hydrogen-bonded complexes as the sum of separate terms: 1) electrostatic interactions, 2) orbital interactions, 3) π-resonance assistance, 4) cooperative effects, 5) steric repulsion, 6) dispersion interactions and 7) secondary electrostatic interactions.

1. Electrostatic interactions

Hydrogen bonding is commonly formed between groups or atoms that are electronically complementary, that is, between a proton acceptor atom with partial negative charge and an opposing proton atom with partial positive charge. The electrostatic interaction will generally get more intense when the partial charges on the frontier atom are enhanced[110]. The electrostatic interaction $\mathbf{\Delta E_{el}}$ between two hydrogen bonded units A and B can be written as:

$$\mathbf{\Delta E_{el}} = \sum_{\alpha \in A, \beta \in B} \frac{Z\alpha Z\beta}{R\alpha\beta} - \int \sum_{\alpha \in A} \frac{Z\alpha \rho B(r)}{|r - R\alpha|} \mathbf{dr} - \int \sum_{\beta \in B} \frac{Z\beta \rho A(r)}{|r - R\beta|} \mathbf{dr} + \iint \frac{\rho A(r1) \rho B}{r12} \mathbf{dr_1 dr_2}$$

where Zα and Rα are the nuclear charge and position of atom α, respectively, and ρ(r) is the molecule's electronic density. The first term is referred to the repulsive Coulombic interaction between the nuclei of module A with those in module B, the second and third terms are the

attractive Coulombic interactions between the electrons of partner A with the nuclei in partner B and *vice versa*, and the last term is the repulsive Coulombic interaction between the electrons in monomer A with those in monomer B. The previous formula highlights how such a semi-classical approach can describe the electrostatic interactions only if the exact electronic density (or a good approximation) is known.

2. Orbital interactions

Orbital interactions or charge transfer (CT) interactions are defined as the transfer of electron density from one molecule to the other molecule upon formation of the hydrogen bonds. The charge transfer mechanism usually takes place from the lone pair orbital on the acceptor atom to the opposing antibonding $\sigma^*_{D\text{-}H}$ orbital on the donor atom, charge transfer interaction can be defined as [111]

$$\mathbf{CT} \propto -\frac{\lambda^2}{|\pi_{occ-\pi_{virt}}|}$$

λ is the orbital overlap and π is the energy difference between the occupied-virtual orbitals. From the previous mathematical expression, it is possible to argue that the orbital interactions are stronger when orbital overlap is larger and orbital energy gap is smaller. Charge transfer interaction is one of the effects that mostly influence hydrogen bond, its formation often results in an elongation of the D-H bond (due to a donation of charge into

the D-H σ* orbital), which is accompanied by a decrease of its stretching vibrational frequency[112].

3. π-Resonance Assistance

The resonance-assisted hydrogen bonding can be seen as synergistic reinforcement between π-resonance and hydrogen bonds[113].

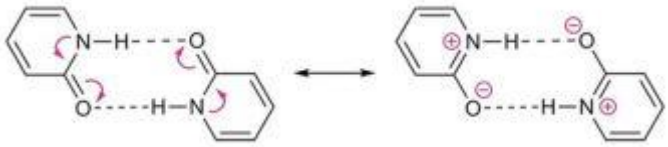

Figure 10. The π-resonance makes the H acceptor more positive and H donor more negative.

The resonance in the π-electron conjugated system performs a partially charge separation, making the H-bonding donor more positively charged and the H-bonding acceptor group more negatively charged (Figure 10).

4. Cooperative effects

Cooperative effects are known to strongly affect the geometrical, energetic, and vibrational properties of hydrogen bonded systems. In particular, such effects strongly favour molecular arrangements where each molecule is simultaneously a donor and an acceptor of hydrogen bonds, regardless of the chemical nature of the monomer subunits[114] (Figure11). A significant

cooperative reinforcement can be found in oligomers (with n>2) or extended non-covalently network such as water molecules[115].

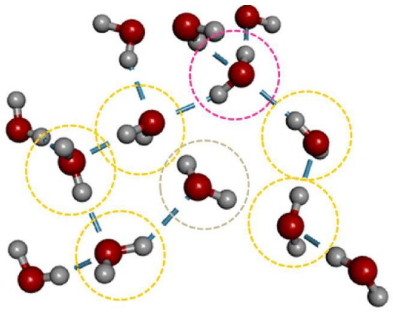

Figure 11. Cooperative effect in water extended hydrogen bonding network.

5. Pauli repulsion

The steric repulsion is defined as the repulsive electronic interactions between the monomer's filled orbitals, it originates from the fact that electrons with the same spin cannot be at the same position in space. Obeying the Pauli principle there will be a depletion of electron density around the hydrogen atoms, which explains the downfield ^{1}H chemical shift upon hydrogen bonding formation[116].

6. Dispersion interaction

The dispersion force is a temporary attractive force that results when the electrons in two adjacent monomers occupy positions that make the atoms form temporary dipoles[117]. This interaction is sometimes called an induced

dipole-induced dipole attraction. Because of the constant motion of the electrons, an acceptor or donor (hydrogen bonding) group can develop a temporary (instantaneous) dipole when its electrons are distributed unsymmetrically about the nucleus. A second acceptor or donor (hydrogen bonding) unit, in turn, can be distorted by the appearance of the dipole in the first acceptor or donor (hydrogen bonding) molecule (because electrons repel one another) which leads to an electrostatic attraction between the monomers (Figure 12).

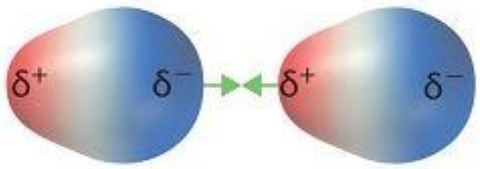

Figure 12. Dispersion forces are present between any two molecules (even polar molecules) when they are almost touching.

[110] C. A. Coulson in *Hydrogen Bonding* (Eds.: D. Hadzi, H. W. Thompson), Pergamon Press, London, **1959**, pp. 339–360.

[111] T. A. Albright, J. K. Burdett, M.-H. Whangbo, *Orbital Interactions in Chemistry*, 2nd ed., Wiley, Hoboken, NJ, **2013**, pp. 15– 24.

[112] G. A. Jeffrey in *An Introduction to Hydrogen Bonding*, Oxford University Press, Inc., New York, **1997**, pp. 217– 218.

[113] G. Gilli, F. Bellucci, V. Ferretti, V. Bertolasi, *J. Am. Chem. Soc.* **1989**, *111*, 1023–1028.

[114] N. Kobko, L. Paraskevas, E. del Rio, J. J. Dannenberg, *J. Am. Chem. Soc.* **2001**, *123*, 4348–4349.

[115] A. S. Mahadevi, G. N. Sastry, *Chem. Rev.* **2016**, *116*, 2775–2825.

[116] M. N. C. Zarycz, C. Fonseca Guerra, *J. Phys. Chem. Lett.* **2018**, *9*, 3720–3724.

[117] B. Brauer, M. K. Kesharwani, S. Kozuch, J. M. L. Martin, *Phys. Chem. Chem. Phys.* **2016**, *18*, 20905 –20925.

ENERGY DECOMPOSITION ANALYSES

Notwithstanding the excellent degree of linearity between total electrostatic forces and interaction energies, SEIs model still gives a rudimentary picture of the bonding mechanism as this description ignores the long-range electrostatic interaction or other components. To understand how this simple model can be refined we performed an energy decomposition analysis[118]. Briefly, EDA provides a powerful method for a quantitative interpretation of hydrogen bonds interaction energy, decomposing the latter into physically meaningful terms:

$$\Delta E = \Delta E_{int} + \Delta E_{pre} \longrightarrow \Delta E_{int} = \Delta E_{el} + \Delta E_{orb} + \Delta E_{pauli} + \Delta E_{disp}$$

The preparation energy (ΔE_{pre}) is the energy necessary to distort structurally and electronically the monomers from their equilibrium geometry to the geometry of the optimized interacting dimer. The focus of the interaction energy (ΔE_{int}) lies on the splitting of several terms:

- ΔEel that is the quasiclassic Coulomb interaction, when the charge densities of the two partners in the complex are frozen;
- ΔEorb is the orbital interaction, and is responsible for charge transfer and polarization effect;
- ΔEpauli represent the repulsive exchange interaction between electrons of the two fragments having the same spin;

- ΔEdisp is due to attractive forces between the temporary dipoles of interacting species.

The energy decomposition analysis (EDA) was performed by *Amsterdam Density Functional* (ADF) software[119]. I adopted the dispersion-corrected BLYP-D3(BJ)[120] functional with a TZ2P basis set, whose combination excellently reproduces the energy properties of hydrogen bonded systems[121].

EDA was carried out scanning the distance between $\mathbf{C_1}$ and $\mathbf{C_2}$ as described above (see Table 10).

As shown in Figure 13, ΔEel (blue curve) and ΔEpauli (red curve) have a very similar reverse trend, in fact from 2.35 to 2.6 Å they tend to cancel each other out. (see Table 10) This means that for distances greater than "interaction distance", ΔEint (purple curve) is mainly composed of ΔEorb (grey curve) and ΔEdisp (yellow curve). Therefore, in the range of long intermolecular distances our dihydrogen bonded system is dominated by not-purely electrostatic interactions (dispersion, polarization and charge transfer effects). This effect can be indirectly seen by evaluating the trend of the spots in Graph 1: after a rapid rise of overcrowded red spots (due to the classic Coulomb electrostatics) the curve easily reaches a plateau.

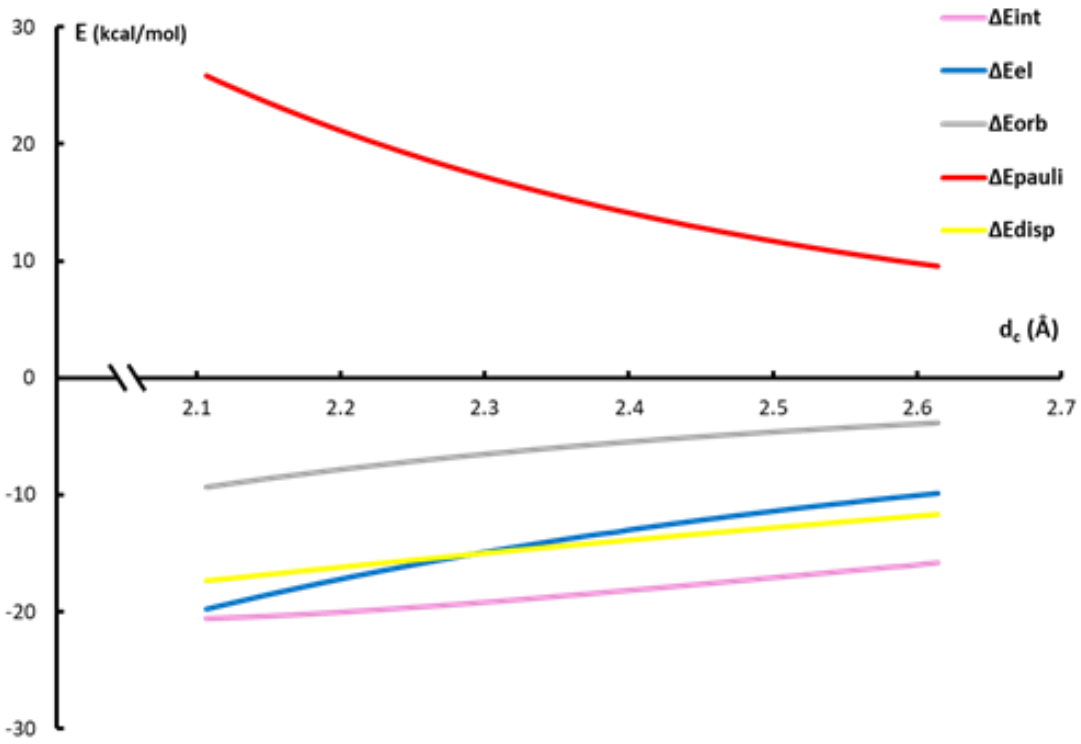

Figure 13. Decomposed energy contributions (kcal/mol) as a function of d_c distance (Å)

Table 10. EDA as a function of $\mathbf{d_c}$ (every term is expressed in kcal/mol) at BLYP-D3(BJ)/TZ2P level.

d_c (Å)	ΔE_{int}	ΔE_{el}	ΔE_{orb}	ΔE_{pauli}	ΔE_{disp}
2.10276	-20.5700	-19.7100	-9.3600	25.8300	-17.3300
2.11276	-20.5300	-19.4100	-9.1800	25.2600	-17.2000
2.12276	-20.4800	-19.1200	-9.0000	24.7200	-17.0800
2.13276	-20.4200	-18.8300	-8.8300	24.1800	-16.9500
2.14276	-20.3700	-18.5400	-8.6500	23.6500	-16.8200
2.15276	-20.3100	-18.2700	-8.4900	23.1400	-16.7000
2.16276	-20.2500	-18.0000	-8.3300	22.6500	-16.5700
2.17276	-20.1800	-17.7300	-8.1700	22.1600	-16.4400
2.18276	-20.1100	-17.4600	-8.0100	21.6900	-16.3200
2.19276	-20.0400	-17.2100	-7.8600	21.2300	-16.2000
2.20276	-19.9600	-16.9500	-7.7100	20.7800	-16.0700
2.21276	-19.8800	-16.7100	-7.5700	20.3400	-15.9500
2.22276	-19.8000	-16.4600	-7.4300	19.9200	-15.8300
2.23276	-19.7200	-16.2300	-7.2900	19.5000	-15.7100
2.24276	-19.6300	-15.9900	-7.1500	19.1000	-15.5900
2.25276	-19.5500	-15.7600	-7.0200	18.7000	-15.4700
2.26276	-19.4600	-15.5400	-6.8900	18.3200	-15.3500

2.27276	-19.3700	-15.3200	-6.7600	17.9400	-15.2300
2.28276	-19.2800	-15.1000	-6.6400	17.5800	-15.1100
2.29276	-19.1800	-14.8900	-6.5200	17.2200	-14.9900
2.30276	-19.0900	-14.6800	-6.4000	16.8700	-14.8800
2.31276	-18.9900	-14.4800	-6.2900	16.5400	-14.7600
2.32276	-18.8900	-14.2800	-6.1700	16.2100	-14.6500
2.33276	-18.7900	-14.0800	-6.0600	15.8900	-14.5300
2.34276	-18.6800	-13.8900	-5.9500	15.5700	-14.4200
2.35276	-18.5800	-13.7000	-5.8400	15.2600	-14.3100
2.36276	-18.4800	-13.5100	-5.7400	14.9700	-14.1900
2.37276	-18.3700	-13.3300	-5.6400	14.6700	-14.0800
2.38276	-18.2600	-13.1900	-5.5400	14.3800	-13.9700
2.39276	-18.1600	-12.9700	-5.4400	14.1100	-13.8600
2.40276	-18.0500	-12.8000	-5.3500	13.8400	-13.7500
2.41276	-17.9500	-12.6300	-5.2500	13.5700	-13.6400
2.42276	-17.8400	-12.4600	-5.1600	13.3200	-13.5300
2.43276	-17.7300	-12.3000	-5.0700	13.0600	-13.4200
2.44276	-17.6200	-12.1300	-4.9900	12.8200	-13.3200
2.45276	-17.5100	-11.9800	-4.9000	12.5800	-13.2100
2.46276	-17.4000	-11.8200	-4.8200	12.3500	-13.1100
2.47276	-17.2900	-11.6700	-4.7400	12.1200	-13.0000
2.48276	-17.1700	-11.5200	-4.6600	11.8900	-12.9000
2.49276	-17.0600	-11.3700	-4.5800	11.6800	-12.7900
2.50276	-16.9500	-11.2200	-4.5000	11.4600	-12.6900
2.51276	-16.8400	-11.0800	-4.4300	11.2500	-12.5900
2.52276	-16.7300	-10.9400	-4.3500	11.0500	-12.4900
2.53276	-16.6200	-10.8000	-4.2800	10.8500	-12.3800
2.54276	-16.5000	-10.6700	-4.2100	10.6600	-12.2800
2.55276	-16.3900	-10.5300	-4.1400	10.4700	-12.1800
2.56276	-16.2800	-10.4000	-4.0800	10.2900	-12.0900
2.57276	-16.1700	-10.2700	-4.0100	10.1000	-11.9900
2.58276	-16.0900	-10.1500	-3.9500	9.9300	-11.8900
2.59276	-15.9400	-10.0200	-3.8800	9.7600	-11.7900
2.60276	-15.8300	-9.9000	-3.8200	9.5900	-11.7000

[118] L. Z. Moritz, V. Hopffgarten, D. M. Andrada, G. Frenking, *Wires. Comput. Mol. Sc.*, **2018**, *8*.

[119] G. Velde, F.M. Bickelhaupt, E.J. Baerends, C. Fonseca Guerra, S.J.A. van Gisbergen, J.G. Snijders, T Ziegler, *J. Comput. Chem.*, **2001**, *22*, 931−967.

[120] S. Grimme, J. Antony, S. Ehrlich, H. Krieg, *J. Chem. Phys.*, **2010**, *132*, 154104.

[121] B. Brauer, M. K. Kesharwani, S. Kozuch, J. M. L. Martin, *Phys. Chem. Chem. Phys.*, **2016**, *18*, 20905–20925.

NCI ANALYSES

NCI is a theoretical method developed to visualize the non-covalent interaction by plotting the electron density versus the reduced density gradient[122]. This approach is based on the fact that critical points of the electron density ($\nabla\rho = 0$) arise when atoms interact, if the interaction is bonding the point is expected to be a first order saddle point. This method was chosen for its ability to highlight interactions in the low density regime. The NCI analysis provides an index that correlates the reduced density gradient (s) and the electron density (ρ) generating a 2D maps:

$$\mathbf{s} = \frac{|\nabla \boldsymbol{\rho}|}{\sqrt[3]{\boldsymbol{\rho}^{\mathbf{4}}}\ \ \mathbf{2}\sqrt[3]{\mathbf{3}\boldsymbol{\pi}^{\mathbf{2}}}}$$

When an inter- or intramolecular interaction is present, there is a marked change in the reduced gradient between the interacting atoms, producing density critical points between interacting fragments. Keeping in mind that the behavior of s at low densities is dominated by ρ, s tends to diverge except in the regions around a density critical point, where $\nabla\rho$ dominates, and s approaches zero. $\nabla\rho$ turns out to be a gauge of the interaction strength, since both attractive and repulsive interactions appear in the

same area of density/reduced gradient space, second derivatives of the density along the main axis of variation are crucial to distinguish between attractive and repulsive interactions (i.e., hydrogen-bonding and steric repulsion). Focusing on the divergence theorem, the sign of the $\nabla^2\rho$ indicates whether the net gradient flux of density is entering ($\nabla^2\rho < 0$) or leaving ($\nabla^2\rho > 0$) an infinitesimal volume around a reference point. Hence, the sign of $\nabla^2\rho$ determines whether the density is concentrated or depleted at that point, relative to the surroundings. However, the sign of the $\nabla^2\rho$ is not sufficient to distinguish between different types of weak interactions, because it is "contaminated" by negative contributions from the nuclei. In these terms, contributions to the $\nabla^2\rho$ along the axes of its maximal variation can help: such contributions are the eigenvalues λi of the electron-density Hessian matrix.

$$\boldsymbol{\nabla^2\rho = \lambda_1 + \lambda_2 + \lambda_3} \text{ such that } \boldsymbol{\lambda_1 < \lambda_2 < \lambda_3}$$

Near the nuclei $\lambda_1 < 0$, $\lambda_2 < 0$, $\lambda_3 < 0$ while away from them, $\lambda_3 > 0$. In molecules or supramolecular aggregates, the λ_3 values vary along the internuclear direction, while λ_1 and λ_2 report the variation of density in the plane normal to the λ_3 eigenvector. It was observed that the second eigenvalue (λ_2) can be either positive or negative, depending on the interaction type. Interactions such as hydrogen bonding are characterized by an accumulation of density perpendicular to the bond ($\lambda_2 < 0$) while electrostatic repulsive interaction produce density depletion ($\lambda_2 > 0$). Finally, an accurate analysis of the sign of λ_2 enables us to distinguish

different types of weak interactions, while the density itself guides us to assess the interaction strength.

[122] J. Contreras-García, E. R. Johnson, S. Keinan, R. Chaudret, J.-P. Piquemal, D.N. Beratan, W. Yang, *J. Chem. Theory Comput.* **2011**, *7*, 625–632.

NON-COVALENT INTERACTIONS MAPPED SURFACES

The mutual spatial communication between frontier hydrogens belonging to two monomers involved in the multiple dihydrogen bond was also investigated by NCI analysis. Despite the electrostatic surface potential maps provide a good qualitative view of the possible interaction regions between the two monomers, they do not allow the discrete visualization of the specific interactions (Figure 14). Taking advantage of the reduced gradient of electron densities it is possible to visualize the non-covalent interaction in low density regime (Figure 15).

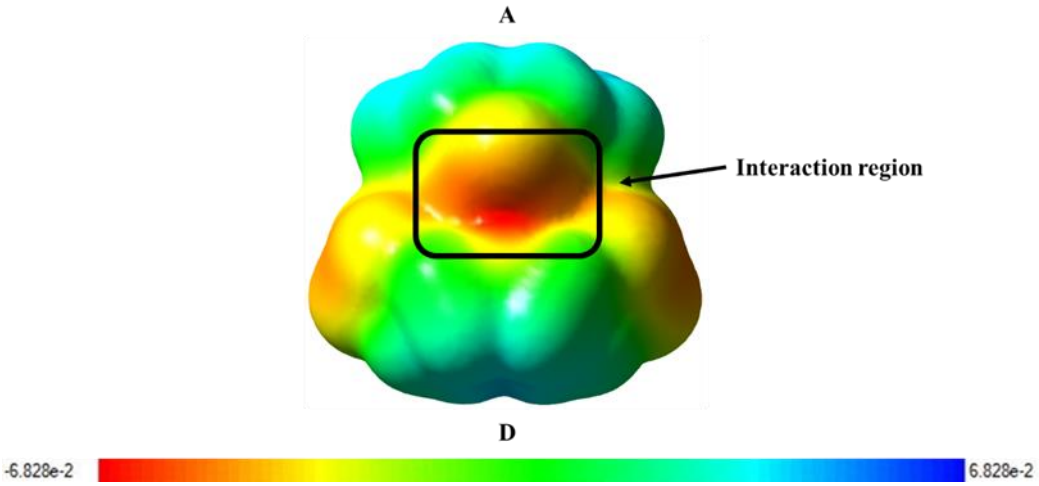

Figure 14. Electrostatic surface potential of the optimized (PBE1PBE/6-311++G) complex**, A** is referred to acceptor partner while **D** to donor one**,** black rectangle indicates the interaction area between the two monomers.

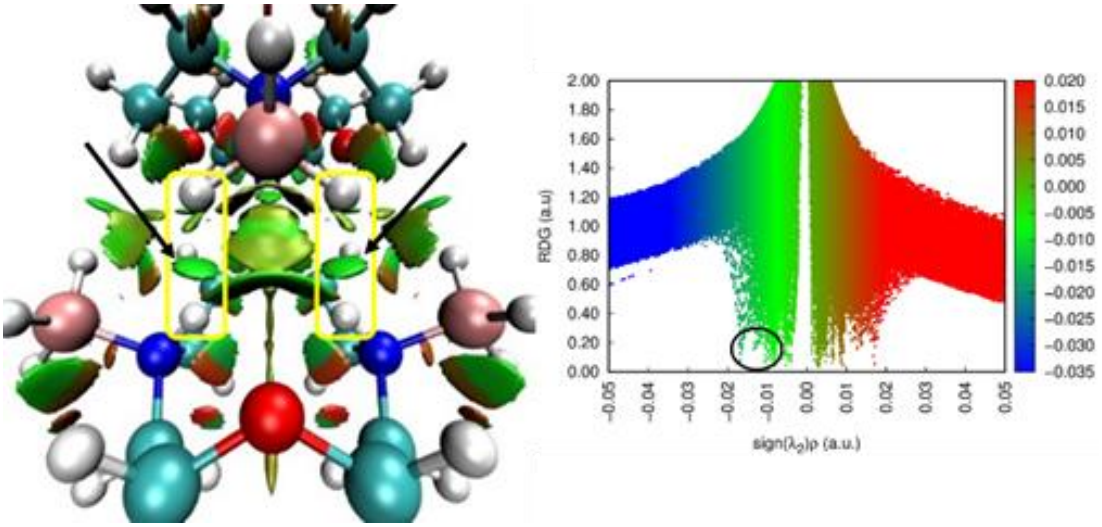

Figure 15. On the left a zoomed vision of the intermolecular interaction surface in the optimized complex (PBE1PBE/6-311++G), on the right the behaviour of reduced gradient as sign(λ_2)ρ varies.

As illustrated in Figure 15, among the many interactions present, proton ad hydridic hydrogens (yellow rectangles) interact symmetrically (as indicated by black arrows) establishing a stable multiple dihydrogen bond

based on AA-DD pattern. These electrostatically favorable relationships were also confirmed by matching the color of the surface with the one of 2D plot (black circle), in fact at low densities regime around the first order saddle points $\nabla\rho$ dominates and RDG (reduced density gradient) approaches zero. The pseudo-circular green surfaces highlighted on the left of Figure 15 are slightly shifted towards the proton hydrogens, this is due to a greater electric charge supported by these hydrogens. Furthermore, these 2D surfaces are moderately inclined in a symmetrical way, this geometric aspect can be considered as a "contamination" of the primary electrostatic interactions on behalf of the diagonal ones.

TOPOLOGICAL FEATURES

Since the time of birth of chemistry, chemists are used to thinking about molecules as geometric entities in which atoms have a certain spatial arrangement. In the last century the introduction of new physical theories has revealed difficulties in bringing the concept of molecular geometry in harmony with the basic principles of quantum theory[123]. The drawback of the geometric approach is that the geometric parameters provide a local characterization of the molecule (i.e. they establish relations between two, three or four atoms) but certain spatial relations in molecules depend on the molecular architecture as a whole. In these cases, we should not focus

on bond lengths and angles but rather the embedding of the molecule as a whole in three-dimensional space. Instead of conventional geometric structures (which are sets of atoms in the two- or three-dimensional space, whose distances are determined by the Euclidean metric), modern topology investigates sets with much more general properties[124]. Changes in the molecular geometry, caused by intramolecular motions or by any kind of external influence (intermolecular interactions), but in which no chemical bond has been broken or formed, are therefore called *topological properties*.

[123] R. G. Woolley, *J. Amer. Chem. Soc.* **1978**,*100*, 1073.

[124] J. Dugundji, Topology. Boston: Allyn and Bacon 1966.

UP-UP OR *UP-DOWN*?

Focusing on the optimized complex structure, it can be noted that there are two different topological approaches for the two monomers: *Up-Down* topology (**A** series, Figure 16) in which the protons bound to the nitrogens are directed towards the oxygen of the ether bridge of the other monomer, establishing a bifurcated hydrogen bond (**A1** cyano rectangle, Figure 16). This interaction causes the two partners to be anchored longitudinally thus being able to form an AA-DD multiple dihydrogen bond (**A2** green

rectangle, and **A3** zoom Figure 16). In the *Up-Up* topology (**B** series, Figure 16) the protons bound to the nitrogens arrange themselves far from the ether bridge of the other partner (**B1**, cyano rectangle, Figure 16). This unconstrained conformation allows the acceptor partner to rotate and thus forming a bifurcated dihydrogen bond (**B2** green rectangle, and **B3** zoom, Figure 16). Our X-ray analysis confirm which the crystalline packing adopts the *Up-Down* topology, this is probably due to a better thermodynamic stability guaranteed by a greater number of electrostatically favorable interactions.

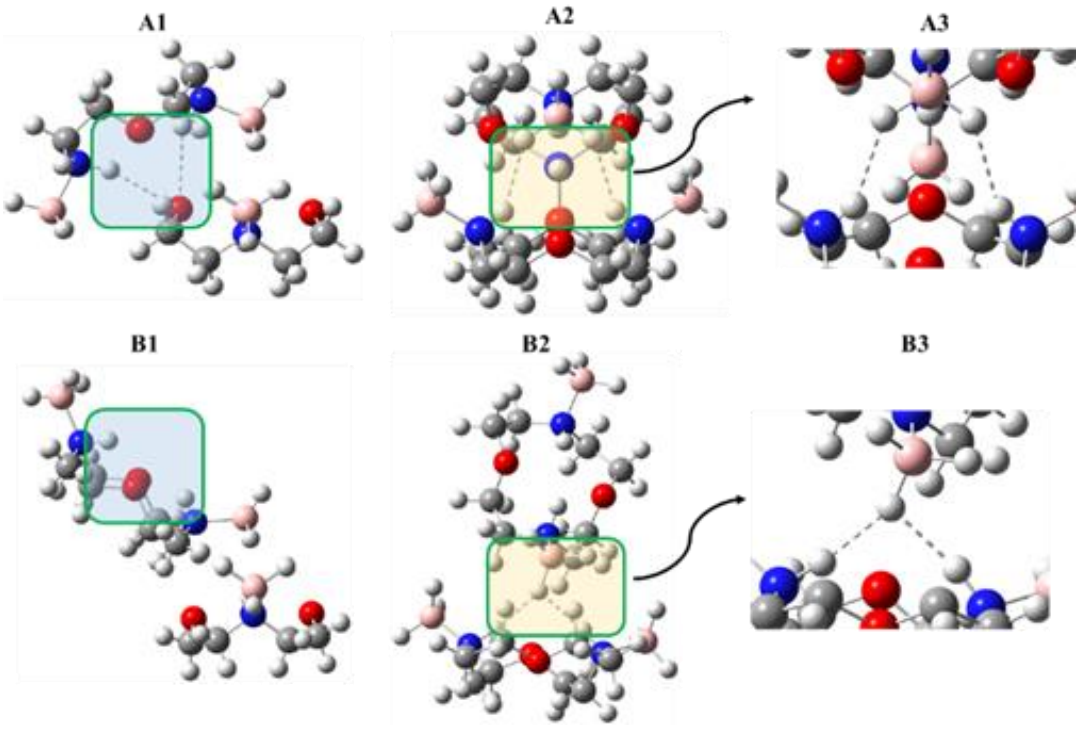

Figure 16. *Up-Up* and *Up-Down* approaches seen from different perspectives, cyano rectangles identify possible hydrogen bonds, while the green ones identify possible dihydrogen bonds. (Dimers were optimized at PBE1PBE/6-311++G level).

In this context, a strategically correct synthesis of the coronand is crucial to ensure an AA-DD interaction, in fact a more extensive chemical skeleton than the oxydiethylene bridge (oxydipropylene, oxydibutylene etc.) would move too far the nitrogen atoms making it impossible to sustain a multiple AA-DD dihydrogen bond. Moreover, it is clear that on the alkyl bridge a heteroatom with available lone pairs (oxygen or sulphur) should be needed to orient the two monomers according to a favorable arrangement. (**A** series, Figure 16).

SCXRD ANALYSIS

Crystal Data for the complex: $C_8H_{24}N_2O_2B_2$ (M =201.91 g/mol) orthorhombic, space group Pnma (no. 62), a = 15.0115(4) Å, b = 14.0176(4) Å, c = 12.3117(4) Å, V = 2590.69(13) Å^3, Z = 8, T = 23 °C, μ(MoKα) = 0.069 mm^{-1}L $Dcalc$ = 1.035 g/cm^3, 19200 reflections measured (5.172° ≤ 2Θ ≤ 52.736°), 2757 unique (R_{int} = 0.0231, R_{sigma} = 0.0180) which were used in all calculations. The final R_1 and GooF were 0.0512 and 1.033 respectively (I > 2σ(I)), while wR_2 was 0.1729 (all data).

Diffraction data were collected at room temperature on a single crystal Bruker APEX-II CCD diffractometer by using APEX2 package [125] which was used for data reduction a structure solution while refinement was

carried out by the wlsqr technique of SHELXL [126] in OLEX2 [127] which has also prepared the publication material.

The asymmetric unit contains only the half moiety of two independent molecules which are placed both on a crystallographic mirror plane. Each ethyl bridge has a significant conformational disorder which was treated by two crossed dispositions with refined occupancy and suitable restrains Hydrogens were placed by geometry of the parent atoms, except the nitrogen Hs which were located and refined by the last difference Fourier syntheses (Figure 17).

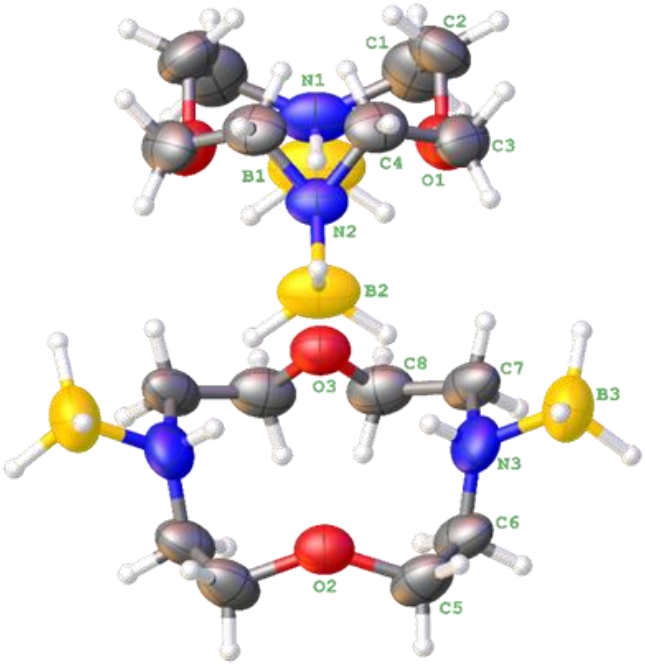

Figure 17. Perspective view showing the two independent molecules placed on a crystallographic mirror plane (symmetry operation: x, 1/2-y, z) with the atomic labels of their moieties in the asymmetric unit only. All the four independent ethyl bridges are disordered and each corresponding lowest occupancy conformation has been omitted for clarity. Displacement ellipsoids are drawn at 50% probability while hydrogen size is arbitrary.

Table 11. Crystal data and structure refinement for the complex (see figure 17).

CCDC deposition n.	2039908
Identification code	**2**
Empirical formula	$C_8H_{24}N_2O_2B_2$
Formula weight	201.91
Temperature/ °C	23
Crystal system	Orthorhombic
Space group	Pnma
a/Å	15.0115(4)
b/Å	14.0176(4)
c/Å	12.3117(4)
α/°	90
ß/°	90
γ/°	90
Volume/Å^3	2590.69(13)
Z	8
ρcalcg/cm^3	1.035
μ/mm 1	0.069
F(000)	896.0
Crystal size/mm^3	0.23 × 0.25 × 0.32
Radiation	MoKα (λ = 0.71073 Å)
2Θ range for data collection/°	5.172 to 52.736
Index ranges	-18 ≤ h ≤ 18, -13 ≤ k ≤ 17, -15 ≤ l ≤ 15
Reflections collected	19200
Independent reflections	2757 [Rint = 0.0231, Rsigma = 0.0180]
Data/restraints/parameters	2757/33/227
Goodness-of-fit on F2	1.033
Final R indexes [I>=2σ (I)]	R1 = 0.0512, wR2 = 0.1544
Final R indexes [all data]	R1 = 0.0694, wR2 = 0.1729
Largest diff. peak/hole / e Å^{-3}	0.27/-0.14

Table 12. Fractional atomic coordinates (×10^4) and occupancy and equivalent isotropic displacement parameters (Å^2×10^3) for the complex (see figure 17). U_{eq} is defined as 1/3 of of the trace of the orthogonalised U_{IJ} tensor.

Atom	occupancy	x	y	z	U(eq)
C1	0.551(8)	5863(4)	3545(5)	5055(6)	95.3(18)
C2	0.551(8)	5606(2)	3801(4)	3914(5)	84.0(16)
C1'	0.449(8)	6042(4)	3140(6)	4828(5)	72.2(16)
C2'	0.449(8)	5481(4)	3992(4)	4678(7)	86(2)
C3	0.519(9)	4235(5)	4014(3)	2897(3)	70.6(13)

C4	0.519(9)	4143(3)	3130(5)	2257(3)	69.2(14)
C3'	0.481(9)	4718(5)	3876(4)	2939(4)	76.3(16)
C4'	0.481(9)	3821(4)	3561(5)	2527(5)	68.2(15)
C5	0.535(7)	376(3)	3507(4)	5074(5)	76.2(15)
C6	0.535(7)	1104(2)	3942(3)	5745(3)	69.9(13)
C5'	0.465(7)	345(4)	3131(5)	5510(5)	70.7(15)
C6'	0.465(7)	702(3)	4058(4)	5138(4)	69.5(14)
C7	0.502(8)	2741(3)	4055(3)	5765(3)	68.6(13)
C8	0.502(8)	2930(3)	3112(5)	6299(4)	72.3(13)
C7'	0.498(8)	2177(4)	3987(3)	6010(3)	74.8(15)
C8'	0.498(8)	3083(3)	3558(4)	5854(5)	70.8(15)
O1	1.0	4666.6(7)	3816.6(8)	4004.4(10)	73.2(4)
O2	0.5	590.1(9)	2500	4728.4(12)	64.8(4)
O3	0.5	3033.6(9)	2500	5459.8(12)	67.8(4)
B1	0.5	5503(2)	2500	6687(2)	114.0(15)
B2	0.5	2530.0(19)	2500	2618(2)	89.4(10)
B3	1.0	1907.3(17)	5056.4(16)	4357(2)	93.1(7)
N1	0.5	5523.9(13)	2500	5394.8(15)	77.7(7)
N2	0.5	3579.5(11)	2500	2823.2(13)	58.5(5)

Table 13. Anisotropic displacement parameters ($Å^2 \times 10^3$) for compound the complex (see figure 17).The anisotropic displacement factor exponent takes the form: $-2\pi^2[h^2a^{*2}U_{11}+2hka^*b^*U_{12}+\ldots]$.

Atom	**U_{11}**	**U_{22}**	**U_{33}**	**U_{23}**	**U_{13}**	**U_{12}**
C1	58(3)	102(5)	126(5)	-14(3)	-22(3)	-11(3)
C2	63(2)	87(3)	102(4)	10(2)	9(2)	-21(2)
C1'	47(2)	99(4)	71(3)	-9(3)	2(2)	-5(3)
C2'	79(3)	70(3)	110(5)	-22(3)	-13(3)	-21(2)
C3	72(3)	71(3)	69(2)	23(2)	10(2)	10(2)
C4	69(2)	93(3)	45(2)	14(2)	6(1)	6(2)
C3'	80(4)	71(3)	78(3)	23(2)	13(3)	-16(3)
C4'	76(3)	72(3)	57(2)	21(2)	-3(2)	-1(2)
C5	48(2)	90(4)	90(4)	-24(3)	-7(2)	11(2)
C6	55(2)	81(2)	74(2)	-26(2)	7(2)	6(1)
C5'	50(2)	99(4)	64(3)	-4(2)	9(2)	11(2)
C6'	52(2)	78(3)	79(3)	-12(2)	-4(2)	17(2)
C7	43(3)	76(3)	87(2)	-31(2)	-2(2)	-3(2)
C8	51(2)	102(3)	64(2)	-11(2)	-6(2)	1(2)
C7'	61(3)	88(3)	75(2)	-25 (2)	-4(2)	15(2)
C8'	47(2)	84(4)	81(3)	-21(3)	-7(2)	1(2)

O1	64.3(7)	69.4(7)	85.9(8)	3.4(6)	-1.8(5)	-10.4(5)
O2	53.8(8)	82(1)	58.3(8)	0	-2.4(6)	0
O3	53.1(8)	83(1)	66.8(9)	0	0.1(6)	0
B1	73(2)	216(5)	54(2)	0	-19(1)	0
B2	55(1)	156(3)	57 (1)	0	-14(1)	0
B3	105(2)	61(1)	114(2)	-4(1)	6(1)	7(1)
N1	48(1)	129(2)	56(1)	0	-11.5(8)	0
N2	51.6(9)	88(1)	35.6(7)	0	-2.7(6)	0
N3	94(1)	56.9(8)	73.5(9)	-16.4(6)	17.5(7)	5.3(7)

Table 14. Bond lengths, angles and torsion angles for the complex **(see figure 17).**

Bond label	**Length (Å)**	**Angle label**	**Angle (°)**	**Dihedral label**	**Angle (°)**
C1 C2	1.500(9)	C2 C1 N1	114.9(3)	C2 C1 N1 B1	-158.6(5)
C5' C6'	1.478(8)	O1 C2 C1	104.2(4)	C2' C1' N1 B1	-88.3(5)
C1' C2'	1.473(9)	N1 C1' C2'	107.6(4)	C3 C4 N2 B2	90.9(4)
C7 C8	1.504(8)	C1' C2' O1	112.1(4)	C3' C4' N2 B2	163.2(6)
C3 C4	1.474(8)	C4 C3 O1	121.1(3)	C5 C6 N3 B3	88.6(4)
C7' C8'	1.500(6)	N2 C4 C3	105.4(3)	C5' C6' N3 B3	166.6(4)
C3' C4'	1.505(9)	O1 C3' C4'	121.0(2)	C8 C7 N3 B3	-166.9(4)
B1 N1	1.591(4)	C3' C4' N2	101.0(2)	C8' C7' N3 B3	-92.3(4)
C5 C6	1.500(6)	C6 C5 O2	121.5(2)	O1 C3 C4 N2	62.0(7)
C6 N3	1.392(3)	N3 C6 C5	122.0(3)	O1 C3' C4' N2	-62.2(9)
C2 O1	1.415(4)	O2 C5' C6'	98.7(2)	O2 C5 C6 N3	70.1(6)
C6' N3	1.673(5)	C5' C6' N3	103.5(2)	O2 C5' C6' N3	-62.3(5)
C2' O1	1.498(6)	C8 C7 N3	114.9(3)	N1 C1 C2 O1	64.4(7)
C8 O3	1.352(4)	O3 C8 C7	104.2(4)	N1 C1' C2' O1	-63.3(8)
C4 N2	1.408(4)	N3 C7' C8'	107.6(4)	N3 C7 C8 O3	62.8(5)
C8' O3	1.562(5)	C7' C8' O3	112.1(4)	N3 C7' C8' O3	-69.4(6)
C4' N2	1.573(5)	C1' N1 B1	121.1(3)		
B3 N3	1.598(3)	B1 N1 C1	105.4(3)		
C1 N1	1.606(6)	C4 N2 B2	121.0(2)		
C5' O2	1.358(5)	C4' N2 B2	101.0(2)		
C1' N1	1.377(7)	C6 N3 B3	121.5(2)		
C7 N3	1.658(5)	C7' N3 B3	122.0(3)		
C3 O1	1.535(5)	B3 N3 C6'	98.7(2)		
C7' N3	1.326(4)	B3 N3 C7	103.5(2)		
C3' O1	1.316(5)				
B2 N2	1.596(3)				
C5 O2	1.508(5)				

Table 15. Hydrogen atom coordinates (Å×10⁴) and occupancy and isotropic displacement parameters (Å²×10³) for the complex (see figure 17). The two hydrogens H1D and H2D are equivalent to H1E and H2E (x, ½-y, z) respect to the crystallographic mirror plane on which the two corresponding parent atoms B1 and B2 lie.

Atom	occupancy	x	y	z	U(eq)
H1	0.5	4980(20)	2500	5190(20)	93
H2	0.5	3706(16)	2500	3520(20)	70
H3	0.5	1866(12)	3620(16)	4593(17)	90
H1A	0.551(8)	5611.2	4011.36	5550.38	114
H1B	0.551(8)	6505.89	3571.94	5123.91	114
H2A	0.551(8)	5840.7	4419.19	3705.37	101
H2B	0.551(8)	5805.03	3322.8	3398.78	101
H1'A	0.449(8)	6216.73	2876.63	4131.48	87
H1'B	0.449(8)	6575.37	3297.55	5235.92	87
H2'A	0.449(8)	5833.64	4487.57	4335.81	104
H2'B	0.449(8)	5298.13	4225.27	5386.02	104
H3A	0.519(9)	3651.32	4295.28	3006.02	85
H3B	0.519(9)	4596.56	4466.97	2497.55	85
H4A	0.519(9)	3892.17	3273.82	1549.56	83
H4B	0.519(9)	4722.72	2838.89	2150.96	83
H3'A	0.481(9)	5184.22	3463.08	2663.58	92
H3'B	0.481(9)	4842.31	4526	2716.09	92
H4'A	0.481(9)	3809	3630.76	1743.41	82
H4'B	0.481(9)	3367.75	3978.82	2825.82	82
H5A	0.535(7)	280.66	3895.28	4432.21	91
H5B	0.535(7)	-172	3505.06	5490.55	91
H6A	0.535(7)	908.82	4541.63	6058.13	84
H6B	0.535(7)	1277.25	3515.26	6327.64	84
H5'A	0.465(7)	597.93	2955.46	6206.69	85
H5'B	0.465(7)	-298.4	3157.12	5577.56	85
H6'A	0.465(7)	512.98	4550.17	5640.73	83
H6'B	0.465(7)	447.03	4205.35	4433.73	83
H7A	0.502(8)	3238.62	4215.32	5296.17	82
H7B	0.502(8)	2706.12	4541.77	6323.69	82
H8A	0.502(8)	3467.39	3144.79	6734.55	87
H8B	0.502(8)	2437.25	2918.94	6758.82	87
H7'A	0.498(8)	1811.24	3571.73	6456.18	90
H7'B	0.498(8)	2225.45	4600.65	6368.4	90
H8'A	0.498(8)	3406.85	3583.91	6535.5	85

H8'B	0.498(8)	3410.39	3931.92	5324.8	85
H1C	0.5	6245(2)	2500.0(2)	7026(2)	137
H1D	0.5	5125(2)	1806.9(4)	7000(2)	137
H1E	0.5	5125(2)	3193.1(4)	7000(2)	137
H2C	0.5	2387.3(19)	2500.0(2)	1667(2)	107
H2D	0.5	2210.0(19)	3193.1(4)	3017(2)	107
H2E	0.5	2210.0(19)	1806.9(4)	3017(2)	107
H3C	1.0	1526.6(17)	4975.9(16)	3514(2)	112
H3D	1.0	1591.3(17)	5697.8(16)	4859(2)	112
H3E	1.0	2674.1(18)	5214.9(16)	4191(2)	112

[125] Bruker, APEX2 Software Package, Bruker AXS Inc., 5465, East Cheryl Parkway, Madison, WI 5317 (**2012**).

[126] G.M. Sheldrick, *Acta Cryst.,* **2015**, *71*, 3-8.

[127] O.V. Dolomanov, L.J. Bourhis, R.J. Gildea, J.A.K. Howard, H. Puschmann, *J. Appl. Cryst.,* **2009**, *42*, 339-341.

SYNTHETIC PATHWAY

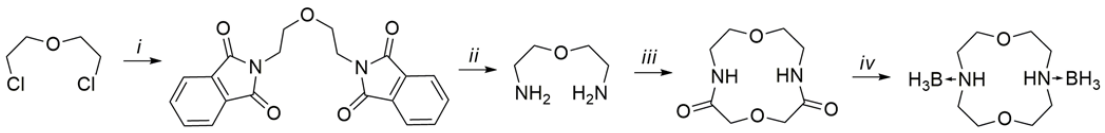

i. potassium phthalimide/DMF; *ii*. 1. NH_2NH_2/EtOH, 2. HCl, 3. NaOH; *iii*. diglycolyl chloride/benzene; *iv*. borane/THF

General notes

Chemicals and solvents were purchased from commercial suppliers and were used without further purification. Column chromatography was performed on silica gel 60 from Merck. For thin layer chromatography (TLC) aluminium backed silica gel was used. Room temperature ^{1}H and ^{13}C NMR spectra were recorded on a Bruker 300 instrument and were referenced internally to residual protio-solvent, and solvent resonances, respectively, are reported relative to tetramethylsilane (δ = 0 ppm).

Synthesis of 2-(2-aminoethoxy) ethylamine

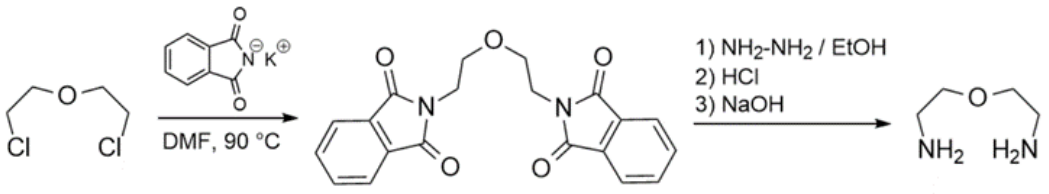

2-(2-aminoethoxy) ethylamine was prepared following the procedure reported in the literature [128].

1,5-dicloro-3-oxapentane (14.3 g, 0.10 mol) and potassium phthalimide (1.35 mol) were dissolved in DMF (100 ml) and heated at 90 °C for 6 h. The hot mixture was poured into crushed ice (500 g) and the precipitated white solid was filtered and washed with water. The solid (27.7g, 0.076 mol), was subsequently dispersed in a solution of hydrazine hydrate 50% (12 ml, 0.19 mol) in ethanol and refluxed for 4 hours to obtain a crude of 2'-oxydiethylamine. After cooling to room temperature, the mixture was filtered to remove insoluble solid and to the solution concentrated hydrochloric acid was added dropwise to adjust at pH 4. The mixture was reduced in volume by removing most of the water by roto-evaporation and which is finally neutralized with sodium hydroxide (50 g) and extracted on a continuous-extraction column with benzene for 48 h The solvent was removed to leave a yellow oil which was vacuum distilled (90 °C, 1 mmHg) to give pure 2-(2-aminoethoxy) ethylamine as a colourless oil to obtain. (6 g, 0.058 mol). The products were characterised by ^{1}H-NMR analysis and the chemical shift values correspond to those reported in the literature.

2-phthalimidoethyl ether: ^{1}H-NMR (300MHz, $CDCl_3$, 25 °C, TMS): δ 7.74-7.64 ppm (m, 8H, Ar-H), 3.84 ppm (t, J= 6 Hz, 4 H, O-CH_2), 3.72 ppm (t, J= 6 Hz, 4 H, N-CH_2).

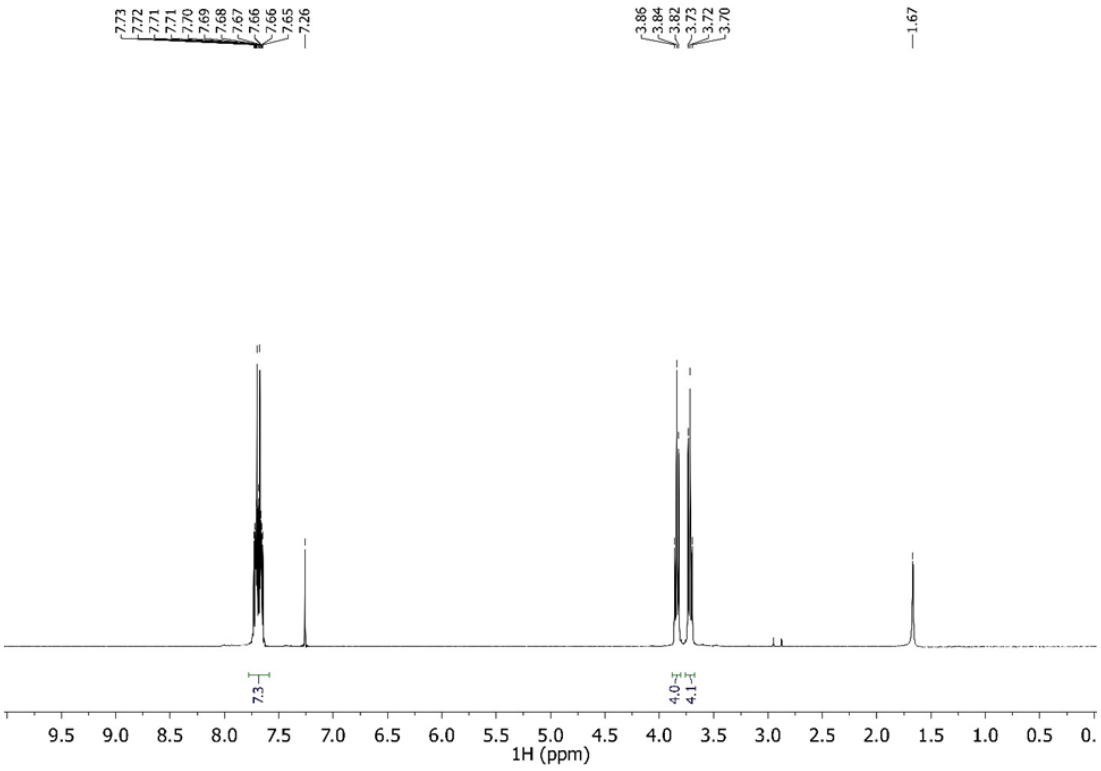

Figure 18. ^{1}H-NMR of 2-phthalimidoethyl ether in $CDCl_3$.

2-(2-aminoethoxy) ethylamine dihydrochloride: ^{1}H-NMR (300MHz, D_2O, 25 °C, TMS): δ 3.63 ppm (t, J= 6 Hz, 4 H, O-CH_2), 3.08 ppm (t, J= 6 Hz, 4 H, N-CH_2).

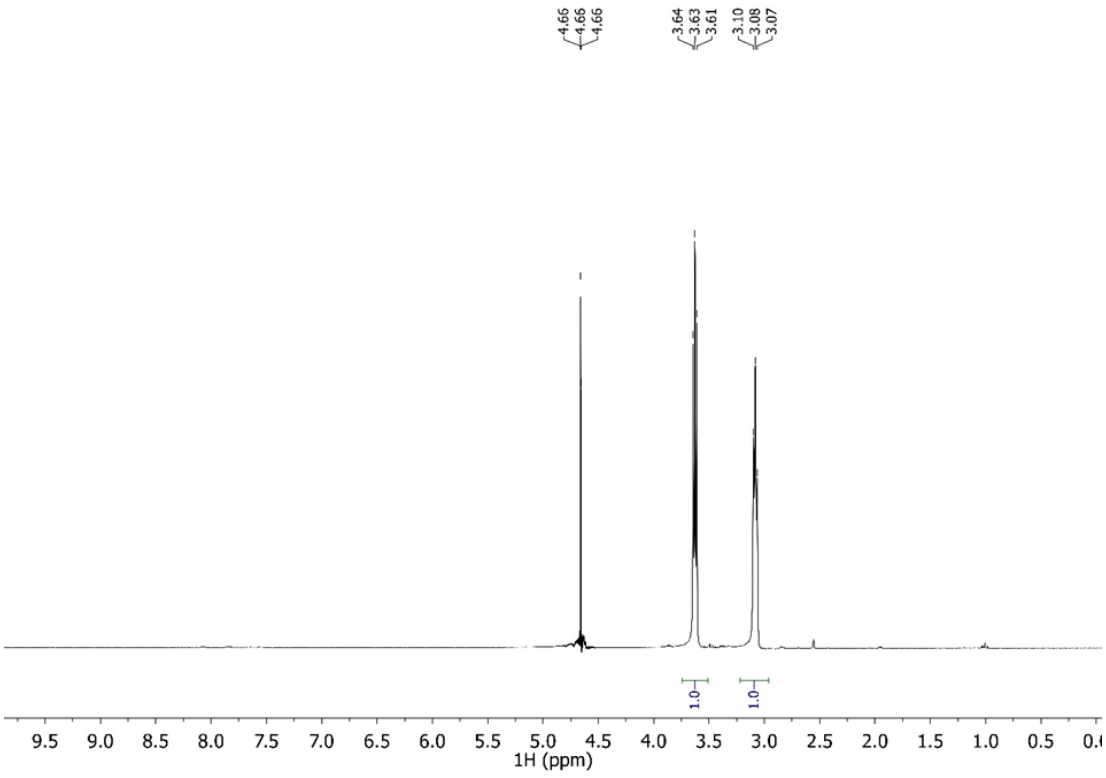

Figure 19. ^{1}H-NMR of 2-(2-aminoethoxy) ethylamine hydrochloride in D_2O.

2-(2-aminoethoxy) ethylamine: ^{1}H-NMR (300MHz, $CDCl_3$, 25 °C, TMS): δ 3.63 ppm (t, J= 6 Hz, 4 H, O-CH_2), 2.82 ppm (t, J= 6 Hz, 4 H, N-CH_2). ^{13}C-NMR (75MHz, $CDCl_3$, 25 °C, TMS): δ 73.10 ppm, 41.77 ppm

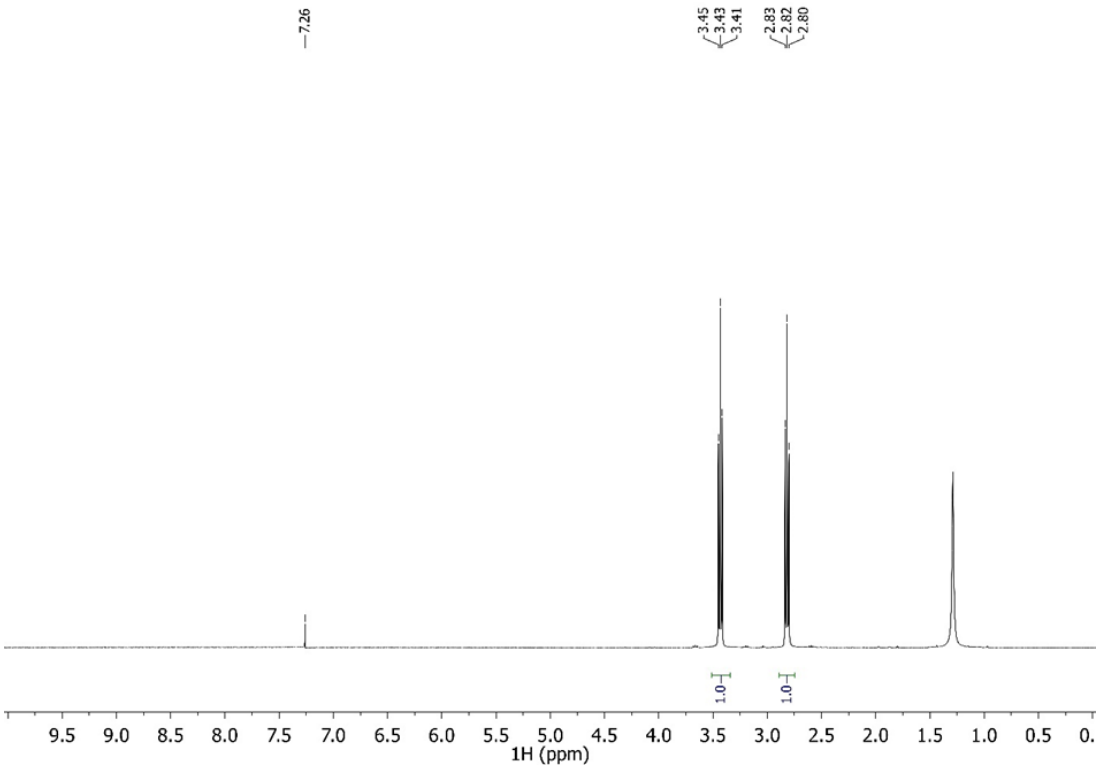

Figure 20. ^{1}H-NMR of 2-(2-aminoethoxy) ethylamine in $CDCl_3$.

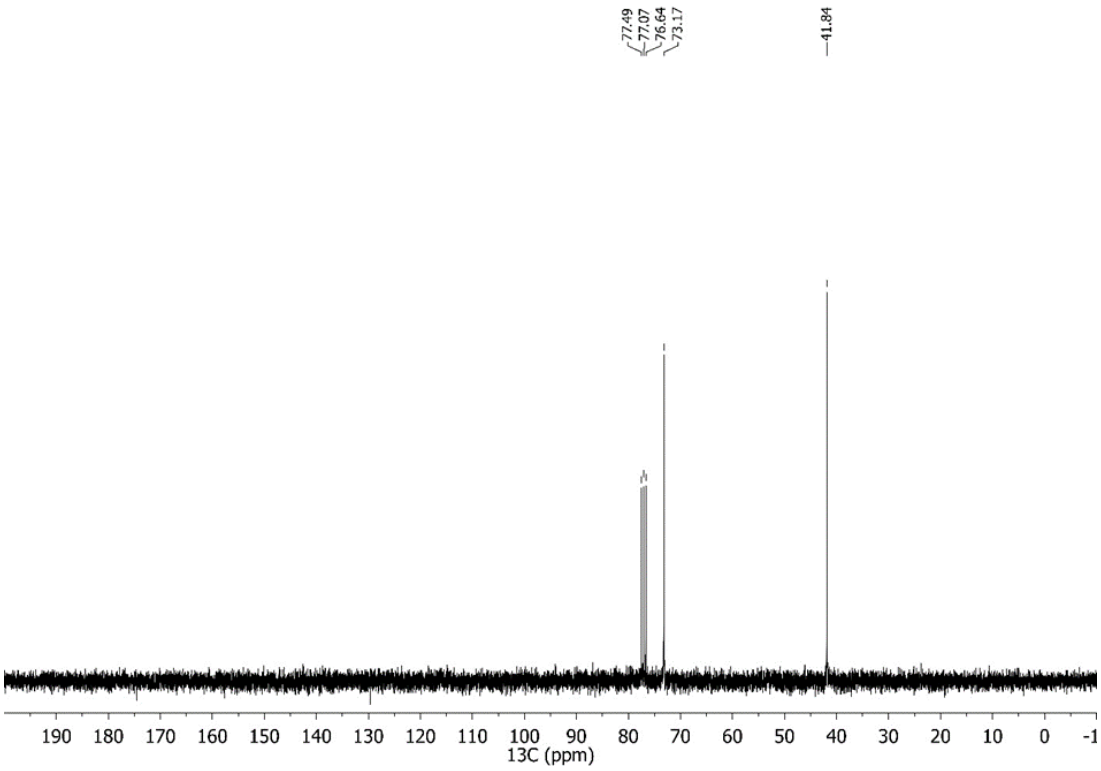

Figure 21. ^{13}C-NMR of 2-(2-aminoethoxy) ethylamine in $CDCl_3$.

Synthesis of 1,7-Dioxa-4,10-diazacyclododecane-3,11-dione

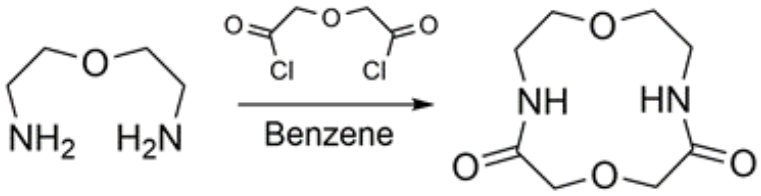

The macrocyclic diamide was obtained by condensation of the diamine (1.04 g, 10 mmol) and diglycolic acid (0.85 g, 5 mmol) in benzene (50 ml). The two reagents were added simultaneously and slowly dropwise over a period of 1 hours and the mixture stirred for 30 min. Afterwards the solid residue formed is filtered and washed with chloroform and the solution was

evaporated. The crude material was purified by chromatographic column using chloroform as eluent. a white crystalline solid (1.21 g, 6 mmol) was isolated after evaporating the solvent and the NMR data confirmed its structure and purity.

1,7-dioxa-4,10-diazacyclododecane-3,11-dione: ^{1}H-NMR (300MHz, $CDCl_3$, 25 °C, TMS): δ 7.08 ppm (s_{broad}, 2H, N-H), 4.10 ppm (s, 4H, CH_2-CO), 3.64 ppm (t, J= 6 Hz, 4 H, O-CH_2), 3.47 ppm (dt, J_1= 6 Hz, J_2= 6 Hz, 4 H, N-CH_2). ^{13}C-NMR (75MHz, $CDCl_3$, 25 °C, TMS): δ 169.92 ppm, 74.04 ppm, 68.70 ppm, 38.79 ppm.

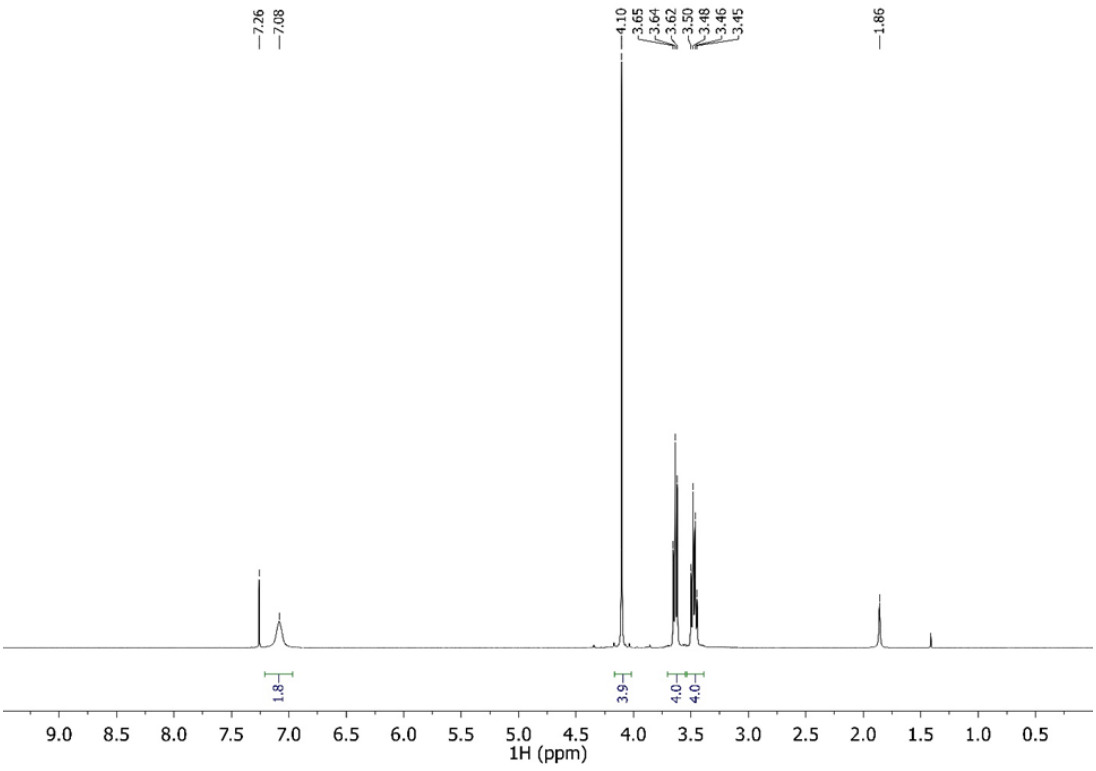

Figure 22. ^{1}H-NMR of 1,7-dioxa-4,10-diazacyclododecane-3,11-dione in $CDCl_3$.

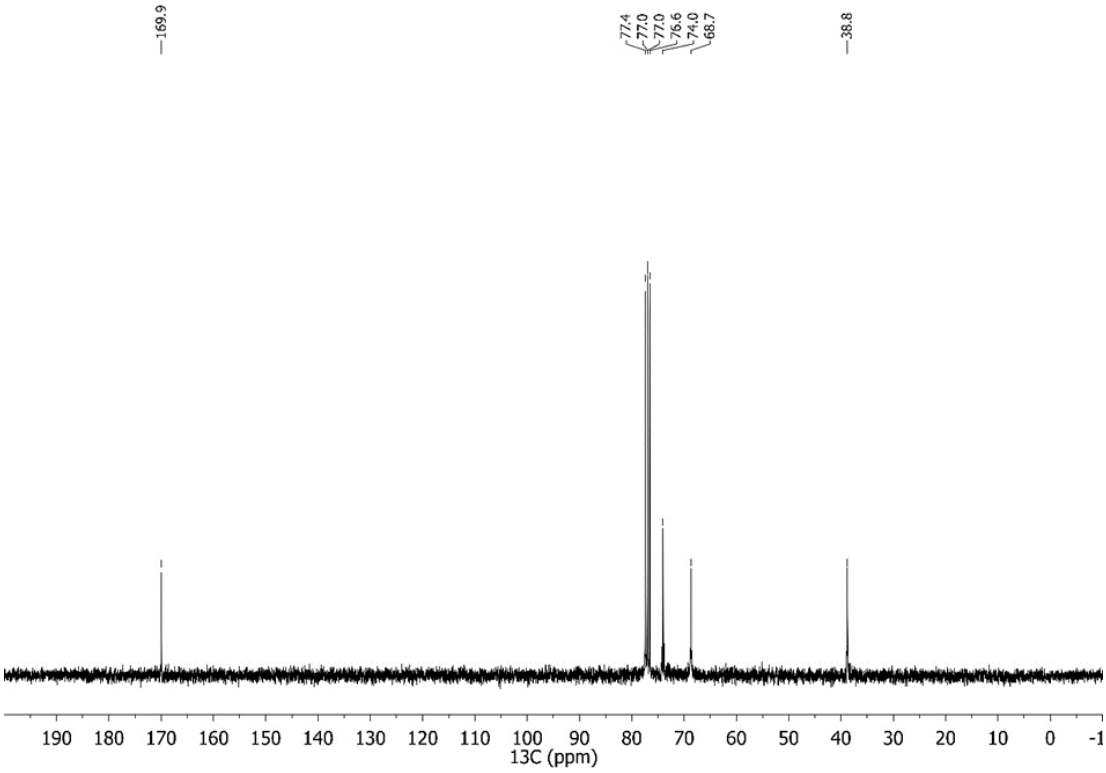

Figure 23. ^{13}C-NMR of 1,7-dioxa-4,10-diazacyclododecane-3,11-dione in $CDCl_3$.

Synthesis of diborane macrocycle

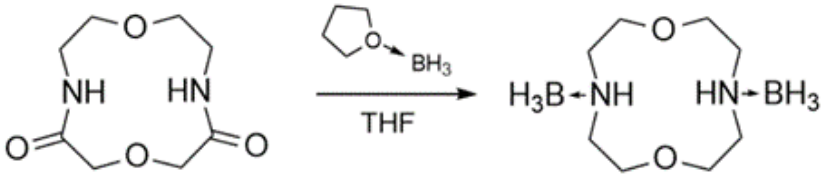

The reduction reaction of macrocyclic diamide was carried out with diborane in THF.

1,7-Dioxa-4,10-diazacyclododecane-3,11-dione (1g, 5 mmol) was dissolved in anhydrous THF (10 ml) in N_2 atmosphere in ice bath, 1 M borane tetrahydrofuran complex solution (1.9 ml, 20 mmol) was added slowly by

syringe and the mixture kept under stirring overnight at room temperature. Then methanol was added, and the mixture was reduced by a third of the volume. A crystalline product (0.65 g) was separated by precipitation from the mother liquors.

^{1}H-NMR (300MHz, $CDCl_3$, 25 °C, TMS): δ 3.82-3.76 ppm (m, 4H, CH), 3.65-3.58 ppm (m, 4H, CH), 3.16-3.08 ppm (m, 4H, CH), 2.92-2.82 ppm (m, 4H, CH).

The mono-borane derivative was also formed in a small percentage and co-crystallizes together with the diborane derivative. The ^{1}H-NMR spectrum shows, in addition to those indicated above, a multitude of proton signals due to the asymmetry of the mono-substituted macrocycle.

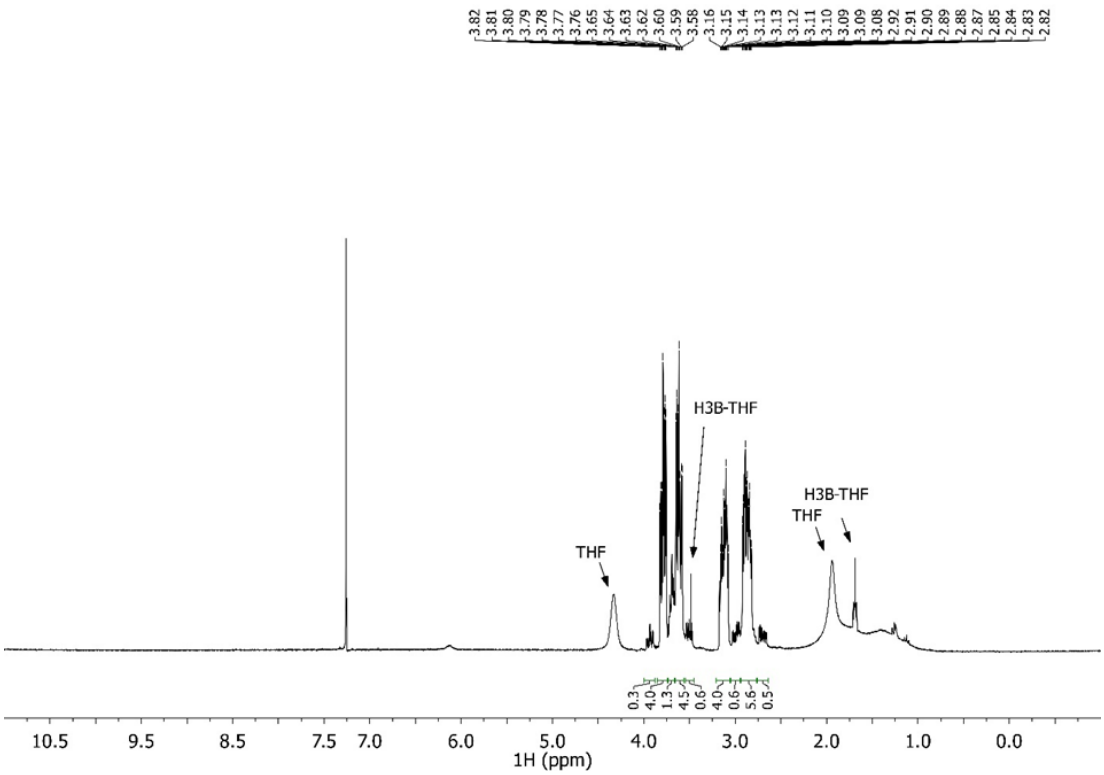

Figure 24. ^{1}H-NMR of macrocycle[12]-diborane in $CDCl_3$.

[128] B. Dietrich, J.M. Lehn, J.P Sauvage, J. Blanzat, *Tetrahedron,* **1973**, *29*, 1629.

CARTESIAN COORDINATES OF THE OPTIMIZED COMPLEX

Tag	Symbol	X	Y	Z
1	O	-1.0934020	3.6785630	0.0000000
2	O	1.0143750	0.1712860	0.0000000
3	N	0.5446290	2.3369140	-1.9701500
4	C	1.7592080	0.2801360	-1.2468820
5	H	2.7549750	-0.1572790	-1.1232650
6	H	1.2015760	-0.3258230	-1.9580410
7	C	0.5758430	3.8199310	-1.7861050

8	H	1.3874450	4.0804260	-1.1017120
9	H	0.7876440	4.2693410	-2.7573140
10	B	-0.0316380	1.9650520	-3.4518420
11	C	-0.7481800	4.3251760	-1.2464590
12	H	-1.5512420	4.0734330	-1.9375440
13	H	-0.7112610	5.4135840	-1.1230630
14	C	1.8803390	1.7050380	-1.7476660
15	H	2.4074600	1.7104310	-2.7033720
16	H	2.4513700	2.3141010	-1.0430690
17	H	0.7559630	2.4702850	-4.2322870
18	H	-1.1448760	2.4382270	-3.5375150
19	H	-0.1095270	1.9520280	-1.2768690
20	H	-0.0422110	0.7546550	-3.5437540
21	N	0.5446290	2.3369140	1.9701500
22	C	1.7592080	0.2801360	1.2468820
23	H	2.7549750	-0.1572790	1.1232650
24	H	1.2015760	-0.3258230	1.9580410
25	C	0.5758430	3.8199310	1.7861050
26	H	1.3874450	4.0804260	1.1017120
27	H	0.7876440	4.2693410	2.7573140
28	B	-0.0316380	1.9650520	3.4518420
29	C	-0.7481800	4.3251760	1.2464590
30	H	-1.5512420	4.0734330	1.9375440
31	H	-0.7112610	5.4135840	1.1230630
32	C	1.8803390	1.7050380	1.7476660
33	H	2.4074600	1.7104310	2.7033720
34	H	2.4513700	2.3141010	1.0430690
35	H	0.7559630	2.4702850	4.2322870
36	H	-1.1448760	2.4382270	3.5375150
37	H	-0.1095270	1.9520280	1.2768690
38	H	-0.0422110	0.7546550	3.5437540
39	O	-0.3911220	-2.1635370	-1.8387960
40	N	-2.2000580	-1.0247640	0.0000000
41	N	1.5235820	-3.2254600	0.0000000
42	B	-2.4967770	0.5758000	0.0000000
43	C	-2.7095660	-1.6681260	-1.2450000
44	H	-2.9932370	-2.7023140	-1.0251990
45	H	-3.6023630	-1.1314360	-1.5676300
46	B	3.1580690	-3.0910870	0.0000000
47	C	1.1022720	-3.9043920	-1.2626830
48	H	1.7988220	-3.5685400	-2.0289640
49	H	1.2496160	-4.9774500	-1.1308560
50	C	-0.3078720	-3.5978020	-1.7195250
51	H	-1.0653510	-3.9781280	-1.0260900
52	H	-0.4777250	-4.0698360	-2.6951500
53	C	-1.6477130	-1.6218350	-2.3262830

54	H	-1.4193370	-0.5966580	-2.6099910
55	H	-1.9796290	-2.1697050	-3.2148880
56	H	-1.1770130	-1.1272700	0.0000000
57	H	-3.7096690	0.6820450	0.0000000
58	H	3.5846360	-4.2302090	0.0000000
59	H	1.1455210	-2.2720320	0.0000000
60	H	3.4550820	-2.4874910	-1.0117350
61	H	-1.9956110	1.0223610	-1.0103720
62	O	-0.3911220	-2.1635370	1.8387960
63	C	-2.7095660	-1.6681260	1.2450000
64	H	-2.9932370	-2.7023140	1.0251990
65	H	-3.6023630	-1.1314360	1.5676300
66	C	1.1022720	-3.9043920	1.2626830
67	H	1.7988220	-3.5685400	2.0289640
68	H	1.2496160	-4.9774500	1.1308560
69	C	-0.3078720	-3.5978020	1.7195250
70	H	-1.0653510	-3.9781280	1.0260900
71	H	-0.4777250	-4.0698360	2.6951500
72	C	-1.6477130	-1.6218350	2.3262830
73	H	-1.4193370	-0.5966580	2.6099910
74	H	-1.9796290	-2.1697050	3.2148880
75	H	3.4550820	-2.4874910	1.0117350
76	H	-1.9956110	1.0223610	1.0103720

PBE1PBE *scf energy:* -1256.28600 a.u

CONCLUSION

The current study presents, as far as we know, the first organic system showing an AA-DD multiple dihydrogen bonds, based on a novel amine borane aza-coronand that was strategically synthetized to guarantee a stable self-assembly. A wide range (270) of DFT functionals were tested to explore the challenging arrangement of the dimer. Among all the functionals applied, the PBE1PBE produced the best agreement between theoretical data and X-ray analysis, providing adequate interaction geometry for our model. In particular, the attention was focused to investigate if the secondary electrostatic interactions (SEIs) influence this particular hydrogen interaction, by using a new vector force model. Through the scan of d_c value, an excellent correlation between the interaction energy and the total electrostatic force was found (R^2=0.91). Moreover, this approach allowed to extrapolate the contributions of the main interaction and the one due to the secondary electrostatic attractions. An accurate analysis showed that, in a range of 0.5 Å from the equilibrium geometry, F_{SEIs} represent 27% of the total forces included in our model. Energy decomposition analysis (EDA) illustrated that in the long-range regime the dihydrogen bond is determined by an interplay of electrostatic and other interaction components (dispersion, charge transfer effect, etc.). Finally, NCI surface illustrated which the hydrogens frontier, involved in the multiple dihydrogen bond, interact symmetrically confirming the line joining C_1 and C_2 as the correct direction along which to calculate the

electrostatic forces. In summary, the importance of the work lies in highlighting that in AA-DD double dihydrogen bonded system, secondary electrostatic interactions play a fundamental role. This evidence can give meaningful understanding for controlling and tuning the properties of self-assembled systems based on multiple dihydrogen bond. Lastly, the transferability of the model proposed above makes it also applicable to other systems (double, triple, fourthly bonded) and other electrostatic interactions (hydrogen, dihydrogen, pnictogen etc.). This can be considered as a clear confirmation of the validity of Newtonian mechanics at the molecular level.

CHAPTER 2

NON-COVALENT CHEMISTRY

Self-organization in programmed structures implies the spontaneous association of molecules through intermolecular interactions[129]. The control over the aggregation process of molecular entities through non-covalent interactions, is a fundamental objective for the realization of new materials, and in general for modern chemistry[130]. Although biological macromolecules are largely composed of covalent bonds, the connections are not always continuous and many important structures, including multimeric proteins and DNA, must be considered "aggregates" and not just "molecules". Many biomolecules have properties that largely derive from their structure, and their specific functions are associated with non-covalent interactions[131]: that is, by hydrophobic, ionic or hydrogen bonding interactions. The detailed knowledge of the non-covalent bond, to use it in the design and preparation of new chemical entities, having the structural and functional complexity of biological macromolecules, requires a fundamentally different intellectual and technical strategy from that used in covalent and non-biological synthesis. In covalent synthesis, the bonds generated are mainly characterized by their enthalpy: in general, bonds and products, once formed, are kinetically stable (although they can be generated by reversible processes).

In non-covalent synthesis, the products are structures in equilibrium, they reflect a balance between enthalpy and entropy: the potential products of these syntheses must be evaluated in terms of thermodynamic minima in equilibrium mixtures. The main challenge is to predict and then influence the position of these equilibria to direct the association towards a specific aggregate.

Many molecular aggregate systems are known in the literature[132], the cyanuric acid-melamine aggregates of G. M. Whitesides[133], and the polypyridine-barbituric acid systems of A. D. Hamilton[134], are just a few examples (Figure 25).

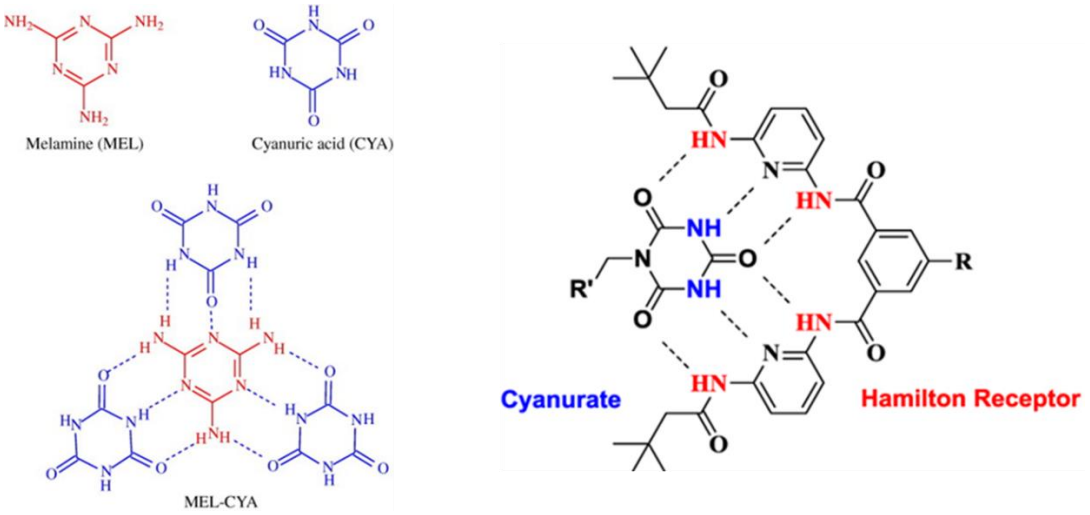

Figure 25. On the left Whitesides aggregates, on the right the Hamilton one.

Assembled multicomponent artificial systems can have applications based on host-guest molecular recognition in the cavity of the cages formed, or as arrays of multi-cromophoric light-harvesting systems[135]. A conclusion that

can be drawn from these numerous studies is that the nature of the bond (covalent, coordination or hydrogen) is just as important to the function of the array as the topology of the chromophores. Therefore, systems formed by the coordination of metal ions have substantially different photophysical properties than analogous systems formed by hydrogen bonding[136]. In virtue of the intimate correlation between structure and function, the spatial mutual organization of the chromophores is of primary importance in directing energy transfer processes and improving the performance of specific devices[137]. In this context, the exploitation of hydrogen bond (H-bond) networks appears particularly convenient with respect to other forms of supramolecular interactions because the possibility of not-chemically "contaminating" the system (as happens with the introduction of coordination metals) has important implications not only for the final geometry of the complexes but also for their electronic properties.

[129] J.-M. Lehn, *Angew. Chem., Int. Ed. Engl.* **1990**, *29*, 1304-1319.

[130] (a) H.-A. Klok, S. Lecommandoux, *Advanced Materials*, **2001**, *13*(16), 1217-1229. (b) Y. Li, T. Liu, H. Liu, M.-Z. Tian, Y. Li, *Accounts of Chemical Research*, **2014**, *47*(4), 1186-1198. (c) S. Yagai, T. Kinoshita, M. Higashi, K. Kishikawa, T. Nakanishi, T. Karatsu, A. Kitamura, *Journal of the American Chemical Society*, **2007**, *129*(43), 13277-13287. (d) W. Decheng, S. Kotaro, K. Masami, *Macromolecules* **2006**, *39*, 6882-6886.

[131] M. Chaplin, *Nat Rev Mol Cell Biol* **2006**, *7*, 861–866.

[132] (a) P.Baxter, J. M. Lehn, A. DeCian, J. Fisher, *Angew. Chem., Int. Ed. Engl.* **1993**,*28*, 89. (b) J. M.Lehn, *Angew. Chem., Int. Ed. Engl.* **1988**, *27*, 89. (c) R. Ballardini, V. Balzani, M. T. Gandolfi, L. Prodi, M. Venturi, D. Philp, H. G. Ricketts, J. F. Stoddart, *Angew. Chem., Int. Ed. Engl.* **1993**, *32*, 1301. (d) J. F. Nierengarten, C. O. Dietrich-Buchecker, J. P. Sauvage, *J. Am. Chem. Soc.* **1994**, *116*, 375.

[133] G.M. Whitesides, E. Simanek, J. Mathias, C. Seto, D. N. Chin, M. Mammen, D. M. Gordon, *Acc. Chem. Res.* **1995**, *28*, 37-44.

[134] (a) A. D. Hamilton, *Advances in Supramolecular Chemistry*, Gokel, G. W., Ed.; **1990**, 1, 1. JAI Press LTD. London, England. (b) S. K. Chang, A. D. Hamilton, *J. Am. Chem. Soc.* **1988**, *110*, 1318.

[135] Ward, D. Michael, R. P. Raithby, *Chemical Society Reviews*, **2013**, *42*(4), 1619-1636.

[136] (a) C. M. Drain, F. Nifiatis, A. Vasenko, J. Batteas, *Angew. Chem., Int. Ed.* **1998**, *37*, 2344-2347. (b) R. V.Slone, J. T. Hupp, *Inorg. Chem.* **1997**, *36*, 5422-5423. (c) P. J. Stang, J. Fan, B. Olenyuk, *Chem. Commun.* **1997**, 1453-1454. (d) J. Fan, J. A. Whiteford, B. Olenyuk, M.D. Levin, P.J Stang, E. B. Fleischer, *J. Am. Chem. Soc.* **1999**, *121*, 2741-2752.

[137] (a) F. Biedermann, H.-J. Schneider, *Chemical Reviews* **2016**, *116*(9), 5216-5300.

PURPOSE OF THE WORK

The main objective of this work is the design and the computational studies of new chromophoric molecules of the BODIPY type (4,4-difluoro-4-bora-3a, 4a-diaza-s-indacene) functionalized with distyryl groups and connected in meso a selected groups to favor the complementary formation of a triple hydrogen bond (Figure 26).

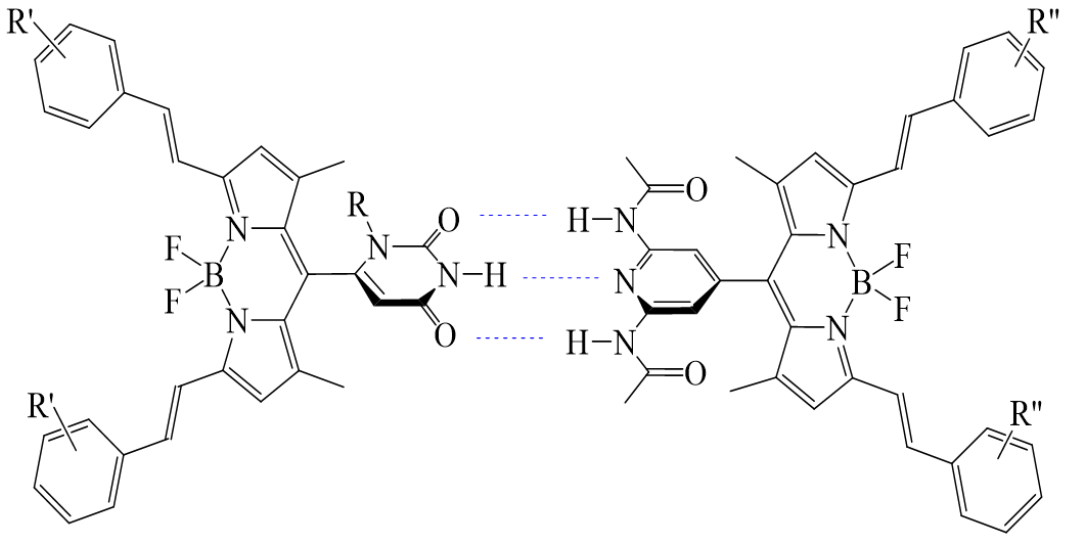

Figure 26. Representation of the complementary BODIPY heterodimer system.

The synthesis and spectroscopic characterization of the complementary derivatives BODIPYs have been the subject of my master's thesis study[138]. BODIPY molecules have been selected as chromophoric building blocks because they are relatively easy to functionalize and present highly promising chemical and photophysical properties. Moreover, these

chromophores have been widely exploited as excellent antenna systems and electron-donor and electron-acceptor molecules in constructing artificial photosynthetic models as flexible platforms to study both energy and charge transfer processes.

[138] a) M. Trapani, M.A. Castriciano, E. Collini, G. Bella, M. Cordaro, *Org. Biomol. Chem.* **2021**, *19*(37), 8118-8127. b) M. Trapani , M. A. Castriciano , J. A. A. W. Elemans , A. Nicosia , P. Mineo , M. Cordaro, *Synlett*, **2021**, *32*(17), 1714-1718.

WHY THE BODIPY?

The ever-increasing interest in BODIPY derivatives is motivated by the particular photochemical properties, their potential use as components of photonic devices on the nanometer scale and as new functional materials[138]. The chemical-physical properties (luminescence, redox, electronics, etc.) of these chromophores can be modified and fine-tuned by means of targeted functionalizations[139]. BODIPYs have high molar extinction coefficients (ε> 50,000 $cm^{-1}M^{-1}$), high quantum yields of fluorescence (which often approaches 1.0, even in water), spectra relatively insensitive to the polarity and pH of the solvent, width of limited bandwidth, relatively long excited state life time (typically 5 ns or more). The fluorescence of alkyl-substituted BODIPY solutions is usually green (absorption-emission maxima around 500-520 nm) but in the presence of substituents conjugated to the central core, both the absorption and emission spectra show a strong bathochromic effect, with possible maximum emissions exceeding 750 nm for some derivatives[140].

To induce a bathochromic shift of excitation and emission in fluorophores, three general strategies are commonly used:

1. The electron density of the dipyrromethenic scaffold is increased, eg. introducing electron-rich substituents such as methoxy or similar groups, preferably in the α or ß positions (Figure 27).

2. The conjugated π system extends.
3. The planarity of the ligand is favored by ringing aromatic / non-aromatic systems to the central structure.

From a synthetic point of view, the main attraction towards BODIPYs is their wide versatility of functionalization [in the positions of the pyrrole C ring (1, 2, 3, 5, 6, 7), central 8- or meso-position, and the boron atom (position 4)] (Figure 27).

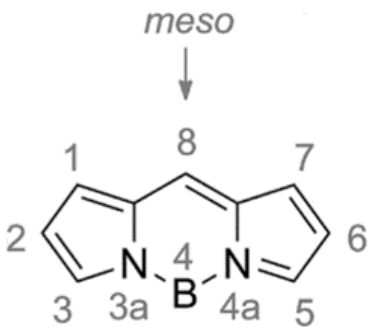

Figure 27. Representation of the "BODIPY core" and the assigned IUPAC numbering. Position 8 is more commonly referred to as meso. Positions 3,5 are indicated as α and positions 1,7 are indicated as β . Common BODIPYs have two fluorine atoms bonded to boron in position 4. All positions are sites of possible functionalization.

The enormous possibility of the synthetic paths of the family of these fluorophores allows the creation of a specific structure based on the chemical-physical characteristics of the desired dye.

[138] (a) A. Loudet, K. Burgess, *Chemical Reviews*, **2007**, *107*(11), 4891-4932; (b) G. Ulrich, R. Ziessel, A. Harriman, *Angewandte Chemie, Int. Ed*. **2008**, *47*(7), 1184-1201; (c) R. Ziessel, G. Ulrich, A. Harriman, A., *New Journal of Chemistry*, **2007**, *31*(4), 496-501; (d) J. Karolin, L. Johansson, L. Strandberg, T. Ny, *J. Am. Chem. Soc.,* **1994**, *116*(17), 7801-6.

[139] A. Burghart, H. Kim, M. B. Welch, L. H. Thoresen, J. Reibenspies, K. Burgess, F. Bergstroem, L. B. Johansson, *J. Org- Chem.*, **1999**, 64(21), 7813-7819; (b) S. Erten-Ela, M. D. Yilmaz, B. Icli, Y. Dede, S. Icli, S E. U. Akkaya, *Organic Letters*, **2008**, 10 (15), 3299-3302.

[140] P. De Bonfils, L. Péault, P. Nun, V. Coeffard, *Eur. J. Org. Chem*. **2021**, 1809 –1824.

SPATIAL COMMUNICATION BETWEEN CHROMOPHORES

Spatial communication between chromophores through non-covalently bridges is important for different types of phenomena, such as energy transfer, electron transfer, superexchange spin coupling etc[141]. In many instances, the chemical nature of the interaction geometry determines how the two connecting parts communicate[142]. Such communications are salient for nanoscale information transfer and for elaborate functionalities in natural and artificial systems[143]. While some of these communications result from structural rearrangements such as conformational changes, certain types of communication are mediated mainly or partially via the electronic system. Taking advantages of the studies carried out on natural and artificial systems, some structural aspects seem to be necessary to favor spatial communication[144]. First of all, a strong interaction between molecules is required to obtain a highly rigid system. It is necessary to maintain an appropriate distance and avoid conjugation between the two chromophores. Furthermore, the planes of the chromophores must be kept as coplanar as possible, and the noncovalent bond should ensure sufficient rigidity and stability of the binary system[145]. With this in mind, hydrogen bonds are particularly suited because they guarantee a most accessible control of orientations, distances, and geometries.

[141] C. Herrmann, *J. Phys. Chem. A,* **2019**, *123*(47), 10205–10223.

[142] V. May, O. Kühn, Charge and Energy Transfer Dynamics in Molecular Systems; Wiley VCH: Weinheim, 2011.

[143] H. J. Wörner, C. A. Arrell, N. Banerji, A. Cannizzo, M. Chergui, A.K. Das, P.Hamm, U. Keller, P. Kraus, E. Liberatore, *Struct. Dyn*. **2017**, *4*, No. 061508.

[144] X. Shi, K. M. Barkigia, J. Fajer, C. M. Drain, *J. Org. Chem*. **2001**, *66*(20), 6513–6522.

[145] E. Fresch, N. Peruffo, M. Trapani, M. Cordaro, G. Bella, M. A. Castriciano, E. Collini, *J. Chem. Phys*. **2021**, *154*, 084201.

ADA – DAD PATTERN

Inspired by nature macrobiomolecules e.g., DNA, where two strands of nucleotides are held together by hydrogen bonding between their base pairs, we tried to extend the concept of designing heterocycles to pair with different multiple hydrogen bonding motifs to the BODIPY scaffold. The design and construction of supramolecular building blocks (SBB) that can be utilized for establishing intermolecular pattern preferences and a relative ranking of competing supramolecular synthons play an important part when it comes to developing transferable strategies for deliberate assembly of molecular aggregates. Such SBB offer two or more electronically and geometrically different binding sites, which can be probed in systematic structural studies using a series of molecular architecture substituted with competing chemical functionalities. When an aromatic N-heterocycle is functionalized with some amine groups, an incident uracil ring displays a preference for the heterocycle as long as this moiety is sufficiently accessible. Such complementary units can also act as synthetic platforms for the construction of extended chromophores with predictable electronic and optical features. To this aim, we designed *meso*-substituted BODIPY bearing 2,6-diacetoamido pyridine (**DAAP- BDP)** as the donor–acceptor–donor (DAD) and uracil (imide) (**URA- BDP**) as the acceptor–donor–acceptor (ADA) moieties, both compounds were also subjected to distyrilation to get **DAAP-DS-BDP** and **URA-DS-BDP** (Figure 28).

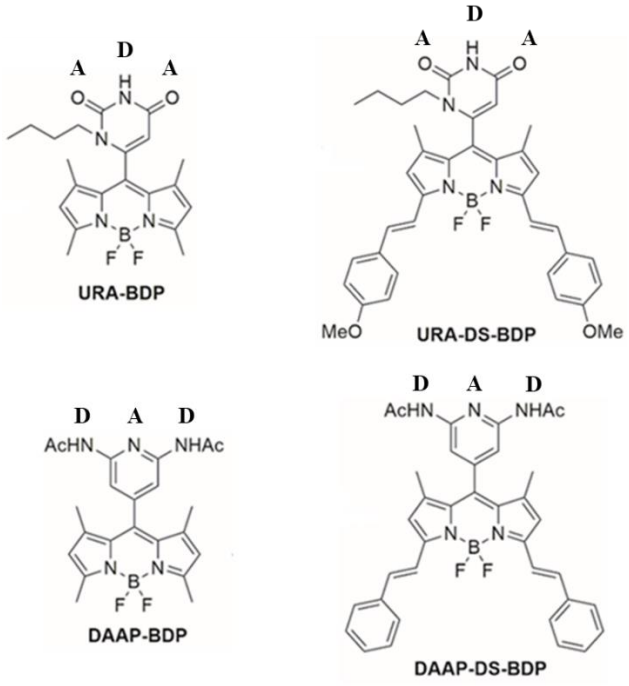

Figure 28. On the top: uracil bodipy (URA-BDP) and uracil distyryl bodipy (URA-DS-BDP). On the bottom: diacetoamido pyridine bodipy (DAAP-BDP) and diacetoamido pyridine distyryl bodipy (DAAP-DS-BDP).

THE GEOMETRY INTERACTION

Once it is verified that the dimer effectively forms in solution (confirmed by downfield shift of the diagnostic peaks referred to the interacting hydrogens of DAAP and URA) (Figure 29), the structure and the electronic properties of the monomers and dimer have been preliminarily investigated through quantum mechanical calculations. Also in this case, the DFT method proved to be

crucial for studying the structural aspects of the single chromophores and providing a useful tool for an accurate analysis of complex chemical species. The specific aim was to gain more insight into the geometry of the dimer and verify the presence of possible modifications in the structure and electronic proprieties promoted by the establishment of hydrogen bonds. In this study, I modelled **DAAP-BDP**, **URA-BDP**, **DAAP-DS-BDP**, **URA-DS-BDP** and their corresponding dimers. All the structures (BODIPYs, distyryl BODIPYs and dimers) were fully optimised without symmetry constraints in chloroform by means of the PCM method using *Gaussian-09* package[105]. The conformational preferences and the electronic features of the aforementioned molecules were analysed by CAM-B3LYP[75] (that combines B3LYP[69,38] with the Coulomb-attenuating method) with a 6-311++G(d,p) basis set, two-electron integrals and their derivatives were calculated using an ultra-fine grid option. Non-covalent interaction (NCI) mapped surfaces were generated by the *Multiwfn* code[146] with a high-quality grid for electron density and visualized using *VMD*[147].

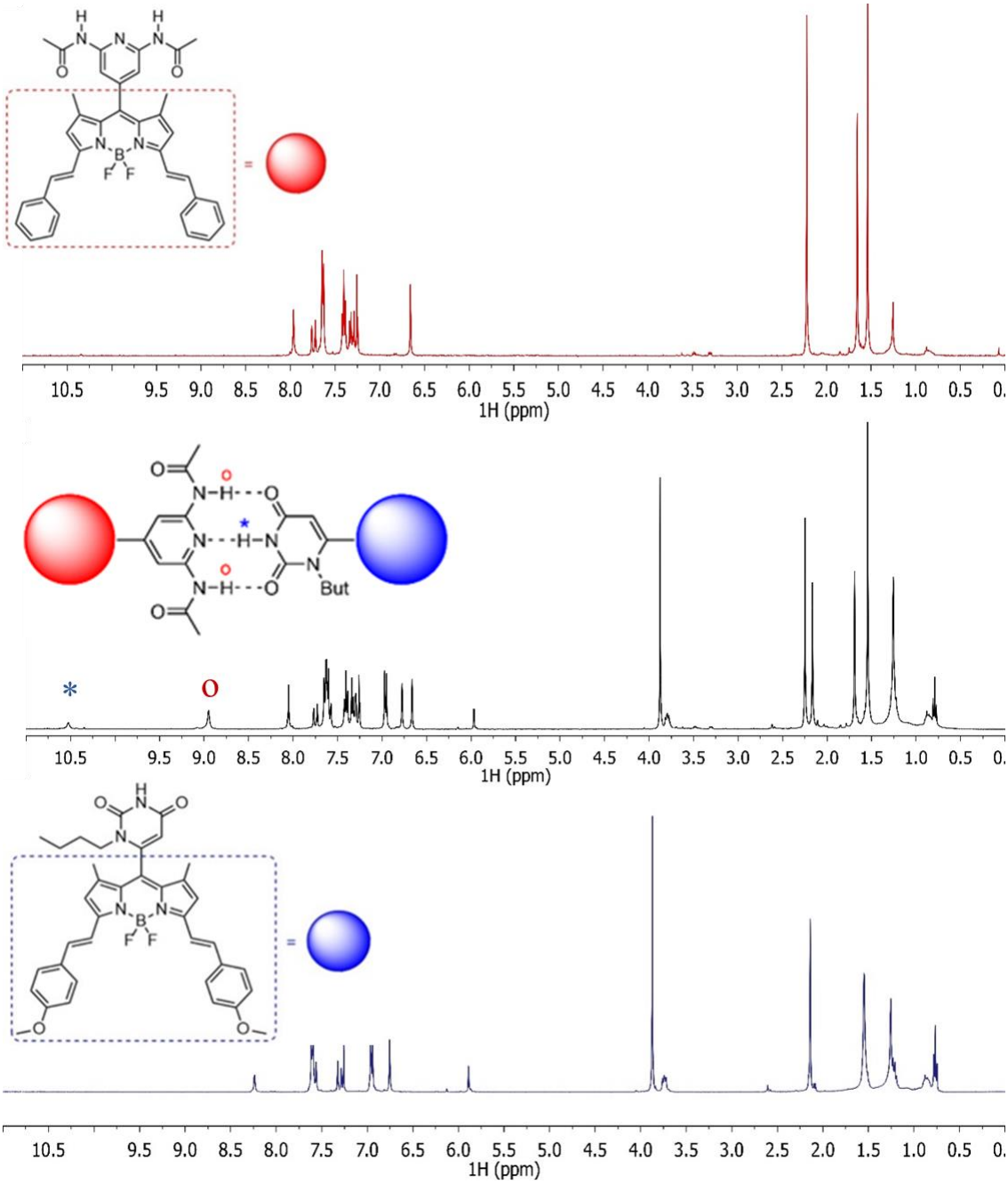

Figure 29. ^{1}H-NMR ($CDCl_3$) of DAAP-DS-BDP, DS-BDP-dimer and URA-DS-BDP, respectively (o NHDAAP; * NHUracil).

Theoretical calculations revealed that the heterocyclic scaffolds linked to the meso positions are perpendicular to the BODIPY core and promote a

triple hydrogen bond based on ADA-DAD pattern (Figure 30). This hydrogen bonding network is further reinforced by the sharing of the methyl hydrogen atoms located on the DAAP moiety. In this context, the arrangement of carbonyl groups is crucial to orient the methyl in the correct position and, at the same time, to generate an intramolecular hydrogen interaction. The optimized association of the two chromophores binary arrays by means of a triple hydrogen bond interaction also revealed the inter-chromophore distance; 1.5nm for distyryl BODIPY dimer and 1.3 nm for BODIPY dimer (Figure 31). This slight difference between the two aggregates is due to the introduction of stiryl functions. At this inter-chromophore distance, we do not expect that a significant electronic coupling between the two monomers can be established.

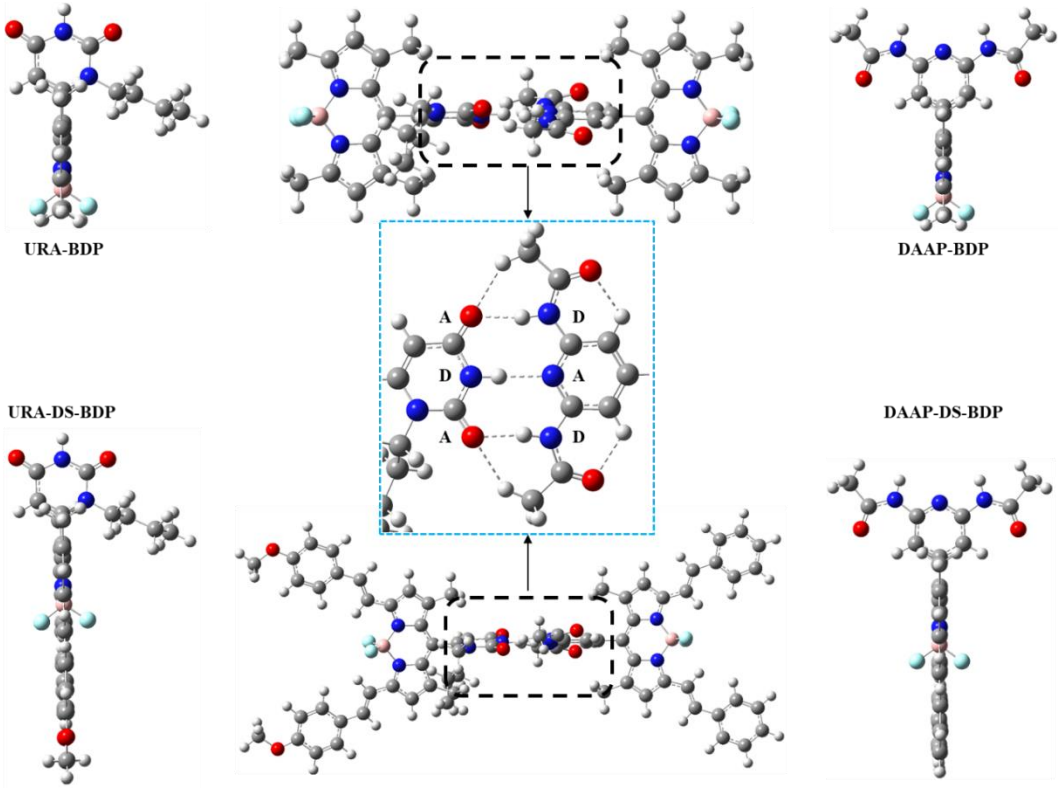

Figure 30. Optimized structures of single monomeric units and their corresponding dimers, central zoom clarifies how the chromophores are arranged to establish an ADA-DAD triple hydrogen bond.

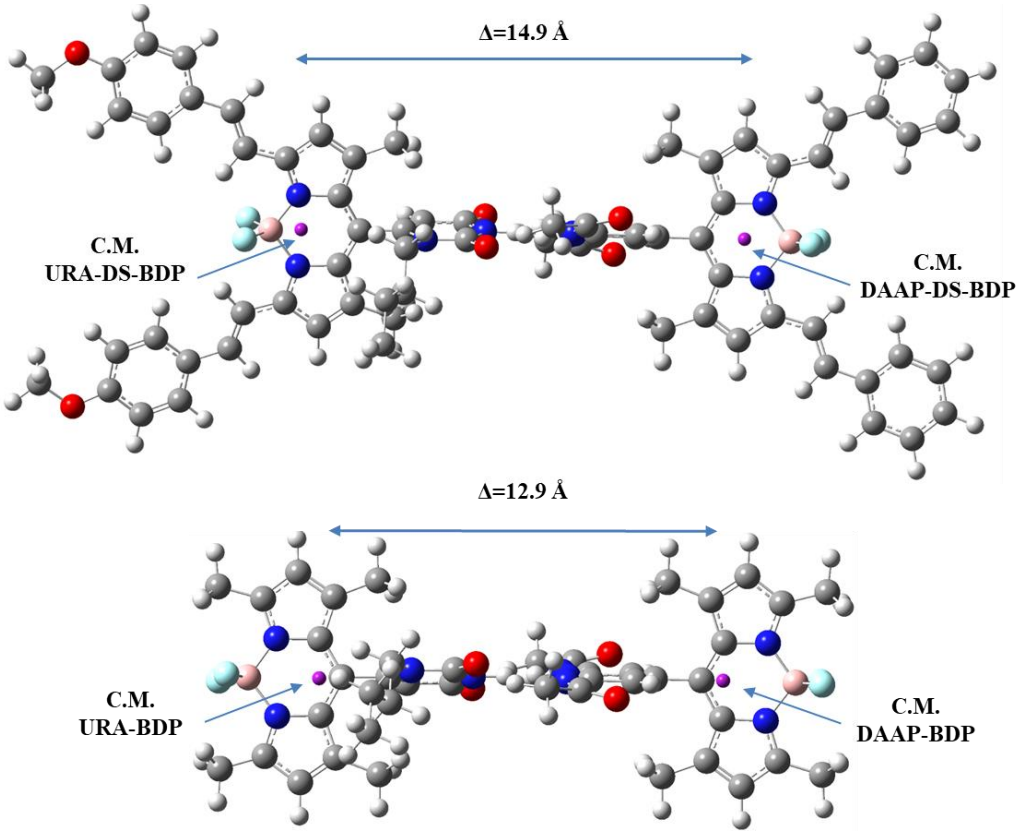

Figure 31. On the top: Association of the distyryl BODIPY dimer. On the bottom: the BODIPY dimer. As emerging from DFT calculations, the center of mass (C.M.) of the two molecular dimers and their distances are pinpointed.

[146] T. Lu, F. Chen, Multiwfn: A multifunctional wavefunction analyzer, *J. Comput. Chem.*, **2012**, *33*, 580-592.

[147] W. Humphrey, A. Dalke , K. Schulten, *J Mol Graph*, **1996**,*14*, 33-38.

ORBITAL ANALYSIS

The DFT computational results clearly suggest a separation of the frontier orbitals in the assembled systems. *De facto,* the HOMO orbital is centered on the **DAAP-BDP** while LUMO on the **URA-BDP** (Figure 32). Both types of orbitals are localized on the BODIPY core, thus highlighting no electronic communication with the groups in the *meso* position. This is most likely due to the perpendicularity of the two fragments. The introduction of distyryl functions on the pyrrole units, hence the extension of the aromaticity, do not cause appreciable changes in the electronic and structural relations between the BODIPY core and the *meso* moieties.

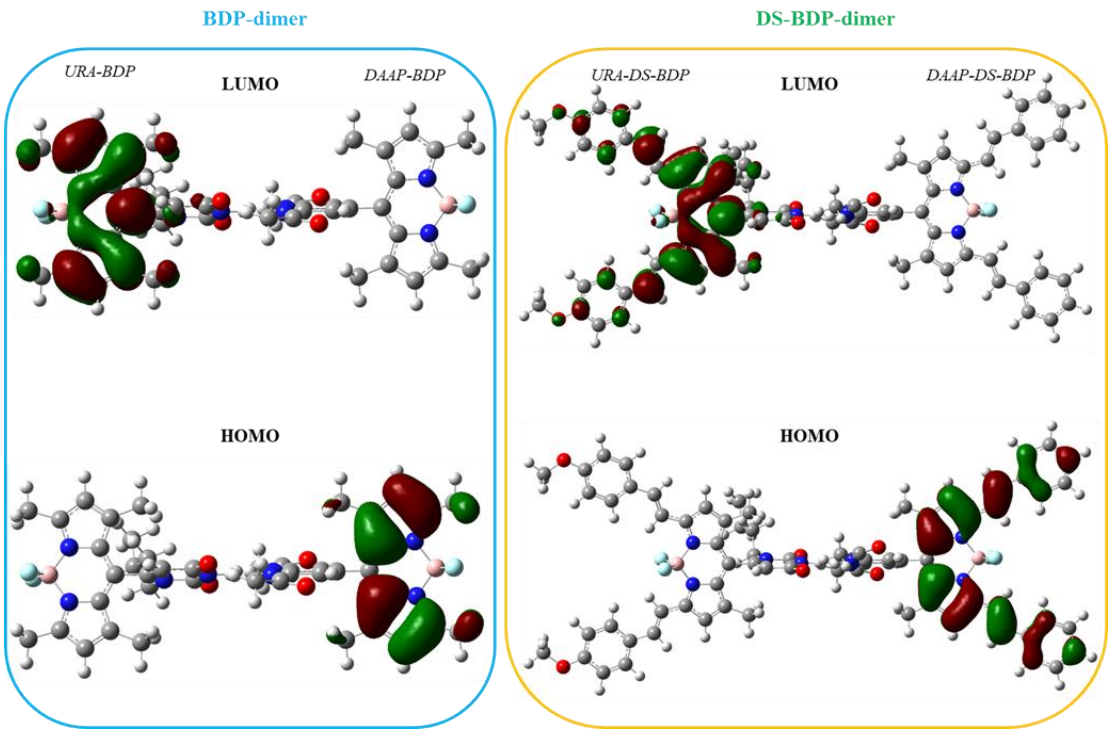

Figure 32. Frontier orbitals related to BODIPY and distyryl-BODIPY dimers.

Focusing on the single monomer molecules it is possible to see that the frontier orbitals are always located on the BODIPY units. This makes clear how the connectivity, between the chromophoric section and the H-bonding units, in *meso* position is regiochemically valid for isolating molecular regions with different functions (Figure 33, 34). The absence of delocalization among the two moieties in the dimers dyads is also confirmed analyzing the energy gap between HOMO and LUMO (Table 16). The high energy differences in the frontier orbitals should not allow a suitable Dexter resonance energy transfer between the choromophores in the assembled systems[148]. Finally, it should be noted that the introduction of distyryl arms leads to a thinning of the LUMO-HOMO energetic gap referred to the not functionalized derivatives (*) (Table 16).

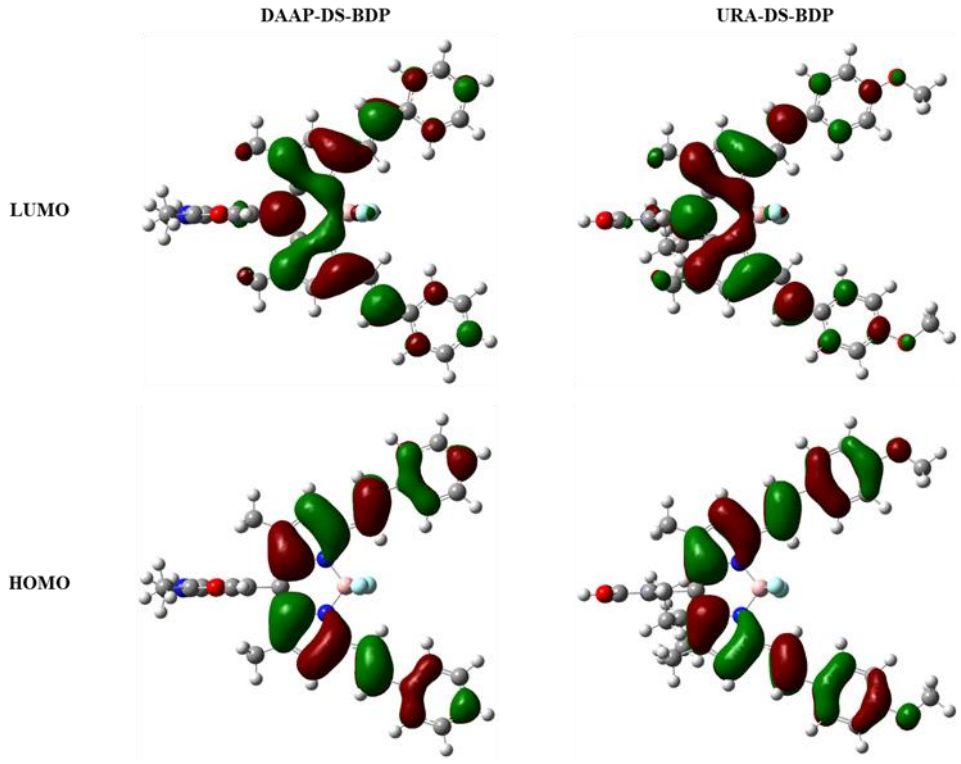

Figure 33. Computed frontier orbitals related to DAAP-DS-BDP and URA-DS-BDP.

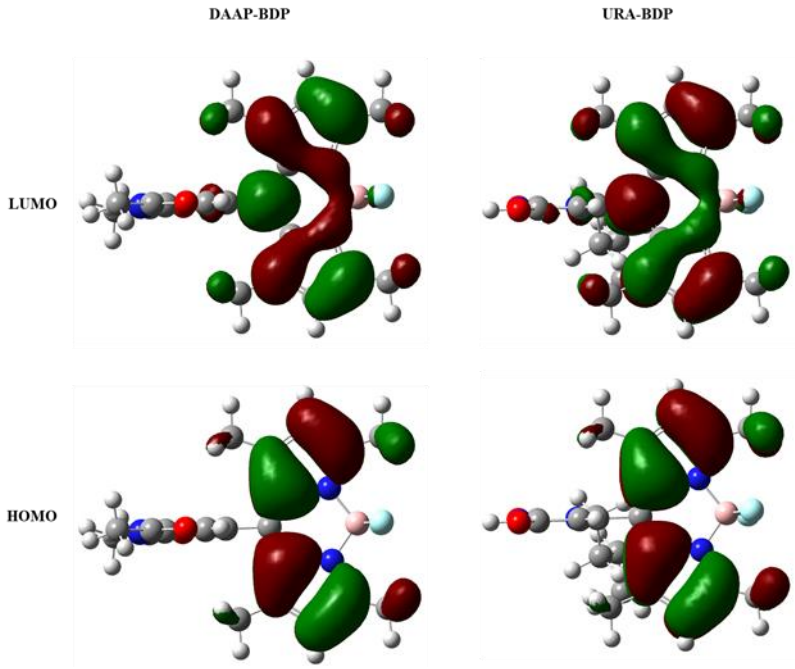

Figure 34. Computed frontier orbitals related to DAAP-BDP and URA-BDP.

Table 16. Electronic properties computed at DFT/CAM-B3LYP/6-311++G(d,p) level.

Chromophores	**$\Delta E_{LUMO-HOMO}$ (eV)**
DAAP-BDP	5.17
DAAP-DS-BDP	4.28*
URA-BDP	5.05
URA-DS-BDP	4.03*
BDP-dimer	4.68
DS-BDP-dimer	4*

[148] J. Otsuki, Y. Kanazawa, A. Kaito, D-M Shafiqul Islam, Y. Araki, O. Ito, *Chem. Eur. J.* **2008**, *14*, 3776-3784.

STAGGERED OR ECLIPSED APPROACH?

Despite the intermolecular distances and the binding energies in the BDP-dimer and DS-BDP-dimer remain quite similar (see Table 17) their mutual arrangement varies according to the presence of the distyryl arms. The rigid perpendicularity of the monomer units may lead to suppose that the chromophores assume an eclipsed configuration upon dimerization. Instead, the potential energy minimum provides for a staggered arrangement. To better visualize the interaction geometry of the dimers, it is convenient to consider the DAAP system placed at the intersection of the Cartesian axes: in the DS-BDP-dimer, the URA moiety shows a clockwise rotation, while in the BDP-dimer, an anti-clockwise rotation is found (Figure 35).

Table 17. Geometric and thermodynamic properties of the dimers. To determinate the binding energy (E_b) between two non-covalently bonded chromophores the following formula was used: $\mathbf{E_b = E_{dimer} (E_{URA} + E_{DAAP})}$ where $\mathbf{E_{dimer}}$ is the energy of the non-covalently bonded complex, $\mathbf{E_{URA}}$ and $\mathbf{E_{DAAP}}$ are the energies of two independently optimized fragments involved in the hydrogen interactions.

Chromophores	$\Delta E_{LUMO-HOMO}$ (eV)	$E_{binding}$ (kcal/mol)	C=O₁---H-N (Å)	N-H---N (Å)	C=O₂---H-N (Å)
BDP-dimer	4.68	-12.1	1.907	1.997	1.925
DS-BDP-dimer	4	-12.3	1.908	1.999	1.924

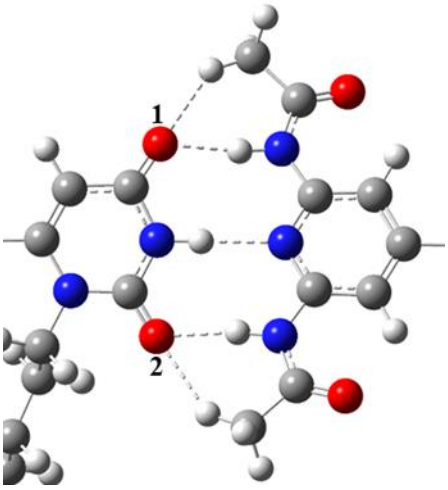

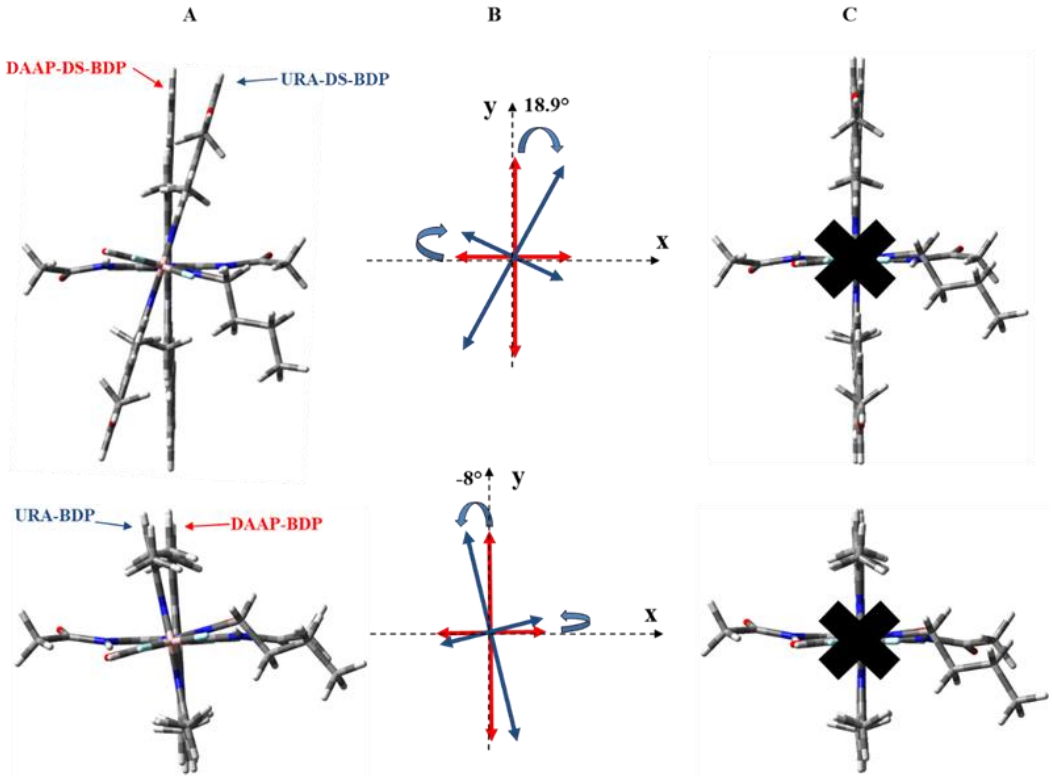

Figure 35. a) Topological approach of DS-BDP-dimer (top) and BDP-dimer (bottom) through tube display format; b) Clockwise (top) and anti-clockwise (bottom) deflection of URA chromophore; c) Ideal eclipsed arrangement not identified in the theoretical calculations.

We believe that the dimers adopt this particular layout in order to assume a suitable angle to maximize the electrostatic interactions between the URA ring and methyl hydrogens on the DAAP substituent (Figure 36). However, it remains unclear why the introduction of the distyryl functions causes an opposite rotation with respect to the non-functionalized BODIPY systems.

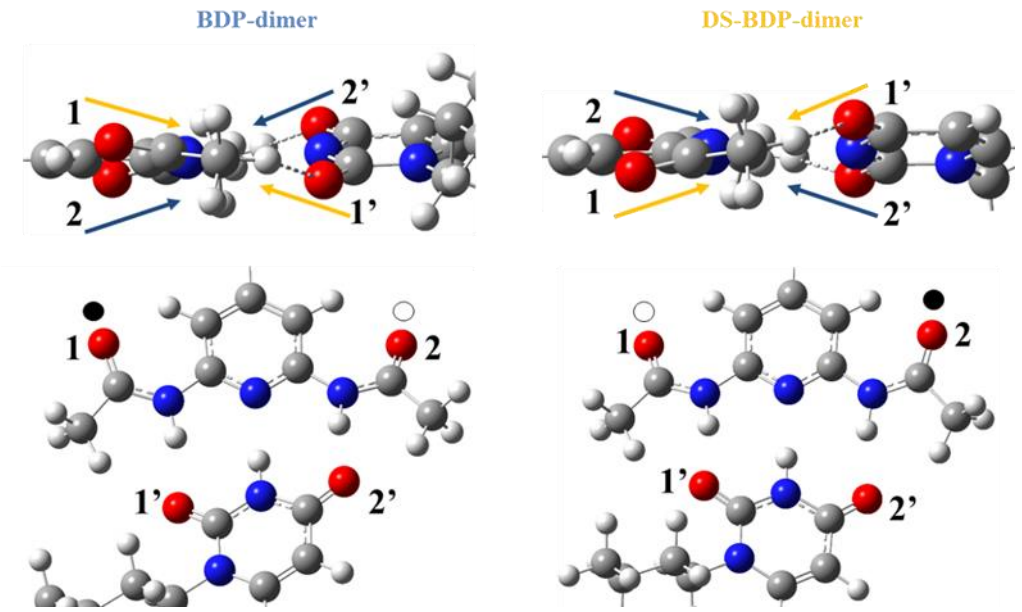

Figure 36. Perspective visions of interaction geometries. Labels 1 and 2 are referred to DAAP oxygen atoms while 1' and 2' to URA ones. The two dimers show an inverse topology. The black (white) circles indicate a shift of the carbonyl group above (below) the pyridine plane. In the top figures, imidic protons were omitted for a better view.

A BETTER LOOK AT THE TRIPLE HYDROGEN INTERACTION

From Figure 36 it is possible to argue that the phase shift of the amide groups, with respect to the plane identified by the pyridine, forces the URA moiety to deflect in order to generate a more stable electrostatic interaction. This aspect was definitively clarified by focusing on NCI mapped surfaces (Figure 37), from which it emerges clearly that the ADA-DAD pattern is well defined by the triple favorable electrostatic interaction (blue pseudo circular surfaces). These electronic effects are also accompanied by secondary repulsive electrostatic interactions (indicated by black stars). Intermolecular diagonally hydrogen interactions between DAAP methyl hydrogens and URA oxygens are finally confirmed and highlighted (black diamonds). Intramolecular six-membered hydrogen cycles on the DAAP ring are denoted by black triangles.

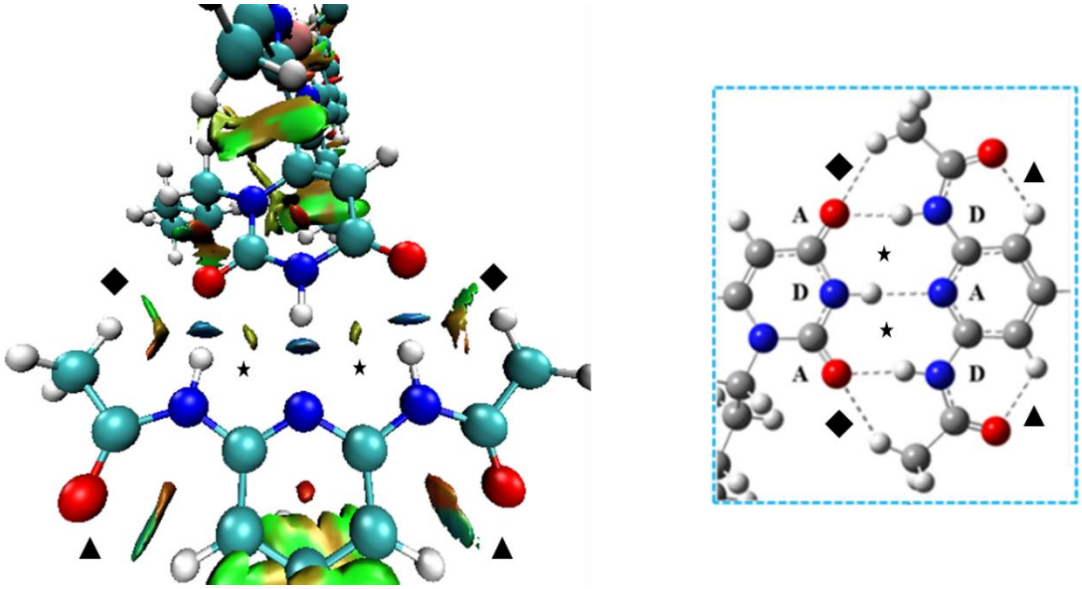

Figure 37. On the left: 3D view of non-covalent electrostatic interactions in the DS-BDP-dimer. The BODIPY dimer presents analogous NCI surfaces and ADA-DAD patterns. On the right: zoomed vision of the interaction geometry in the optimized DS-BD-DIMER.

The complementary H-bonding units, URA and DAAP, was also investigated focusing on their electrostatic potential energy maps. These colored surfaces illustrate the appropriate combination between the two heterocycle rings. Figures 38, 39 show how the acceptor-donor-acceptor/donor-acceptor-donor pattern is electronically established: in the DAAP systems an accumulation of positive charge (blue areas) is located on the N-H acetyl groups (donor motifs) while a depletion of positive charge (light green) is concentrated on the N-endocyclic pyridine atom (acceptor element). The URA scaffold presents a reverse colored codified situation: carbonyl groups bear an high density of negative charge (red shells) and

act as acceptor components, while the uracil N-H constitutes a spot of positive charges (light blue circle) and is referred to the donor part.

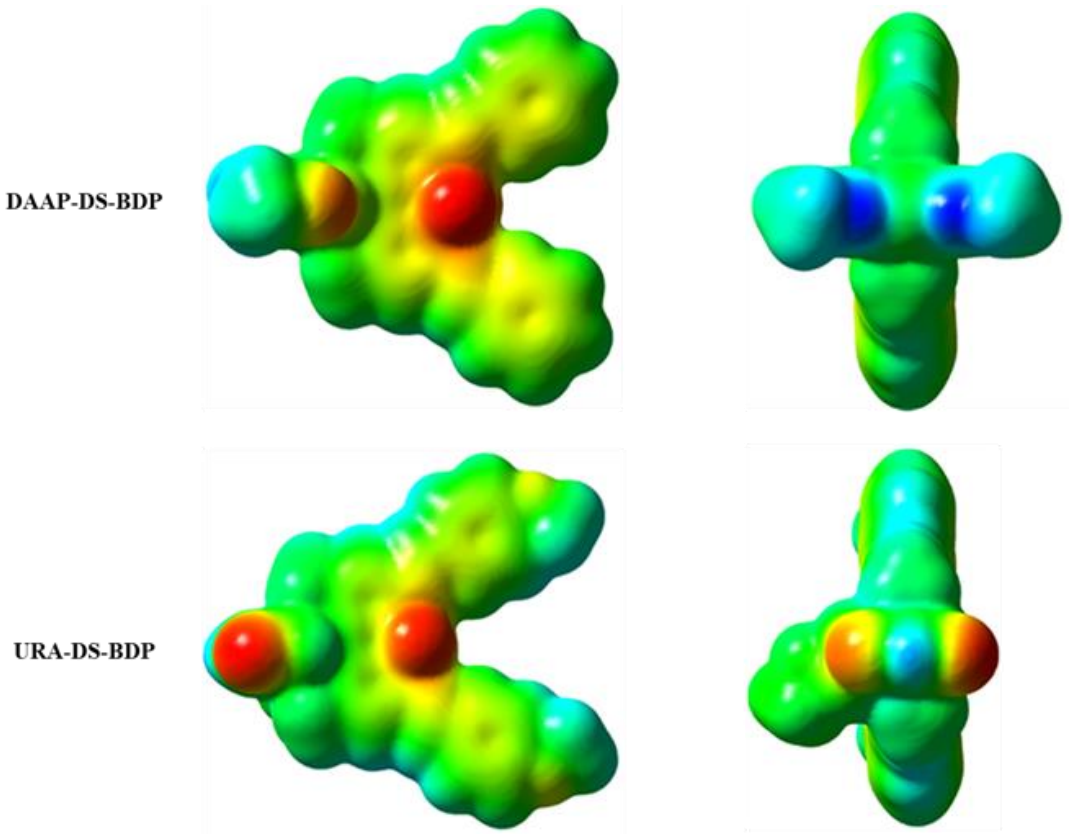

Figure 38. Different perspective views of the electrostatic potential energy maps of DAAP-DS-BDP and URA-DS-BDP. The frontal view shows the complementarity of the two chromophores by means of a triple hydrogen bond.

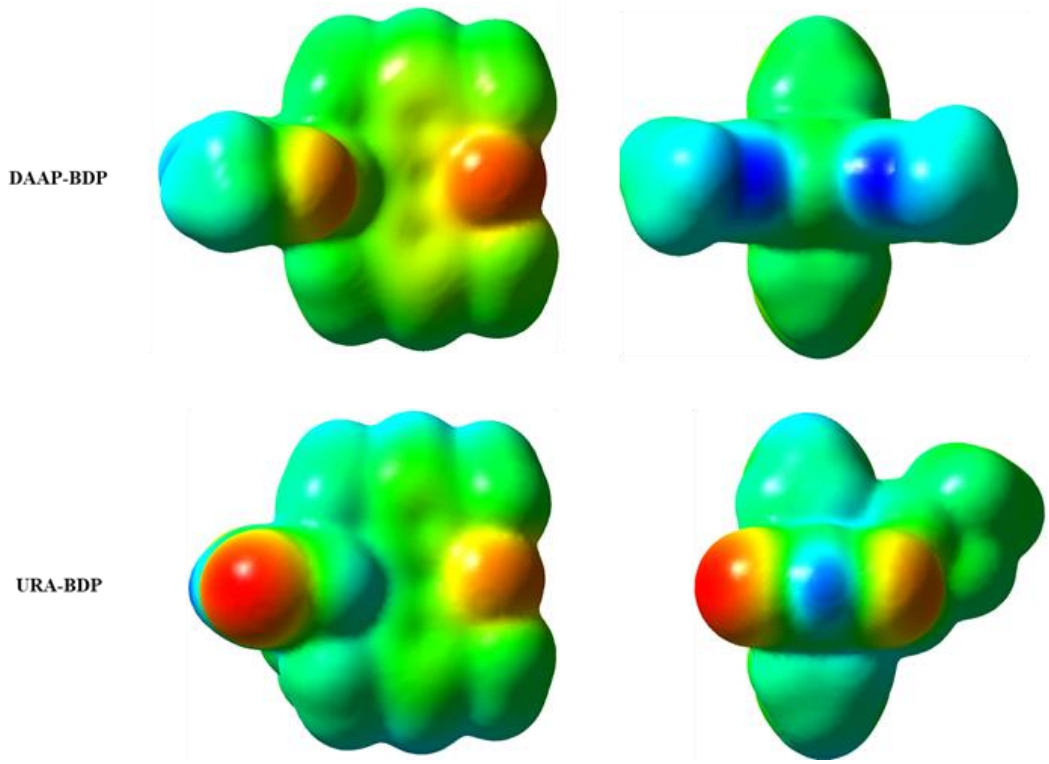

Figure 39. Different perspective views of the electrostatic potential energy maps of DAAP-BDP and URA-BDP, the frontal view shows the complementarity of the two chromophores by means of a triple hydrogen bond.

Finally, in the assembled systems it is clear that is not possible to distinguish accumulation and depletion charge areas in the H-bonding substituents, there is a sort of fusion between the electrostatic maps (Figure 40). However, with some visual effort, it is possible to discern a line of contact (dark blue arrows) which separates the chromophores.

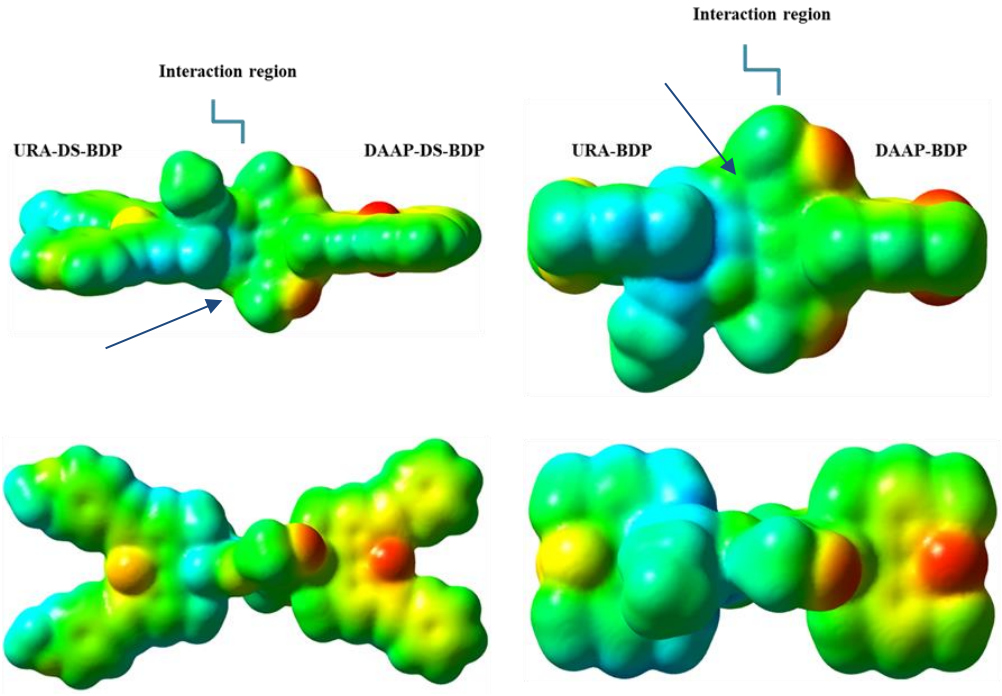

Figure 40. Different perspective views of the electrostatic potential energy maps of BDP-dimer and DS-BDP-dimers.

CONCLUSION

In summary, I reported the computational studies and theoretical analysis of new BODIPY derivatives functionalized with DAAP and URA moieties in meso position. The BODIPY moieties have been designed to have in *meso* position complementary donor–acceptor-donor/acceptor–donor-acceptor patterns able to induce a triple hydrogen bond through mutual interactions. Useful structural and electronic information both on single monomer units and on dimer derivatives in solutions have been obtained through computational data analysis. Various peculiarities concerning the effects of the interaction geometry on the stability of the H-bonded systems have been also investigated. The DFT calculation unveiled new meaningful understanding for controlling and tuning the properties of hetero-assembled chromophoric systems based on multiple hydrogen bonding. Lastly, this theoretical approach provides a better vision of the intimate correlation between structure and function, the spatial mutual organization of the chromophores is of primary importance in directing energy transfer processes and improving the performance of specific devices.

CARTESIAN COORDINATES OF THE OPTIMIZED DIMERS AND MONOMERS

Tag	Symbol	X	Y	Z
1	C	2.9050530	-1.1459150	0.0063750
2	C	1.5143090	-1.2062450	0.0066300
3	C	0.8294700	0.0001260	0.0001720
4	C	1.5153720	1.2058740	-0.0063690
5	C	2.9060710	1.1442910	-0.0062580
6	N	3.5810090	-0.0011110	0.0000250
7	H	1.0048490	-2.1556780	0.0121970
8	H	1.0067710	2.1557680	-0.0119630
9	N	3.7374990	-2.2696480	0.0149440
10	N	3.7395190	2.2672720	-0.0150070
11	H	4.7197470	-2.0349790	0.0132730
12	C	-0.6611270	0.0005920	0.0001060
13	C	-1.3433690	-0.0006310	1.2162480
14	C	-1.3431500	0.0021470	-1.2161490
15	N	-2.7413020	-0.0011180	1.2400550
16	N	-2.7410710	0.0025050	-1.2402330
17	C	-0.8881890	-0.0005700	2.5664790
18	C	-0.8876870	0.0033940	-2.5662730
19	C	-2.0256010	-0.0012360	3.3552230
20	C	-2.0249360	0.0046490	-3.3552540
21	C	-3.1486010	0.0040870	-2.5159640
22	C	-3.1490950	-0.0015970	2.5157010
23	C	0.5080920	0.0002950	3.0997950
24	C	-4.5824240	-0.0016610	2.9145100
25	C	0.5087110	0.0034970	-3.0992840
26	C	-4.5818530	0.0050800	-2.9150390
27	H	1.0671090	0.8772140	2.7698730
28	H	0.4821760	0.0045080	4.1895620
29	H	1.0654440	-0.8802470	2.7767850
30	H	1.0688490	-0.8721680	-2.7680030
31	H	0.4830430	-0.0022050	-4.1890490
32	H	1.0647940	0.8852740	-2.7773800
33	B	-3.6535250	-0.0010570	-0.0001780
34	H	-2.0556920	0.0056690	-4.4343110
35	H	-2.0565800	-0.0015120	4.4342750
36	F	-4.4782240	1.1384240	0.0015030

37	F	-4.4735250	-1.1441990	-0.0020200
38	C	3.3996930	3.5962460	-0.0112910
39	C	3.3964480	-3.5983030	0.0112770
40	C	4.5713520	4.5440000	0.0271810
41	H	5.5067700	4.0862650	-0.2929780
42	H	4.3477130	5.4011560	-0.6054980
43	H	4.6913850	4.9045150	1.0511720
44	O	2.2487190	3.9904770	-0.0158430
45	C	4.5671510	-4.5472380	-0.0271080
46	H	4.6845950	-4.9106180	-1.0503750
47	H	5.5037120	-4.0896640	0.2899040
48	H	4.3439860	-5.4025330	0.6082830
49	O	2.2451130	-3.9914810	0.0161390
50	H	4.7215550	2.0317030	-0.0135450
51	H	-4.6685070	-0.0105600	3.9999140
52	H	-5.0917670	0.8815620	2.5249800
53	H	-5.0962290	-0.8752660	2.5097330
54	H	-4.6677130	0.0004680	-4.0004870
55	H	-5.0953240	-0.8704130	-2.5138990
56	H	-5.0917030	0.8864420	-2.5220190

DAAP-BDP *SCF ENERGY:* -1501.51788 a.u

Tag	SymboL	X	Y	Z
1	C	-3.2945720	-1.4404160	-1.8566900
2	C	-1.8749780	-1.2395450	-1.6832020
3	C	-1.3984970	-0.6360620	-0.5787830
4	C	-3.6004470	-0.3503030	0.3520440
5	N	-4.0527880	-0.9616620	-0.7946920
6	H	-1.2092690	-1.5815570	-2.4606740
7	C	0.0730120	-0.4395240	-0.4273070
8	C	0.6657150	0.6789530	-1.0053320
9	C	0.8178240	-1.3978910	0.2571790
10	N	2.0433380	0.8800470	-0.8808690
11	N	2.1976910	-1.2399690	0.4022510
12	C	0.1352500	1.7631520	-1.7690770
13	C	0.4483930	-2.6163980	0.8983970
14	C	1.2094560	2.5776100	-2.0712250
15	C	1.6183920	-3.1508760	1.4056060
16	C	2.6778710	-2.2859240	1.0876470
17	C	2.3694710	2.0124810	-1.5149460
18	C	-1.2683400	2.0172180	-2.2163240

19	C	3.7589340	2.5367120	-1.5862760
20	C	-0.9022860	-3.2419970	1.0300420
21	C	4.1173180	-2.4502290	1.4227480
22	H	-1.9866060	1.9630620	-1.3976220
23	H	-1.3362220	3.0129970	-2.6541200
24	H	-1.5801590	1.2951980	-2.9731080
25	H	-1.3510630	-3.4451880	0.0565880
26	H	-0.8184190	-4.1859610	1.5677500
27	H	-1.5946120	-2.6057340	1.5850650
28	B	3.0189810	-0.0485650	-0.1282740
29	H	1.7155460	-4.0758400	1.9533550
30	H	1.1779780	3.4937670	-2.6410300
31	F	3.6177510	0.6421440	0.9393280
32	F	4.0252280	-0.4990360	-0.9958130
33	N	-2.2233260	-0.1877940	0.4359020
34	O	-3.8318220	-1.9669790	-2.8142030
35	H	-5.0570640	-1.0768170	-0.8568360
36	O	-4.3579180	0.0166230	1.2267120
37	C	-1.7204540	0.4603210	1.6644170
38	H	-0.6980390	0.1249190	1.8220950
39	H	-2.3261500	0.0805480	2.4857540
40	C	-1.7902300	1.9813670	1.6246340
41	H	-1.1460840	2.3581920	0.8252050
42	H	-2.8138000	2.2885850	1.3939450
43	C	-1.3581050	2.5935320	2.9543720
44	H	-0.3431140	2.2601750	3.1953490
45	H	-2.0054540	2.2156770	3.7524790
46	C	-1.4036040	4.1175030	2.9379390
47	H	-0.7399860	4.5225300	2.1695160
48	H	-2.4142020	4.4780340	2.7291410
49	H	-1.0932710	4.5331920	3.8986350
50	H	4.4059390	1.8387130	-2.1209510
51	H	3.7718390	3.4960870	-2.1005850
52	H	4.1767180	2.6611150	-0.5859820
53	H	4.4966840	-1.5709840	1.9456840
54	H	4.2574050	-3.3277390	2.0517080
55	H	4.7124640	-2.5677310	0.5149760

URA-BDP *SCF ENERGY:* -1409.26190 a.u

Tag	Symbol	X	Y	Z
1	C	-5.0275560	-0.0233790	1.1459800
2	C	-3.6367040	-0.0243590	1.2056370
3	C	-2.9516590	0.0008200	-0.0005480

4	C	-3.6384400	0.0260800	-1.2056050
5	C	-5.0292520	0.0255260	-1.1438140
6	N	-5.7038680	0.0011630	0.0015490
7	H	-3.1270250	-0.0448590	2.1547600
8	H	-3.1302760	0.0461660	-2.1555590
9	N	-5.8596550	-0.0505490	2.2695730
10	N	-5.8629740	0.0530470	-2.2662100
11	H	-6.8420550	-0.0441540	2.0353820
12	C	-1.4608500	0.0005930	-0.0009530
13	C	-0.7775390	-1.2155450	-0.0095660
14	C	-0.7770450	1.2165170	0.0078160
15	N	0.6148300	-1.2425790	-0.0076900
16	N	0.6153410	1.2429240	0.0063100
17	C	-1.2383190	-2.5678040	-0.0224050
18	C	-1.2371970	2.5690010	0.0191030
19	C	-0.1118570	-3.3611040	-0.0273080
20	C	-0.1103590	3.3617990	0.0228370
21	C	1.0255610	2.5258720	0.0148800
22	C	1.0244530	-2.5256940	-0.0174720
23	C	-2.6377010	-3.0934630	-0.0302810
24	C	2.4237420	-2.8913400	-0.0173630
25	C	-2.6362860	3.0954650	0.0262770
26	C	2.4250130	2.8909030	0.0141200
27	H	-3.1960960	-2.7454010	-0.9003360
28	H	-2.6172940	-4.1831080	-0.0533160
29	H	-3.1911730	-2.7828740	0.8570050
30	H	-3.1954060	2.7474670	0.8958830
31	H	-2.6152460	4.1850930	0.0496040
32	H	-3.1894220	2.7854930	-0.8614340
33	B	1.5251180	-0.0000070	-0.0033360
34	H	3.1282940	-2.0708460	-0.0131120
35	H	3.1291870	2.0701050	0.0068330
36	C	2.8565880	4.1595960	0.0220000
37	C	2.8547750	-4.1602390	-0.0198930
38	H	2.1230820	4.9602700	0.0312180
39	H	-0.1000810	4.4403090	0.0316570
40	H	-0.1020610	-4.4396110	-0.0368130
41	H	2.1209540	-4.9606760	-0.0205650
42	C	4.2476570	-4.6098740	-0.0194800
43	C	4.2496300	4.6087380	0.0205990
44	C	5.3373960	-3.7307330	-0.0411150
45	C	4.5068430	-5.9837520	0.0032510
46	C	5.3390060	3.7293880	-0.0093930
47	C	4.5093570	5.9823890	0.0498130
48	C	5.8069190	-6.4680440	0.0063270
49	C	6.6346400	-4.2135990	-0.0382970

50	C	6.6364090	4.2118340	-0.0086530
51	C	5.8095910	6.4662660	0.0506970
52	C	6.8765010	-5.5839630	-0.0142810
53	H	5.1734980	-2.6606950	-0.0616760
54	H	3.6742690	-6.6784690	0.0193710
55	H	5.9838540	-7.5367590	0.0246530
56	H	7.4650080	-3.5178240	-0.0555540
57	C	6.8788030	5.5819810	0.0215590
58	H	3.6770800	6.6772720	0.0725320
59	H	5.9869350	7.5348180	0.0739500
60	H	5.1747090	2.6595140	-0.0347260
61	H	7.4664820	3.5158990	-0.0324090
62	F	2.3464690	0.0061360	-1.1454250
63	F	2.3536430	-0.0065070	1.1331840
64	C	-5.5236380	0.0697460	-3.5954720
65	C	-5.5182670	-0.0707440	3.5982700
66	C	-6.6970690	0.0468730	-4.5417430
67	H	-7.6233670	0.3945740	-4.0853660
68	H	-6.4602100	0.6636440	-5.4067030
69	H	-6.8429860	-0.9785150	-4.8887650
70	O	-4.3731010	0.0797900	-3.9901010
71	C	-6.6900670	-0.0462890	4.5464960
72	H	-6.8316250	0.9786180	4.8967350
73	H	-7.6183920	-0.3893180	4.0907340
74	H	-6.4539970	-0.6663800	5.4093000
75	O	-4.3671280	-0.0832170	3.9910650
76	H	7.8959230	5.9548760	0.0218110
77	H	7.8934980	-5.9571860	-0.0122870
78	H	-6.8450190	0.0485500	-2.0305120

DAAP-DS-BDP *SCF ENERGY:* -2039.62210 a.u

Tag	Symbol	X	Y	Z
1	C	-6.2258080	-0.4719160	-2.0909120
2	C	-4.7917100	-0.3889490	-1.9450430
3	C	-4.2247180	-0.3840850	-0.7242700
4	C	-6.3558150	-0.5551720	0.3858900
5	N	-6.8999080	-0.5475390	-0.8778890
6	H	-4.1880420	-0.3265330	-2.8373760
7	C	-2.7411360	-0.2906320	-0.6004100
8	C	-2.1404850	0.9650890	-0.6153470
9	C	-1.9918500	-1.4623030	-0.5033240
10	N	-0.7570200	1.0790710	-0.4983180

11	N	-0.6057200	-1.4020030	-0.3948550
12	C	-2.6784910	2.2862570	-0.7348820
13	C	-2.3725590	-2.8391850	-0.4897750
14	C	-1.6063750	3.1456400	-0.6796760
15	C	-1.2063850	-3.5614400	-0.3760590
16	C	-0.1216420	-2.6583800	-0.3173490
17	C	-0.4242530	2.3842100	-0.5327040
18	C	-4.0971860	2.7226210	-0.9166310
19	C	0.9402070	2.8391940	-0.4241270
20	C	-3.7383600	-3.4403910	-0.5787520
21	C	1.2883920	-2.9384920	-0.1932900
22	H	-4.7661920	2.2948010	-0.1693750
23	H	-4.1567780	3.8078230	-0.8342090
24	H	-4.4784770	2.4380970	-1.8986980
25	H	-4.2421090	-3.1655420	-1.5064510
26	H	-3.6625310	-4.5268820	-0.5444570
27	H	-4.3782220	-3.1276300	0.2487720
28	B	0.2219740	-0.1031730	-0.3476310
29	H	1.6919440	2.0689790	-0.3196150
30	H	1.9443470	-2.0789040	-0.1749630
31	C	1.7889830	-4.1811200	-0.1065630
32	C	1.2886270	4.1357060	-0.4459320
33	H	1.1008720	-5.0212280	-0.1311750
34	H	-1.1343710	-4.6368980	-0.3404730
35	H	-1.6597060	4.2209410	-0.7429770
36	H	0.5063070	4.8816760	-0.5522710
37	C	2.6365870	4.6817430	-0.3387680
38	C	3.1937440	-4.5530650	0.0195320
39	C	3.7800100	3.8916110	-0.2007370
40	C	2.8106650	6.0726810	-0.3730380
41	C	4.2359140	-3.6251690	0.0777570
42	C	3.5322780	-5.9120580	0.0865610
43	C	4.0605530	6.6469710	-0.2735750
44	C	5.0427670	4.4526270	-0.0998930
45	C	5.5576400	-4.0237190	0.1964110
46	C	4.8427310	-6.3254320	0.2046670
47	C	5.1894310	5.8392620	-0.1355310
48	H	3.6952940	2.8124920	-0.1701970
49	H	1.9419070	6.7127200	-0.4798970
50	H	4.1879710	7.7218180	-0.3002260
51	H	5.9011300	3.8046160	0.0053120
52	C	5.8684750	-5.3818730	0.2604030
53	H	2.7448000	-6.6563470	0.0442930
54	H	5.0971090	-7.3766020	0.2554310
55	H	4.0233310	-2.5644140	0.0306900
56	H	6.3335620	-3.2726620	0.2379140

57	F	0.9117880	-0.0100190	0.8748060
58	F	1.1660800	-0.0871050	-1.3887380
59	N	-4.9711730	-0.4641530	0.4376670
60	O	-6.8405560	-0.4772190	-3.1424520
61	H	-7.9099620	-0.6104810	-0.9151270
62	O	-7.0453690	-0.6396900	1.3817620
63	C	-4.3702520	-0.4878310	1.7867390
64	H	-3.3552990	-0.8661680	1.6910180
65	H	-4.9419760	-1.2093560	2.3686140
66	C	-4.3768040	0.8668940	2.4825590
67	H	-3.7708270	1.5760000	1.9116050
68	H	-5.3989480	1.2539570	2.5076570
69	C	-3.8309330	0.7644460	3.9042270
70	H	-2.8170780	0.3513990	3.8750040
71	H	-4.4384570	0.0532070	4.4733770
72	C	-3.8128500	2.1097360	4.6215450
73	H	-3.1855500	2.8301560	4.0901740
74	H	-4.8190460	2.5312810	4.6910170
75	H	-3.4214160	2.0122300	5.6361210
76	O	6.3767420	6.4833500	-0.0441740
77	O	7.1253170	-5.8723110	0.3764120
78	C	7.5607320	5.7130320	0.1030380
79	C	8.2107370	-4.9584940	0.4340860
80	H	9.1078290	-5.5656530	0.5250180
81	H	8.2693950	-4.3579490	-0.4772040
82	H	8.1273710	-4.3012220	1.3033010
83	H	8.3776280	6.4282630	0.1559790
84	H	7.5348880	5.1223550	1.0222510
85	H	7.7111240	5.0529040	-0.7549020

URA-DS-BDP *SCF ENERGY:* -2176.39502 a.u

Tag	Symbol	X	Y	Z
1	C	2.2964470	0.7641580	-0.5347780
2	C	3.6833660	0.8808310	-0.5690110
3	C	4.4276500	-0.1151900	0.0401220
4	C	3.7998870	-1.1829740	0.6579290
5	C	2.4076150	-1.2124930	0.6435860
6	N	1.6707130	-0.2590550	0.0600290
7	H	4.1454950	1.7238840	-1.0538780
8	H	4.3546210	-1.9728910	1.1351440
9	N	1.4467370	1.6949070	-1.1386910
10	N	1.6703090	-2.2277670	1.2577240
11	H	0.4647830	1.4300530	-1.2040840

12	H	0.6694770	-2.0584280	1.3655860
13	C	5.9157920	-0.0364830	0.0305560
14	C	6.5685670	0.6586520	1.0480300
15	C	6.6252740	-0.6598450	-0.9952260
16	N	7.9637780	0.7482550	1.0574020
17	N	8.0218910	-0.6008970	-1.0228880
18	C	6.0826910	1.3603470	2.1888220
19	C	6.2019050	-1.4134220	-2.1279410
20	C	7.2000360	1.8487130	2.8438980
21	C	7.3561730	-1.7828990	-2.7965770
22	C	8.4587540	-1.2717010	-2.0965670
23	C	8.3412720	1.4589520	2.1280070
24	C	4.6761290	1.5700270	2.6489210
25	C	9.7631900	1.7531850	2.4524890
26	C	4.8196550	-1.7739470	-2.5677110
27	C	9.8997140	-1.4189230	-2.4365070
28	H	4.1560820	0.6246890	2.8099170
29	H	4.6785740	2.1213640	3.5893370
30	H	4.0951930	2.1407290	1.9226310
31	H	4.1990270	-0.8903250	-2.7230530
32	H	4.8679370	-2.3251910	-3.5069240
33	H	4.3135620	-2.4011080	-1.8320490
34	B	8.9034640	0.1262680	0.0085390
35	H	7.4121410	-2.3654330	-3.7037100
36	H	7.2057050	2.4313200	3.7526450
37	F	9.7862440	-0.7811960	0.6214700
38	F	9.6631860	1.1297210	-0.6208780
39	C	-1.9200150	-1.2875740	1.0323530
40	C	-3.3588820	-1.2934800	1.0382050
41	C	-4.0429190	-0.4700770	0.2210250
42	C	-2.0273700	0.4467030	-0.6994990
43	N	-1.3558720	-0.3945240	0.1440850
44	H	-3.8716770	-1.9659500	1.7085190
45	C	-5.5346090	-0.4831720	0.2377160
46	C	-6.2019440	0.2845470	1.1871910
47	C	-6.2149480	-1.2869490	-0.6748900
48	N	-7.5993410	0.2892930	1.2193980
49	N	-7.6109510	-1.3166730	-0.6747070
50	C	-5.7404640	1.1419080	2.2335030
51	C	-5.7603400	-2.1684480	-1.6997490
52	C	-6.8738210	1.6329350	2.8509260
53	C	-6.8976070	-2.6985350	-2.2794570
54	C	-8.0211280	-2.1586260	-1.6320680
55	C	-8.0023730	1.0940120	2.2092990
56	C	-4.3439990	1.4670260	2.6570790
57	C	-9.4326830	1.3365990	2.5338620

58	C	-4.3622680	-2.4993730	-2.1115100
59	C	-9.4538940	-2.4419720	-1.9108340
60	H	-3.7265520	1.8232650	1.8316170
61	H	-4.3678500	2.2499030	3.4148600
62	H	-3.8454200	0.5973790	3.0885200
63	H	-3.7902390	-2.9329990	-1.2899260
64	H	-4.3824470	-3.2224090	-2.9263210
65	H	-3.8193880	-1.6201340	-2.4642720
66	B	-8.5200440	-0.4935540	0.2594980
67	H	-6.9306930	-3.4093010	-3.0910700
68	H	-6.9024430	2.3127830	3.6887700
69	F	-9.3045890	0.3986840	-0.4908240
70	F	-9.3670320	-1.3420900	0.9857420
71	N	-3.4079420	0.3973110	-0.6477840
72	O	-1.2015660	-1.9929190	1.7321420
73	H	-0.3242380	-0.3483330	0.1025890
74	O	-1.4303470	1.1982110	-1.4564290
75	C	-4.1323300	1.3017820	-1.5670060
76	H	-5.1082650	0.8627390	-1.7597780
77	H	-3.5759750	1.3022860	-2.5029260
78	C	-4.2726960	2.7225670	-1.0370330
79	H	-4.8594310	2.7139500	-0.1142640
80	H	-3.2825510	3.1164090	-0.7922530
81	C	-4.9493260	3.6320740	-2.0592370
82	H	-5.9289850	3.2185930	-2.3207850
83	H	-4.3603470	3.6391180	-2.9822210
84	C	-5.1181340	5.0588630	-1.5489310
85	H	-5.7316810	5.0828900	-0.6446580
86	H	-4.1509810	5.5074180	-1.3074200
87	H	-5.6014750	5.6912790	-2.2960760
88	C	2.1344600	-3.4296220	1.7339320
89	C	1.7782250	2.9198420	-1.6645110
90	C	1.0833550	-4.3128030	2.3568370
91	H	0.0899420	-3.8704390	2.3583080
92	H	1.0638380	-5.2571320	1.8107290
93	H	1.3874420	-4.5337520	3.3809420
94	O	3.2990900	-3.7813830	1.6653030
95	C	0.6304130	3.6704320	-2.2908660
96	H	-0.3380860	3.2096190	-2.1105230
97	H	0.6371870	4.6906170	-1.9072340
98	H	0.8063330	3.7228860	-3.3671790
99	O	2.9048350	3.3829760	-1.6461380
100	H	-9.5477470	-3.0427390	-2.8138700
101	H	-9.9057500	-2.9859790	-1.0786460
102	H	-10.0168400	-1.5161130	-2.0356000
103	H	-9.5171080	2.0928510	3.3122760

104	H	-9.9795600	1.6689970	1.6502860
105	H	-9.9085160	0.4171070	2.8805060
106	H	10.4282680	-1.9601490	-1.6494930
107	H	10.0091130	-1.9627710	-3.3734360
108	H	10.3771720	-0.4425890	-2.5328130
109	H	10.2418760	2.2962200	1.6357810
110	H	9.8233990	2.3520320	3.3598760
111	H	10.3254430	0.8292160	2.5985890

BDP-dimer *SCF ENERGY:* -2910.79907 a.u

Tag	Symbol	X	Y	Z
1	C	3.0345700	0.3077350	0.9407210
2	C	4.4249680	0.3040750	1.0135320
3	C	5.1299530	0.0761610	-0.1562300
4	C	4.4603920	-0.1362760	-1.3490390
5	C	3.0680030	-0.1095000	-1.3249260
6	N	2.3693040	0.1062060	-0.2033540
7	H	4.9198860	0.4761570	1.9542250
8	H	4.9835610	-0.3195370	-2.2721390
9	N	2.2218150	0.4988110	2.0615100
10	N	2.2915660	-0.2816440	-2.4734020
11	H	1.2287430	0.3074690	1.9340420
12	H	1.2987330	-0.0602510	-2.3859090
13	C	6.6201100	0.0593080	-0.1308520
14	C	7.2862880	-1.1466430	0.0878110
15	C	7.3206710	1.2494990	-0.3263190
16	N	8.6780260	-1.1888410	0.1174360
17	N	8.7132190	1.2597280	-0.3086050
18	C	6.8062820	-2.4733440	0.3108950
19	C	6.8790690	2.5867630	-0.5657050
20	C	7.9212400	-3.2676270	0.4674580
21	C	8.0166300	3.3551470	-0.6840520
22	C	9.1408000	2.5190730	-0.5224690
23	C	9.0691440	-2.4576650	0.3450360
24	C	5.3998000	-2.9759020	0.3730550
25	C	10.4628190	-2.8338990	0.4344830
26	C	5.4872540	3.1206640	-0.6770730
27	C	10.5450020	2.8628360	-0.5644390
28	H	4.8702760	-2.8100200	-0.5662110
29	H	5.4046010	-4.0470370	0.5755090
30	H	4.8277530	-2.4834910	1.1605970
31	H	4.9212030	2.9664350	0.2426840
32	H	5.5229220	4.1914260	-0.8783250

33	H	4.9326210	2.6411470	-1.4847690
34	B	9.6052760	0.0252330	-0.0790200
35	H	11.1790130	-2.0341560	0.3037700
36	H	11.2376200	2.0448730	-0.4203640
37	C	10.9943100	4.1090750	-0.7664690
38	C	10.8756270	-4.0878960	0.6645440
39	H	10.2723430	4.9087660	-0.9027700
40	H	8.0416430	4.4173180	-0.8697630
41	H	7.9152130	-4.3303400	0.6515110
42	H	10.1307670	-4.8681340	0.7899230
43	C	12.2618460	-4.5459840	0.7696890
44	C	12.3936840	4.5344360	-0.8243890
45	C	13.3636870	-3.6897960	0.6524810
46	C	12.5016540	-5.9043280	0.9990500
47	C	13.4706290	3.6475210	-0.7042100
48	C	12.6728390	5.8919510	-1.0099060
49	C	13.7944760	-6.3958750	1.1072930
50	C	14.6537110	-4.1798610	0.7605430
51	C	14.7747480	4.1073950	-0.7660790
52	C	13.9797880	6.3532620	-1.0715710
53	C	14.8762340	-5.5347040	0.9882750
54	H	13.2148970	-2.6318820	0.4764800
55	H	11.6596700	-6.5813070	1.0927000
56	H	13.9562000	-7.4523460	1.2848190
57	H	15.4936220	-3.5017980	0.6672720
58	C	15.0365000	5.4619240	-0.9496580
59	H	11.8505290	6.5923830	-1.1058310
60	H	14.1720960	7.4097450	-1.2153250
61	H	13.2913110	2.5890610	-0.5633740
62	H	15.5949270	3.4057440	-0.6716170
63	F	10.4489800	-0.1792580	-1.1862300
64	F	10.4126130	0.2112350	1.0580680
65	C	-1.2640960	0.2141290	-1.5068330
66	C	-2.7020680	0.2183810	-1.4715700
67	C	-3.3530340	0.1302230	-0.2953700
68	C	-1.2982490	0.0500000	0.9404060
69	N	-0.6623500	0.1249810	-0.2679610
70	H	-3.2428700	0.2850480	-2.4029710
71	C	-4.8439960	0.1233920	-0.2726340
72	C	-5.5150880	-1.0827200	-0.4521140
73	C	-5.5259260	1.3279420	-0.1066490
74	N	-6.9076440	-1.1144770	-0.4393670
75	N	-6.9172290	1.3502080	-0.0990010
76	C	-5.0501620	-2.4202190	-0.6655380
77	C	-5.0655760	2.6687670	0.0723680
78	C	-6.1727390	-3.2071030	-0.7666190

79	C	-6.1912600	3.4529290	0.1786900
80	C	-7.3297990	2.6228690	0.0707980
81	C	-7.3149970	-2.3851440	-0.6253070
82	C	-3.6508560	-2.9318910	-0.7944630
83	C	-8.7079150	-2.7562360	-0.6578300
84	C	-3.6633680	3.1828660	0.1401460
85	C	-8.7252460	2.9844330	0.1224110
86	H	-3.0169640	-2.6351070	0.0418740
87	H	-3.6645080	-4.0211570	-0.8294320
88	H	-3.1778800	-2.5725280	-1.7097650
89	H	-3.1043180	2.9589860	-0.7693890
90	H	-3.6766090	4.2646840	0.2699220
91	H	-3.1116690	2.7572340	0.9808550
92	B	-7.8232820	0.1121350	-0.2463190
93	H	-9.4189320	-1.9524060	-0.5251300
94	H	-9.4318680	2.1730330	0.0135090
95	C	-9.1529740	4.2460230	0.2904470
96	C	-9.1278300	-4.0188780	-0.8393140
97	H	-8.4131810	5.0348330	0.3917010
98	H	-6.2013950	4.5222660	0.3185870
99	H	-6.1797860	-4.2729910	-0.9309080
100	H	-8.3831710	-4.7991210	-0.9672940
101	C	-10.5080150	-4.4857190	-0.8859920
102	C	-10.5365430	4.7021550	0.3533620
103	C	-11.6131740	-3.6406970	-0.7611580
104	C	-10.7554540	-5.8542590	-1.0657690
105	C	-11.6366000	3.8465310	0.2608260
106	C	-10.7925310	6.0713070	0.5150250
107	C	-12.0390700	-6.3553760	-1.1169420
108	C	-12.9090490	-4.1279680	-0.8106450
109	C	-12.9356200	4.3241600	0.3241680
110	C	-12.0793250	6.5628940	0.5798160
111	C	-13.1288690	-5.4938610	-0.9894720
112	H	-11.4712970	-2.5760700	-0.6233710
113	H	-9.9175630	-6.5351230	-1.1665850
114	H	-12.2235860	-7.4131400	-1.2557520
115	H	-13.7361490	-3.4396680	-0.7104250
116	C	-13.1638890	5.6908610	0.4844390
117	H	-9.9588070	6.7605790	0.5901680
118	H	-12.2701420	7.6213380	0.7042300
119	H	-11.4883140	2.7809880	0.1374470
120	H	-13.7584830	3.6276520	0.2486470
121	F	-8.6165960	-0.0501820	0.9033160
122	F	-8.6750760	0.2602330	-1.3539540
123	N	-2.6798680	0.0459640	0.9096700
124	O	-0.5748410	0.2763720	-2.5194870

125	H	0.3704200	0.1203020	-0.2374270
126	O	-0.6691470	-0.0055280	1.9874280
127	C	-3.3654620	-0.0190300	2.2183870
128	H	-4.3498700	0.4257850	2.0958420
129	H	-2.7957230	0.6120660	2.8986800
130	C	-3.4764540	-1.4306110	2.7788420
131	H	-4.0892810	-2.0431350	2.1116560
132	H	-2.4819580	-1.8829920	2.8191020
133	C	-4.0957850	-1.4259140	4.1740060
134	H	-5.0796690	-0.9469030	4.1332350
135	H	-3.4802570	-0.8121610	4.8398710
136	C	-4.2351800	-2.8285030	4.7552430
137	H	-4.8736620	-3.4533200	4.1254560
138	H	-3.2618200	-3.3196470	4.8345120
139	H	-4.6769330	-2.8007830	5.7532210
140	O	-14.3531300	-6.0674890	-1.0516840
141	O	-14.3919490	6.2557590	0.5576450
142	C	-15.5011800	-5.2398750	-0.9321290
143	C	-15.5347010	5.4174860	0.4663860
144	H	-16.3955240	6.0760420	0.5496990
145	H	-15.5667220	4.8977290	-0.4944900
146	H	-15.5549150	4.6885110	1.2804200
147	H	-16.3577830	-5.9042070	-1.0128310
148	H	-15.5236050	-4.7343480	0.0365410
149	H	-15.5385920	-4.4995620	-1.7351990
150	C	2.7077810	-0.7110220	-3.7100980
151	C	2.6026580	0.9071490	3.3163260
152	C	1.6273030	-0.7610610	-4.7603440
153	H	0.6399460	-0.5114220	-4.3791680
154	H	1.8951280	-0.0638650	-5.5561900
155	H	1.6162260	-1.7621760	-5.1927140
156	O	3.8554910	-1.0313510	-3.9651650
157	C	1.4829770	0.9881420	4.3229170
158	H	0.5038100	0.7754920	3.9003550
159	H	1.6936610	0.2770220	5.1235650
160	H	1.4888560	1.9863660	4.7619120
161	O	3.7490480	1.1867400	3.6194640
162	H	16.0588200	5.8170920	-0.9977170
163	H	15.8876650	-5.9135780	1.0722380

DS-BDP dimer *SCF ENERGY:* -4216.03679 a.u